HIGH-THROUGHPUT TOOLS AND TECHNIQUES TO INVESTIGATE ENVIRONMENTAL EFFECTS ON AGING BEHAVIORS IN *CAENORHABDITIS ELEGANS*

A Dissertation
Presented to
The Academic Faculty

by

Kim Ngoc Le

In Partial Fulfillment
of the Requirements for the Degree
Doctor of Philosophy in the
Wallace H. Coulter Department of Biomedical Engineering

Emory University &
Georgia Institute of Technology
December 2021

HIGH-THROUGHPUT TOOLS AND TECHNIQUES TO INVESTIGATE ENVIRONMENTAL EFFECTS ON AGING BEHAVIORS IN *CAENORHABDITIS ELEGANS*

Approved by:

Dr. Hang Lu, Advisor
School of Chemical & Biomolecular Engineering
Georgia Institute of Technology

Dr. Annalise Paaby
School of Biology
Georgia Institute of Technology

Dr. Gordon Berman
Department of Biology
Emory University & Georgia Institute of Technology

Dr. Shuichi Takayama
Department of Biomedical Engineering
Georgia Institute of Technology

Dr. Patrick McGrath
School of Biology
Georgia Institute of Technology

Date Approved: November 18, 2021

To Má and Bố, for their love and support.

ACKNOWLEDGEMENTS

There are many people I would like to thank who have helped make this dissertation possible. First and foremost, I want to thank my advisor, Hang Lu, who has provided tremendous support, encouragement, and advice throughout these past years. I would not be the researcher that I am today without her mentorship. I would also like to thank my committee members for providing constructive feedback and guidance in my work. Additionally, I would like to thank all members of the Lu Lab – both past and present – for their invaluable support, camaraderie, and insightful scientific feedback. In particular, I want to thank Dr. Yongmin Cho and Dr. Dhaval Patel for their mentorship and guidance during my first few years in the lab, along with Dr. Kathleen Bates for her vital help in the last, computationally-focused, year. Special thanks to the aging crew – Yongmin, Dhaval, and Jason Wan – for their support in brainstorming, troubleshooting, and helping to run some of those fun, long-term aging experiments. Thank you to Weipeng Zhuo and Seleipiri Charles for your friendship and crucial pep talks whenever experiments have failed. Additionally, I want to thank Kirby Broderick, Lushuang Zhang, and Madison Green, dedicated undergraduate students who have immensely contributed to this work.

Last but not least, I would like to thank my friends and family for their support throughout these past few years. Thank you to Sophie for being the best writing companion a person could hope for. Thank you to Mai, Lan, and Byron for your love, support, and the countless care packages to get me through the worst of it. Finally, thank you to Mom and Dad for your unconditional love and support – I am forever grateful to have you both as my parents and role models in life.

TABLE OF CONTENTS

LIST OF TABLES

LIST OF FIGURES

LIST OF SYMBOLS AND ABBREVIATIONS

C. elegans	*Caenorhabditis elegans*
IIS	Insulin/insulin-like growth factor signaling
E. coli	*Escherichia coli*
PEG	Polyethylene glycol
PDMS	Polydimethylsiloxane
HeALTH	Health and Lifespan Testing Hub
OP50	Strain of *E. coli* used for culturing *C. elegans*
HB101	Strain of *E. coli* used for culturing *C. elegans*
C22	Small molecule used for progeny prevention in *C. elegans*
DR	Dietary restriction
NGM	Nematode Growth Medium
S-Medium	Buffer used for *C. elegans* culture and handling
FUdR	5-fluoro-2'-deoxyuridine, used for progeny prevention in *C. elegans*
CNN	Convolutional Neural Network
Mask R-CNN	Mask Region-Based Convolutional Neural Network
Faster R-CNN	Faster Region-Based Convolutional Neural Network
IoU	Intersection over the union
AP	Average precision
AR	Average recall
mAP	Mean average precision
ROI	Region of interest
RPN	Region proposal network

CR	Caloric restriction
IF	Intermittent fasting

SUMMARY

Aging is modulated by genetic and environmental cues; however, it is difficult to study how these perturbations modulate the aging process in a robust, high-throughput manner. Methods to gather large-scale behavioral data for aging studies are labor-intensive, lack individual-level resolution, or lack precise spatiotemporal environmental control. In addition, tools to analyze large-scale behavioral data sets are difficult to scale, unable to be broadly applied across complex environments, or fail to detect subtle behavioral changes.

In this thesis I develop tools to enable robust, microfluidic culture and behavioral analysis of *C. elegans* to examine how environmental cues, such as dietary restriction, influence longevity and behavior with age. In Aim 1, I engineer a robust pipeline for the long-term longitudinal culture and behavioral monitoring of *C. elegans* in aging studies with precise spatiotemporal environmental control. In Aim 2, I develop a flexible deep learning based pipeline for detecting and extracting postural information from large-scale behavioral datasets across heterogeneous environments. In Aim 3, I characterize how the full behavioral repertoire of individuals change with age, along with examining how these age-related behavioral changes are modulated by different dietary restriction regimes. The completion of this thesis provides 1) a new toolset to robustly explore how genetic or environmental effects influence longevity and healthspan, 2) a flexible pipeline for analyzing large-scale behavioral data in *C. elegans*, and 3) insight into how environmental perturbations influence health through age-related changes in behavior.

CHAPTER 1. INTRODUCTION

In the past few decades, global lifespans have dramatically increased due to advancements in medicine. However, with this rise in lifespan, there is an accompanying rise in age-related diseases. Cases of cardiovascular disease have almost doubled to 523 million in the thirty years, costing $363 billion annually in the United States alone.[1,2] Global rates of cancer are expected to increase by 47% within the next twenty years, while neurodegenerative diseases in the United States are expected to double by 2060 to 13.9 million cases.[3,4] Although these illnesses vary in physical, mental, and societal impacts they all have a shared, underlying cause – aging.

Aging, the functional decline of an organism over time, is largely universal across species. Once thought of as an inherent part of the human experience, the past few decades have brought new insights into the underlying causes of aging. For instance, factors such as cellular senescence, deregulated nutrient sensing, or a breakdown in mitochondrial regulation and proteostasis have been shown to drive the aging process across species.[5] However, it is difficult to examine how these biological causes are driven and modulated by genetic or environmental factors, particularly in mammalian organisms. As a result, it is difficult to design interventions to delay the aging process in order to not just prolong lifespan, but also extend the period of healthy, disease-free functional living (i.e. the healthspan) or an individual.

Caenorhabditis elegans (C. elegans) is a commonly used model organism for aging studies. It already has demonstrated its usefulness in discovering how different molecular pathways, such as the insulin/IGF-1-like (IIS) pathway, can dramatically alter the aging

process.[5,6] However, although these organisms are easy to cultivate and study throughout their entire lifespan, there are some key technical difficulties in performing precisely controlled large-scale aging studies, in terms of data collection, data analysis, and subsequent interpretation.

In this thesis, I detail robust and high-throughput tools and techniques to better study the aging process in *C. elegans*, along with biological applications demonstrating the impact of genetic and environmental perturbations on aging behaviors. The following sections serve as a brief review on prior literature and research on aging in *C. elegans* (with a particular focus on healthspan), detail the limitations of existing technologies, and introduce the objectives of this work.

1.1 Aging in *C. elegans*

Aging studies in humans and mammalian models can be difficult to perform due to their long natural lifespans, environmental complexity, and high cost.[7] As a result, *C. elegans* is a commonly used, powerful, and tractable tool for aging studies. This 1 millimeter long nematode has a relatively short lifespan (~2-3 weeks) making it possible to monitor individuals throughout their entire adult lifespan. It is relatively easy to culture and maintain large populations of animals, and there are a wide range of established tools for genetic manipulation allowing researchers to examine how environmental and genetic perturbations influence the aging process. The organism produces large, isogenic populations making it amenable for large scale studies. Lastly, it has a significant degree of genetic homology to humans (~38% for protein-coding genes)[8] potentially making identified pathways or transcription factors in worms translatable across species.

1.1.1 Genetic effects on aging

This organism has already been used to identify key genes and signal pathways involved in the aging process. A canonical example is the IIS pathway, in where it was discovered that a mutation in the *daf-2* receptor in the nematode dramatically results in individuals that live twice as long as wild-type individuals.[9,10] Additional downstream transcription factors in the pathway - such as DAF-16/FOXO, HSF-1, or SKN-1 – also impact longevity in the worm, and are associated with stress response, cytoskeletal integrity, and protein quality control.[9–17] Crucially, the pathway's effect on longevity is conserved across species, ranging from *Drosophila melanogaster*, mice, and humans.[18–21] In addition to the IIS pathway, a wide variety of other conserved pathways and factors have also been implicated in regulating lifespan, and largely are associated with stress-response or nutrient sensing genes that respond to environmental cues.[22–26]

1.1.2 Environmental effects on aging

Response to stressors and nutrient availability is perhaps best exemplified by the case of dietary restriction (DR). This evolutionarily conserved process, first demonstrated in rats but later found across species from yeast to potentially humans, is a prime example of how environmental or sensory cues can have a large influence on longevity.[27–33] DR has been shown to largely activate either the IIS or target of rapamycin (TOR) pathways; however, different regimes of DR (such as altering the food levels, frequency, or method of restriction) have been shown to trigger different nutrient sensors and subsequent transcription factors, indicating a flexibility and wide variety of responses to different environmental cues .[34,35] Even just sensory cues in response to food have been shown to

influence longevity across species.[36–39] In addition to nutrient availability, a wide range of stressors have also been shown to impact longevity. For instance, modulating body temperature has been shown to have similar effects on longevity in both *C. elegans* invertebrates and mammalian models.[40–43] Thus, the interactions between environmental conditions, the individual's perception of its surroundings, and resulting genetic response strongly influence the aging process.

1.1.3 Healthspan in C. elegans

Aging encompasses both an increased risk of death and increased frailty, whether it be an increased risk for age-related diseases, declines in sensory abilities (such as vision, hearing, or even taste), or reduced physical capabilities.[44] As such, it is crucial to measure not just the longevity of the individual in response to targeted perturbations, but also the health throughout its lifespan to also ensure a prolonged healthspan. For example, if an intervention increases the lifespan of the individual without proportionally maintaining or extending its health, there is still a substantial disease burden on the individual, making it undesirable to pursue.

There is no set method to measure health and healthspan. For instance, in humans this can be done through tracking metrics ranging from the maximum amount of oxygen consumption during exercise as a measure of cardiorespiratory fitness, mental health assessments to characterize cognitive decline, to a short physical performance battery (SPPB) test in a clinical setting as a measure of physical ability.[45–47] Similarly, there are many ways to gauge healthspan in *C. elegans.* Prior work has examined physiological markers such as mitochondrial morphology, muscular structure, or autofluorescence to

measure lipofuscin accumulation.[48–52] However, perhaps the most common method of measuring healthspan is by gauging sarcopenia or physical ability through examining basic behavioral metrics (such as maximum velocity traveled over a set period of time or thrashing rates in liquid).[48,50,51,53,54] To consistently track these metrics over time requires significant time and labor and often is unscalable for large-scale aging studies, particularly if using traditional data collection and analysis tools.

1.2 Existing tools to measure and analyze aging in *C. elegans*

Traditionally researchers have used lifespan as the measure of aging, with researchers equating longer lifespans with slower rates of aging. Conventional lifespan assays for *C. elegans* require the periodic assessment of motility after mechanical stimulation, with a lack of response indicating death.[55] They are often done manually, with researchers tracking populations on agar plates seeded with *E. coli*, stimulating each worm with a metal every other day, with the average lifespan on the population indicating the overall effectiveness of the intervention of interest. Similar to traditional lifespan studies, the more recent healthspan assays typically require the periodic manual subsampling of a population and manually counting or measuring the phenotype of interest under a microscope.[48–51,53,54,56] Both assays require large amounts of manual labor, can be prone to experimenter bias, and lack precise environmental control over time. For example, although plates are typically kept within temperature-controlled incubators, the plates are periodically removed for scoring, resulting in unintended and uncontrolled temperature fluctuations, which may influence phenotypes of interest, such as behavior or lifespan. Specific behavioral metrics, such as the extent of movement or the types of behaviors performed, are time-consuming, prone to bias, and difficult to quantify on a large-scale.

Furthermore, they often fail to study these trends at an individual-level resolution, therefore masking any intrapopulation variability or trends that may point to different aging trends within the population.

It is extremely difficult to perform large-scale aging studies (in terms of examining both longevity or health metrics of interest) both on a collection and analysis front using the conventional techniques. Although there are some existing methods that have attempted to address and reduce this barrier for large-scale analysis in terms of both data collection and subsequent analysis, they too have limitations, as detailed below.

1.2.1 Existing techniques for large-scale data collection for aging studies in C. elegans

A major difficulty in performing large-scale aging studies is the amount of manual labor required to culture, perturb, collect, and finally analyze aging data. The subsequent sections detail two distinct veins of approaches that aim to address this challenge. First, I discuss a variety of methods for collecting large-scale data sets and examine the existing limitations with those approaches. Second, I discuss the lack of behavioral analysis methods able to accurately analyze the large sets of data generated from the recent advancements in data collection.

1.2.1.1 Automated methods for aging studies

To address the challenge of performing large-scale lifespan studies, researchers have recently developed methods designed to automate the assay process. For instance, the Lifespan Machine uses modified flatbed scanners as a low-cost large-scale imaging tool, allowing researchers to periodically scan and observe movement across large swaths of

different populations cultured on standard agar plates.[57] Although easily amendable to large-scale studies and traditional lifespan assay protocols,[58] there are limitations to this technique. For example, due to the use of scanners as an imaging tool, it is difficult to obtain frequent imaging timepoints, preventing the acquisition of high-content behavioral data to examine healthspan.

There are several *C. elegans* longitudinal culture devices that could be used to examine behavior or health metrics over long periods of time (i.e. on the time scale of days). These systems culture individual worms on a solid substrate (either agar or a PEG gel) and use several low-cost cameras or modified robotic handlers to automate the imaging process to automatically record activity over time.[59–62] They obtain high-content health information on a large scale, with many doing so on an individual worm level resolution, allowing researchers to better observe variability in aging within the isogenic population. However, they are all "closed-system" culture devices, therefore lacking precise control in regulating the organism's immediate environment. For instance, many individuals are given *ad libitum* amounts of food at the beginning of the experiment, with the amount of food changing and decreasing based on the worm's consumption rate. Furthermore, one is unable to introduce dynamic stimulus into the environment (such as pharmaceutical intervention or altering their diet midway through their lifespan), limiting the types of studies and extent of effects one could investigate.[29,63,64] While these technologies address the data collection bottleneck through the automated data collection, they lack the required precise environmental control ideal for lifespan and aging studies.

1.2.1.2 Microfluidic approaches towards aging studies

Microfluidic devices have been a relatively recent tool in the manipulation and culture of *C. elegans*.[65–70] Their ability to handle small volumes of liquid, the biocompatibility and tunable mechanical properties of polydimethylsiloxane (PDMS), the elastomer used to create these devices, and the similar sized scaled features to that of *C. elegans* allows these devices to easily handle and manipulate organisms while providing precise spatiotemporal environmental control.[71–73]

As such, as there a variety of existing devices that could be adapted to measure phenotypes linked to healthspan, along with devices explicitly designed for performing lifespan assays. For example, devices designed to enable high-throughput imaging of worms at high levels of magnification could be used to measure physiological traits, such as autofluorescence or the structure and organization of the musculature.[65,74–76] There are devices specifically designed to measure traits such as fecundity or pharyngeal pumping rates, metrics that have previously been used to determine the health of individuals.[77,78] However, while these devices are adept at measuring specific phenotypes of interest, they are unable to culture worms for long-periods of time, particularly on the scale of their entire lifespan.

In contrast, there are devices specifically designed for long-term culture for aging studies.[79–82] These devices are often limited in the range of environmental conditions they are able to provide, culturing worms in axenic media or low food conditions that are atypical of conventional lifespan assays. The micro-scale size of the device features results in extreme difficultly to robustly flow bacterial food into the device for the duration of the worm's lifespan. Due to the known impact of food and dietary restriction on lifespan, these reduced long-term food levels could likely result in confounding lifespan results.[82]

Additionally, these devices are often not easily scalable. They either lack the capability to culture large numbers of worms on a single device (due to having a large footprint for each individual) or simply culture worms as a large population, preventing experimenters from tracking individuals on a longitudinal basis. Thus, although existing microfluidic devices for studying *C. elegans* lifespans allow for precise spatiotemporal environmental control, they either lack experimental robustness, longitudinal tracking, are limited to low food levels, or have not demonstrated the ability to scale up for high-throughput studies.

1.2.1.3 Automated methods of quantifying aging in *C. elegans*

With the strides in collecting large-scale data for aging studies for *C. elegans*, there is a need to analyze the large sets of generated data in a scalable, robust manner. Typical methods of measuring lifespan – manual inspection of individuals under a microscopy for signs of movement after a mechanical stimulus – are infeasible to perform at scale. Therefore, there is a need for automated methods to extract and quantify phenotypes of interest.

Within the past few years, there have been a rise in the number of analysis pipelines designed to address this gap. For instance, when performing lifespan assays, experimenters track and measure the extent of coarse movement to automatically determine whether an individual is dead without the need for manual assessment.[57,60,62] For more complex information, such as examining behavior with age, there are a plethora of tools that can aide experimenters in easily measuring and calculating metrics of interest.[83–87] For example, Tierpsy Tracker is a popular worm-focused software that allows experimenters to track and extract behavioral information of individuals, such as the speed of the worm

and basic postural information, throughout the video.[83] It uses basic image processing techniques, such as background subtraction and intensity based thresholding, which are parameters optimized by the experimenter, and are subsequently used to extract out the worms of interest. Though these tools are highly advantageous for conventional experimental conditions (such as when a worm is cultured on a high-contrast environmental condition with no other objects nearby) they can be difficult to accurately use and scale across heterogeneous environments or experimental conditions.

1.3 Thesis Objective

Although there are existing tools that have reduced the burden of performing large-scale aging studies in *C. elegans*, they still have significant limitations in terms providing flexibility for exploring the impact of environment on the aging process. The purpose of this thesis is to develop robust, flexible, and automated methods to study the aging process in *C. elegans* under precise environmental conditions. This encompasses both the long-term culture and subsequent behavioral analysis of large populations and culminates in examining how the behavioral repertoire changes with age and how different forms of dietary restriction modulate those changes.

1.4 Thesis Outline

This thesis consists of five chapters. **Chapter Two** presents an automated microfluidic-based platform and robust pipeline for large-scale, long-term aging studies. This chapter details improvements to both the system's design and culture protocol for increased experimental viability and usability. It then demonstrates the system's potential application in large-scale aging studies, exploring how genetic and environmental

perturbations influence longevity and behavioral decline over time, displaying individual-level resolution. **Chapter Three** discusses the development of a flexible, deep-learning segmentation pipeline for extracting behavioral metrics from worms cultured in complex and heterogenous environments. In this work, deep learning is applied to extract meaningful, biological data on a large-scale. **Chapter Four** presents a biological application of the long-term culture and behavioral analysis developed in previous chapters, exploring how health and aging are influenced by the environment. This work defines the behavior repertoire of aging with single animal resolution and examines how the repertoire changes within an isogenic population and across different dietary restriction regimes. Lastly, **Chapter Five** provides a conclusion and suggestions for future work.

CHAPTER 2. A ROBUST PIPELINE FOR THE LONG-TERM CULTURE AND LARGE-SCALE BEHAVIORAL MONITORING OF *C. ELEGANS* FOR AGING STUDIES

This chapter is adapted from a research article entitled "An automated platform to monitor long-term behavior and healthspan in *Caenorhabditis elegans* under precise environmental control" published in Nature Communications Biology in 2020.[88] This was co-authored in collaboration with Dr. Mei Zhan and Dr. Yongmin Cho.

2.1 Introduction

In this chapter I discuss the development and optimization of an automated microfluidic-based platform designed to capture high-throughput, long-term, longitudinal behavioral recordings under precise spatiotemporal environmental control, resulting in the Health And Lifespan Testing Hub (HeALTH). To demonstrate the versatility and robustness of the platform, several large-scale aging studies were performed, examining how longevity and behaivoral decline varied across 1) IIS mutants, 2) chronic caloric restriction, and 3) culture temperture.

2.2 Background

Environmental factors play a major role in the health and longevity of an individual.[39] However, existing methods of studying lifespan and healthspan in *C. elegans* are limited and lack the ability to provide precise environmental control. Traditional lifespan and healthspan assays require large amounts of manual labor, making it difficult to scale for

different genotypes or environmental conditions.[89] Recent high-throughput methods developed for scoring longevity or observing behavior over time lack precise control in regulating the organism's immediate environment.[57,59,60,62] For instance, dietary restriction (DR), an evolutionarily conserved environmental perturbation that modulates aging, cannot be studied as food levels deplete over time within these closed culture systems. Existing microfluidic devices for studying *C. elegans* lifespans allow for precise spatiotemporal environmental control, but often lack experimental robustness, longitudinal tracking, are limited to a range of low food levels, or have not feasibly demonstrated the ability to scale up for high-throughput studies.[79–82] As a result, there is a need for a robust method to probe a wide variety of environmental conditions in a high-throughput manner, providing precise spatiotemporal control throughout the entirety of the organism's lifespan.

To address these limitations, previous members of the lab, Dr. Mei Zhan and Dr. Yongmin Cho, developed a platform designed to provide automated behavioral monitoring of individuals throughout the adult lifespan (from Day 2 Adult to death) under precisely controlled environmental conditions as shown in **Figure 2.1**.[90] The platform uses a time-shared, low-cost CMOS camera mounted on an automated x-y stage to allow for automated acquisition of behavioral data in scalable manner, while still being both cost and space-effective. A commercially available white LED ring was mounted to the end of the collimator, providing constant illumination to the worms. A Peltier-based, thermal control module was developed to maintain the desired temperature throughout the lifespan of the worms. A microfluidic chamber array, previously used for observing behavior for chemical screening with single-animal resolution, was adapted for use (**Figure 2.1b,c**).[91] The device was designed for Day 2 adult animals and consists of 1.5 mm circular chambers connected

by a larger serpentine channel, and allowed for robust, characterized fluid exchange across the population. The microfluidic device coupled with a custom-made pressure-driven food delivery system provided continuous flow to the animals, providing constant exposure to the desired food concentration.

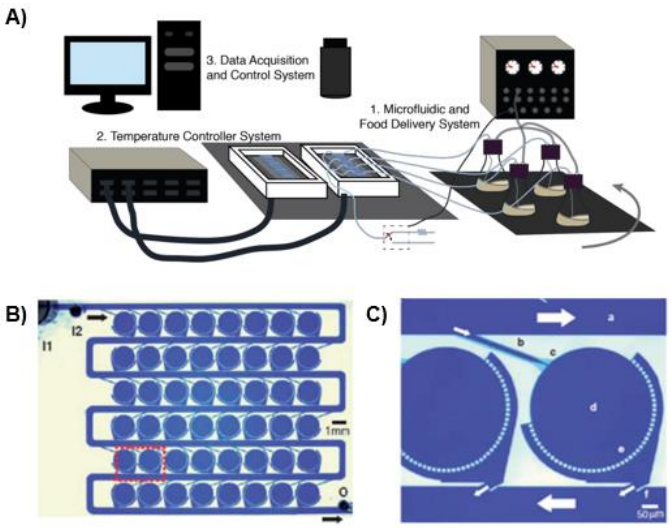

Figure 2.1. Overview of the original platform. A) Main modules of the system. Image credit from Dr. Mei Zhan's thesis.[90] B) Worm chamber array and zoomed-in insert showing the loading channel (b), restriction point (c), culture chamber (d), and small outlet channels (e).[91]

As a proof of concept, an initial trial of experiments was conducted across a variety of genetic and environmental conditions. While the lifespans of the individuals appeared comparable to traditional plate assays under certain conditions, there were indications that the culture resulted in adverse effects for a few of the experimental conditions, resulting in unexpected longevity trends across genotypes and different environmental conditions (**Figure 2.2a,b**). For example, although literature has established *daf-16* as a short-lived strain, in the initial set of experiments its average lifespan surpassed that of the wild-type and was comparable to the *daf-2* population. Additionally, when exposing wild-type worms

to a range of static, thermal conditions (ranging from 15°C to 25°C) the population reared at the 15°C had a significantly shorter lifespan than those reared at warmer temperatures, a trend contradicting known literature.[41,42] In addition, a large subset of data was unable to be analyzed due to poor imaging conditions. For example, the population cultured under $OD_{600}5$ had extremely poor contrast and visibility, making it difficult to accurately quantify and assess its behavioral decline over time (**Figure 2.2c)**. Lastly, these experiments were extremely difficult to perform and lacked robustness. The experiment required constant hourly monitoring throughout the entirety of the experiment to ensure and prevent clogging or contamination in the device. Although the hardware was engineered for scalability, there was a strong need to modify and optimize the platform and experimental culture protocol to improve the throughput and ease of the experiments.

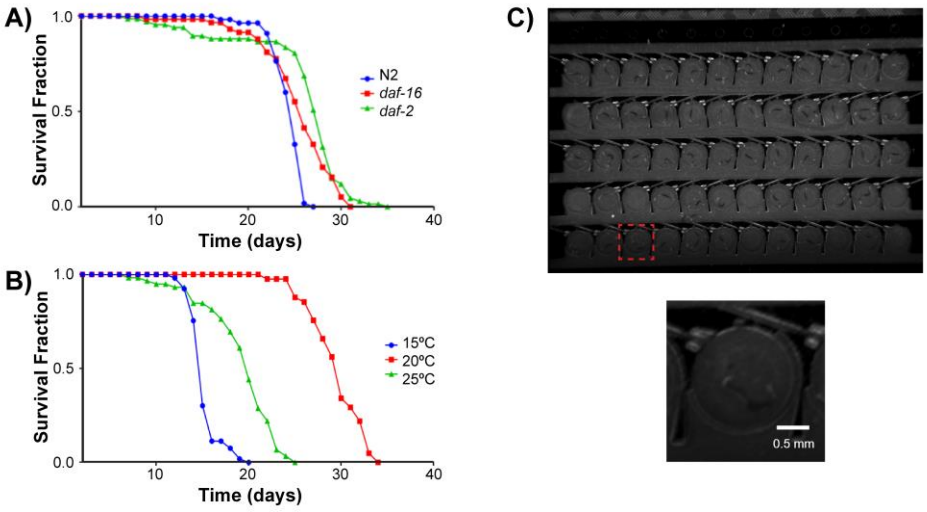

Figure 2.2. Preliminary longevity studies and behavioral recordings. A) Longevity of IIS mutants. B) Longevity of WT individuals under thermal perturbations. C) *(top)* Image of the device, with the red box insert highlighting (*bottom)* the magnified chamber.

2.3 Materials and Methods

2.3.1 C. elegans *culture*

The following strains were used: N2, QL12 *daf-16(mu86)* I, and QL390 *daf-2(e1368)* III. Worms were grown at 20°C and fed live *E. coli* OP50 on agar plates for two generations. The synchronized progeny of the F2 generation was obtained within a six-hour period, grown at 20°C, and fed live *E. coli* OP50 on agar plates until the L4-stage where the worms were either loaded into the microfluidic device or used for manual lifespan assays.

2.3.2 Microfluidic device fabrication

Microfluidic devices were fabricated from PDMS using standard soft lithography techniques and bonded to a glass coverslip using plasma bonding. Devices were sterilized by autoclaving before usage.

2.3.3 E. coli *culture and preparation*

Bacterial culture protocols are similar to previously published protocols.[92] We grew *E. coli* (HB101) overnight in filtered LB at 37°C within a shaking incubator. We then spiked the culture with carbenicillin (50µg/ml) continued culturing for an additional 30 minutes and chilled it at 4°C to inhibit growth. We spun down the cultures at 2400 rcf at 4C for 20 minutes and re-suspended the pelleted bacteria in S Medium with Pluronic F-127 (0.005%), carbenicillin (50µg/ml), and kanamycin (50µg/ml) to prevent the risk of bacterial aggregation and contamination during subsequent culture. Bacterial growth was measured by sampling a five-fold dilution of the culture before centrifugation and measuring the OD_{600} of the sample. The samples were resuspended to concentrations of

OD_{600} 10 and kept at 4°C until use. For DR experiments, the OD_{600} 10 stock was diluted with S Medium with Pluronic, carbenicillin, and kanamycin until reaching the desired concentration.

2.3.4 C. elegans *culture on-chip*

Worms are loaded into the microfluidic device using a two-step pressurized loading process previously developed in our lab.[91] They are then mounted onto a temperature control module and cultured at 20°C in bacterial concentrations of OD_{600} 10 with 5uM C22 on-chip to mitigate any effects DR may have on the developmental process and prevent progeny. When mounting devices on the temperature control module, a thin layer of silicon oil was applied between the silicon surface and the glass coverslip for enhanced thermal conductivity and improved contrast for imaging. At Day 2 of adulthood, worms were then shifted to the desired temperature and food level. Every other day, upstream in-line filters were changed to prevent excessive bacterial accumulation. Every four days, we exchanged upstream and downstream tubing and downstream resistance devices to prevent bacterial accumulation and added new bacteria at the desired concentration with 5uM C22 to the pressurized food source. All filters, tubing, and food source bottles were sterilized by autoclaving before use to prevent potential contamination.

Custom reservoirs filled with the bacteria are pressurized by the pressure box to creating flow through the device. A 0.22um filter is placed between the pressure source and reservoir to reduce the risk of contamination. To prevent accumulation, the bacteria within the pressurized reservoirs is continuously agitated with a stir bar. Additionally, a series of mesh filters are placed between the reservoir and device to prevent any bacteria

aggregates from entering and clogging the microfluidic device. The resistance device downstream of the device and pressure sensor limits the flow rate of the device. We used an average flow rate of approximately 15µL/min across all conditions. Every hour, devices underwent an increased 'pulsed' flow for 5 seconds, with an average flow rate of approximately 275 µL/min, to provide additional mechanical stimulation and to help reduce bacterial accumulation within the upstream tubing.

2.3.5 Manual lifespan assays

Manual lifespan assay protocols are similar to previously published work.[92] 6cm Nematode Growth Medium (NGM) plates were supplemented with 5uM C22 and 50ug/ml carbenicillin to prevent progeny and potential contamination. For the first two days, worms were placed on plates seeded with lawns of HB101 concentrated at OD_{600} 10 and cultured at 20°C. At Day 2 of adulthood worms were transferred to the desired environmental conditions and subsequently transferred regularly to fresh plates until the end of the reproductive period. Worms were gently stimulated with a platinum wire pick every other day to assay for movement; lack of response was scored as death. We performed at least three different biological replicates for each genotype examined in the manual assays. Raw lifespan data for the plate assays are included in **Appendix A.2.1**.

2.3.6 Video acquisition

Videos were taken twice an hour for 10 seconds at an acquisition rate of 14 fps using a 1.3 Megapixel monochrome CMOS camera (Thorlabs DCC1545M camera) coupled with a 10X close focus zoom lens (Edmund #54-363). The magnification was set to allow all chambers to be within the field of view (24 mm x 19.2 mm). Illumination was

provided by a set of concentric red LED rings (Super Bright LEDs 60 and 80mm LED Halo Headlight Accent Lights) to reduce the amount of blue light exposed to the worm. To prevent excessive, strong light exposure to the worm, the LED was on only while viewing devices or during video recordings.

2.3.7 Behavioral analysis

To analyze the generated behavioral recordings, we developed a custom MATLAB code. The user is presented with a background-subtracted frame of the device and selects the center locations of the four corner chambers of the device. The center locations of the chambers within the device are then interpolated and recorded, giving us the region of interest (ROI) for each worm. To account for potential shifts in the device placement over time, we select a static portion of the initial device video – typically a patterned feature in the microfluidic chip separate from the fluid flow path. We then perform image registration using cross-correlation for the patterned feature for each video and translate shifts in the patterned feature to the chamber locations. After extracting the location of each worm, we measure raw movement within the chamber (in the form of the pixel difference across frames in a video) and track this metric as the worms age. Worms are scored as dead if no raw movement is detected after a period of two days. We validated a sample of the lifespan results automatically generated with our code with manual curation of the videos and have found no significant difference between the two conditions **(Appendix A.2.2**).

Due to the large volume and frequency of behavioral recordings, we examined a subset of our data, looking at behavior every 12 hours. For each time point, we sampled a video of worms undergoing a constant flow rate and a video of worms immediately after

experiencing an increased, ‘pulsed’ flow. When examining behavior immediately after switching to 15°C for the thermal oscillatory case, we examined videos every other hour for increased temporal resolution.

A major behavioral characteristic we examined was the duration of high activity movement. To characterize whether the behavior was seen as high or low activity, we performed k-means clustering with two groups using the built-in MATLAB function. The clustering was done within each experimental group.

To examine intrapopulation differences we divided each experimental condition into cohorts based on their lifespan. The shortest-lived cohort consisted of the bottom 20^{th} percentile, while the longest-lived cohort consisted of the top 20^{th} percentile for each experimental condition. Relative behavioral decline within experimental conditions was compared for the shortest and longest-lived cohorts, using the Kolmogorov-Smirnov test; no significant difference was found.

2.3.8 Statistical analysis

For each experimental condition, we performed at least three different biological replicates. Raw lifespan data for each analyzed individual cultured on HeALTH, along with corresponding experimental conditions and trial information, is included in **Appendix A.1**. To identify and characterize the sources of variance across experimental trials we performed a mix-model approach. Similar to previously published work we used GLMs using the *lme4* v.1.12 package in R.[93] We accounted for variance due to different trials, and devices or plates within the trial; however, we did not include variance due to different batches of bacterial food.

Lifespans for both on-chip and plate experiments were analyzed via Kaplan-Meier and significance was calculated with the log-rank test in JMP Pro14. Two-sample Kolmogorov-Smirnov tests were performed in MATLAB (2018b) using a built-in function. Remaining statistical tests (such as one-way ANOVA followed by Tukey's HSD test, Pearson's correlation coefficient) were performed in GraphPad Prism 5.

2.4 Results and Discussion

2.4.1 Engineering the culture system for improved experimental robustness

To address some of the irregularities previously obtained, along with increasing the feasibility of using the system on a large-scale basis, several modifications were introduced. The sections below detail changes made on the system hardware, microfluidic device design, and experimental protocol. These modifications were made to improve the experimental robustness and ease-of-use of the system, increase the amount of gathered behavioral information, and reduce any potential stressors to the individuals, thus resulting in prematurely shortened lifespans.

2.4.1.1 System optimization: Modifications of the microfluidic device

The initial microfluidic device was designed to load and culture worms on Day 2 of adulthood. To extend the period of monitoring and reduce environmental variability early in life the worm chamber array device was adapted to L4 animals, scaling the loading channel dimensions for the smaller sized individuals (**Figure 2.3**). This was non-trivial since the loading channel dimensions need to balance being able to effectively trap and hold a single L4 to ensure single loading, while avoiding extremely small feature sizes that

are easily susceptible to clogging during long-term culture. This dimensional scaling did reduce the loading efficiency of the device (45% compared to 56% singly loaded chambers), since the smaller size of the worm allows for multiple individuals to bypass the restriction channel more easily (**Figure 2.3d**); however, it still is able to effect trap a large number of single individuals within chambers as shown in **Figure 2.3c.**

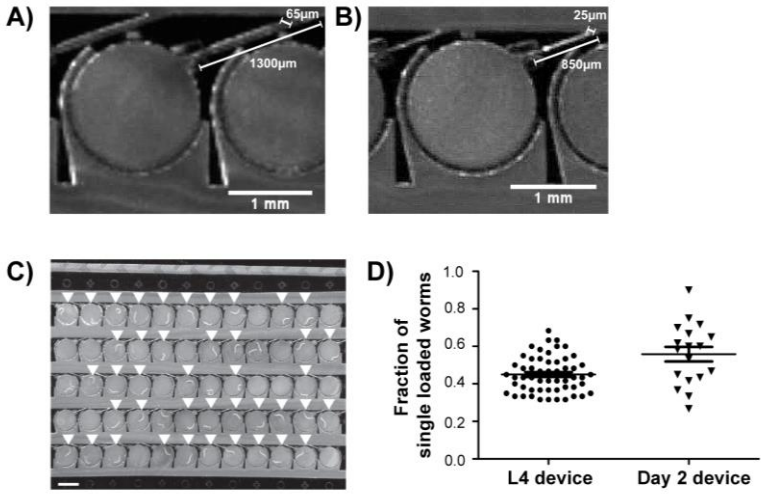

Figure 2.3. Worm chamber array device for L4-stage worms. A) Initial chamber array device sized for Day 2 of adulthood. B) Modified chamber array device sized for loading L4-stage worms. C) L4 sized device loaded with worms. White arrows indicate chambers with single-loaded worms (n = 42 individuals). D) Loading efficiency of single-loaded worms of the L4 device (27 ± 0.76 single individuals, n = 56 devices) and the Day 2 device (33.5 ± 2.31 single individuals, n= 18 devices).

2.4.1.2 System optimization: Modifying the illumination system

Another concern was the extent of light exposure on the worms. Literature has hinted at the damaging effects high levels of light exposure, particularly blue light, have on the health and longevity of *C. elegans*; by constantly exposing them to white LEDs for imaging illumination, it could potentially result in adverse stress and shortened lifespans.[94,95] An additional concern was the constant long-term exposure to visible light

due to the use of a commercially available white LED ring. To mitigate this, the commercial LED ring were replaced with a set of custom concentric red LED rings that were integrated and controlled by the system GUI, with illumination only occurring during recording periods. This minimized light exposure in the blue wavelength, reducing its deleterious impact on longevity.

2.4.1.3 System optimization: The addition of a pressure monitoring system

A major technical hurdle is the difficulty of maintaining long-term culture on-chip throughout the lifespan of the worms. One of the major points of failure in experiments was the frequency of bacterial clogging and accumulation within the device. Over time, accumulation results in the formation of biofilms, blocking the micrometer-scale features of the device and clogging and preventing fluid flow, and causes the premature death of the population cultured within the device. This accumulation can be difficult to catch by eye and would require near constant monitoring to ensure that no significant clog would form within the device, significantly limiting the scale and robustness of the experiment.

Prior published work that flows bacteria within microfluidic devices either 1) uses shorter timescales (on the scale of hours to days) or 2) uses much lower concentration levels to reduce the incidence of accumulation over the period of week.[76,77,79–82] As such, there was no established way of being able to monitor and reduce the rate of bacterial aggregation and clogging in a robust manner. To address this limitation, a clog detection system was created, consisting of miniature pressure sensors that continuously monitor the pressure detected downstream of the device (**Figure 2.4**). Variations and drops in pressure correlate to changes in flow rate indicating the presence of bacterial accumulation or

clogging in the upstream filter. The system provides real-time measurements of the pressure and is fully integrated to the system and user GUI. Drops below a set threshold are reported in real-time to the experimenter via text, alerting the user to either exchange upstream filters or tubing.

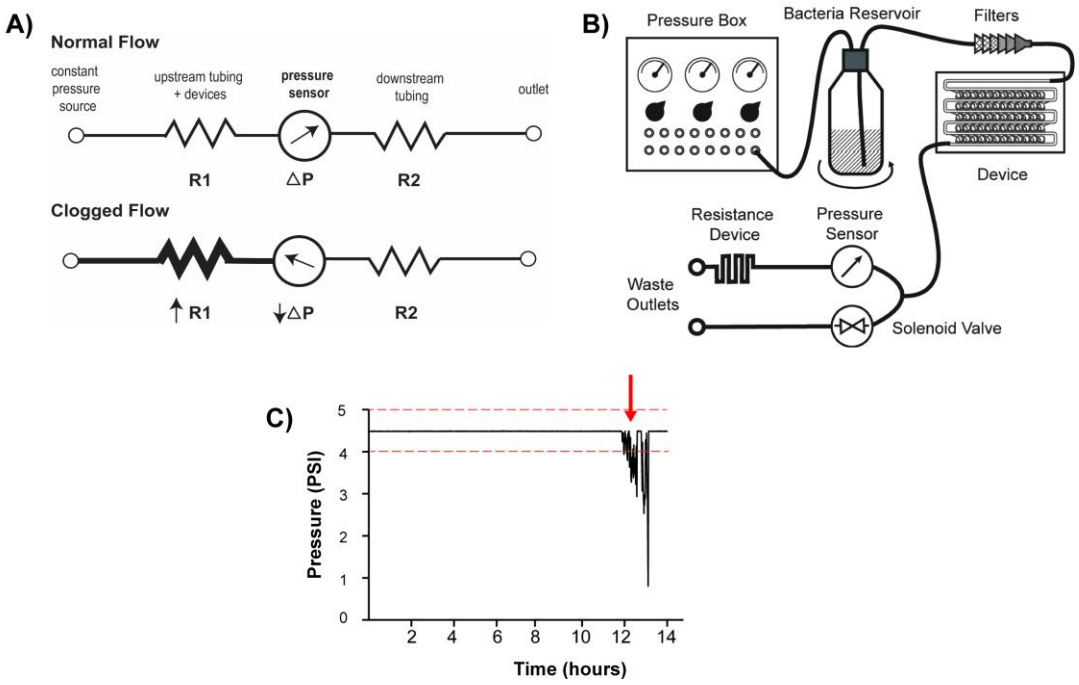

Figure 2.4. Overview of the clog detection system. A) Conceptual diagram of the clog detection system based off the continuous pressure-drive flow. B) Flow diagram of the system and location of the pressure sensor. C) Representative example of monitored pressure over time and the presence of a clog (indicated by the red arrow). Red dashed lines indicate pressure thresholds of when the experimenter is notified by the system for irregularities in flow.

2.4.1.4 Protocol optimization: The use of C22 for progeny prevention

A common method of preventing progeny in aging studies is through the use of 5-fluoro-2'-deoxyuridine (FUdR), which inhibits the germline.[57,60,93,96,97] However, recent studies have indicated that the use of FUdR may have gene-specific effects on lifespan,

hinting at unknown, downstream effects on longevity and increased lifespans.[98,99] To avoid these confounding effects, egg-5(RNAi) was initially used to prevent eggshell formation of the fertilized embryos.[92] Although effective on plate, it was not fully effective in liquid, resulting in the bag of worms phenotype and live progeny within the device. Due to issues with the efficacy of egg-5 RNAi for progeny blocking, we used C22, a small molecule that impairs eggshell integrity leading to embryonic lethality.[100] This drug preserves the reproductive system and fecundity of animals, while preventing the occurrence of viable progeny without any adverse effects on health. It has been shown to be widely applicable across genotypes and environmental conditions.

To verify the efficacy of the drug in our hands, we performed an initial proof of concept trial of progeny preventing using C22 in liquid culture. L4 stage N2 worms were cultured in 48-well plates in OP50 (OD_{600}5), with C22 concentrations of 0, 1.25, 2.5, 5, and 10μM (n = 10 worms per condition). With the exception of the control condition, no progeny was seen across a 72 hour period, and after 240 hours only worms cultured in the 1.25 μM condition contained progeny. This validates the effectiveness of C22 as a method of progeny prevention in microfluidic and liquid environments.

2.4.1.5 Protocol optimization: On-chip bacterial food conditions

Another potential issue is whether the initial culture and behavioral monitoring protocol resulted in inadvertent stress on the developmental stages of individuals, causing increased levels of stress and premature death in certain experimental conditions. For example, the observed bagging phenotypes could indicate stress related to food availability.

To reduce those potential stressors, I aimed to culture the worms in higher concentrations of *E. coli*. Balancing optical visibility, contrast between the worm and bacteria, and the desire to have high bacterial concentration levels, the concentration of $OD_{600}10$ was selected. Being twice the concentration of the highest food level initially examined in the device, it was crucial to ensure that the bacteria would be able to robustly flow for long periods of time without accumulation within the small microfluidic features or clogging within the device. This concern was further exacerbated by the transition to the L4 device, due to the smaller dimension of the loading channel. In addition to the implementation of the clog detection system to HeALTH, the strain of *E. coli* was altered, transition from using OP50 to HB101, commonly used in *C. elegans* liquid culture used for its reduced tendency for aggregation compared to OP50.[101]

2.4.2 HeALTH recapitulates known behavior and longevity trends in IIS mutants

A major challenge when developing long-term culture systems is to preserve known longevity trends across populations and to ensure no adverse effects prematurely shorten the lifespan of the population. To validate the system, we measured the lifespan of a wild-type (N2) population, along with two different insulin/IGF-1 pathway mutants, *daf-2(e1368)* and *daf-16 (mu86)*, which are well-known long- and short-lived mutants respectively. Longevity assays performed in HeALTH are comparable to lifespans done using traditional plate assay, for both wild-type and mutant populations (**Figure 2.5**). Importantly, our platform exhibits similar variability (including trial-to-trial, across devices or plates, and individual variation) across all replicates compared to plate-based trials, indicating similar experimental reproducibility **(Appendix A.2.3, Appendix A.2.4)**.[93] This ability to recapitulate both the average lifespan length and variability in

comparison to plate assays underscores the viability of using HeALTH to perform lifespan studies.

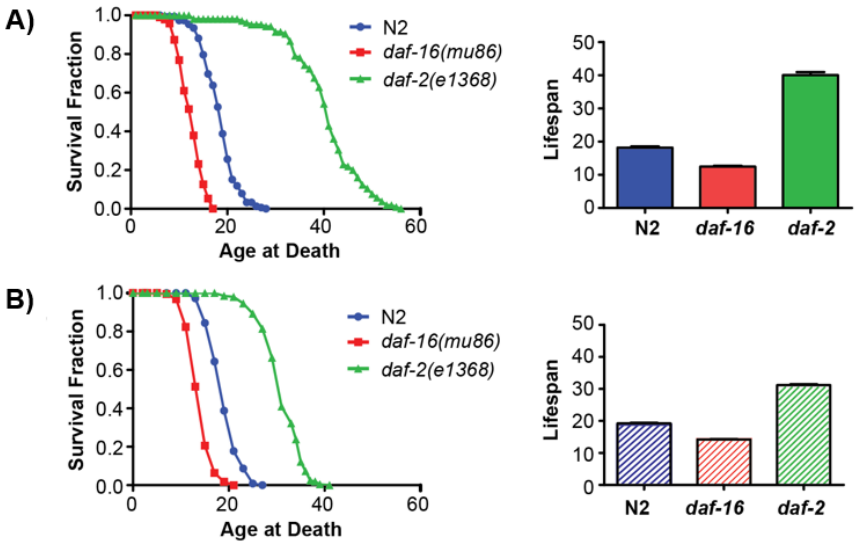

Figure 2.5. Longevity of IIS mutants cultured on HeALTH. A) *(left)* Lifespan curves for wild-type N2 (18.00 ± 0.23, n = 245 individuals), *daf-16(mu86)* (12.49 ± 0.26, n = 95), and *daf-2(e1368)* (40.32 ± 0.74, n = 105) populations cultured on the platform and *(right)* bar graph with the average lifespan for each genotype (error bars are SEM, $p < 0.0001$, via log-rank test). B) *(left)* Lifespan curves and *(right)* bar graph for N2 (19.25 ± 0.21, n = 220), *daf-16* (14.18 ± 0.17, n = 221), and *daf-2* (31.20 ± 0.28, n = 206) for corresponding plate controls (error bars are SEM, $p < 0.0001$, via log-rank test).

Next, we examined how health is impacted during aging by monitoring behavioral decline (**Figure 2.6**). To do so, we examined how raw movement – measured in terms of pixel differences from the first and last frame of the video – changed for each individual across time. Previous literature demonstrated the need to look at evoked behavior as an accurate measure of behavioral decline during aging.[51,60,102] Our microfluidic device provides mechanical stimulus through fluid flow, allowing us to observe how stimulated locomotion changes as individuals age; however, for our environment the mechanical

stimulus resulted in no significant difference in average movement with age (**Appendix A.2.5)**.

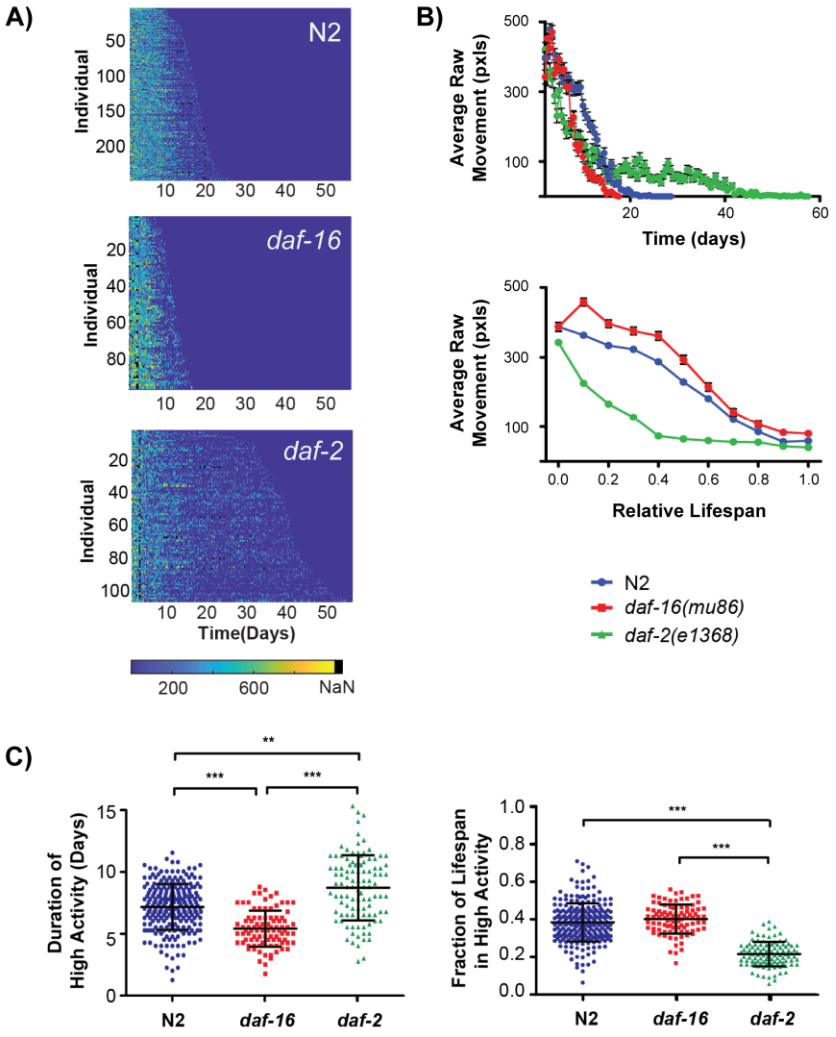

Figure 2.6. Movement decline across IIS mutants. A) Heatmaps showing individual behavioral decline for different behavioral metrics across different genotypes over time. B) (*top)* Population averaged raw movement across mutants (error bars are SEM). (*bottom)* Relative population average activity for raw movement normalized to lifespan across mutants (error bars are SEM). Relative behavioral decline of *daf-2* is statistically significant from the other conditions. (Kolmogorov-Smirnov test, p = 0.0121). c) *(left)* Duration of high activity for raw movement across genotypes and *(right)* relative fraction of life in high activity for raw movement for each genotype (error bars are SD, *** p < 0.0001, via one-way ANOVA followed by Tukey's HSD test. Non-significant differences are not marked).

Similar to previous studies, across all genotypes there appears to be a consistent initial period of frequent 'high activity' movement, followed by a period of sporadic 'low activity' movement until the individual's death.[50,51,60,103] Bouts of consistent movement suggest an initial period of good health for the worm, which may indicate a lack of sarcopenia or cognitive decline. We examined how mutations impact the duration of 'high activity' as a proxy of their health and decline with age. Using the raw movement metric, we quantified the duration and relative time (normalized to each individual's lifespan) of the high activity period across all genotypes (**Figure 2.6c**)**.** Average duration of high activity correlated with the average lifespan for each genotype. When normalized by lifespan, both N2 and *daf-16* spend equivalent proportions of their life in the high activity period. However, the *daf-2* mutant spends a significantly lower proportion of its life in the high activity period than the wild-type animals ($p < 0.0001$, one-way ANOVA followed by Tukey's HSD test), likely due to increased *odr-10* expression resulting in preference for food over exploration and movement.[51] Thus, we show that our system recapitulates known behavioral trends on an individual-level with high temporal resolution.

2.4.3 Effects of DR on longevity and behavior

We next asked how environmental perturbations influence behavioral decline during the aging process. While dietary restriction has been shown to significantly alter aging in *C. elegans*, the interpretation of experimental results can be complex, as it can be difficult to perform precisely controlled DR experiments using conventional closed-culture systems due to depleting food levels over time. To prevent this variability in food levels,

we take advantage of the ability of microfluidics to deliver a constant perfusion of bacteria, allowing for precisely controlled food levels over time. To maintain the steady flow of bacteria over long periods of time without the formation of biofilms or bacterial aggregation on the small features of the device, we use our pressure monitoring system, allowing us to culture worms in concentrations up to OD_{600} of 10 (OD 10).

We examined the effects of DR on both the lifespan and healthspan of worms. Unsurprisingly we see a significant decrease in lifespan for worms cultured at OD 10 compared to those at the lower concentration levels ($p < 0.0001$, log-rank, **Figure 2.7**). The behavior over time was also impacted by DR (**Figure 2.8**). The population average of raw movement across the three food levels had similar decline rates later in life; however, their initial level of movement differed, with worms in higher food concentrations having lower amounts of movement (**Figure 2.8a,b**). This early difference may be attributed to food searching behavior, with worms in DR having increased movement to search for areas with higher food concentrations. The duration and normalized period of high activity movement increases with decreased food concentration (**Figure 2.8c**), with animals at OD 10 having a significantly lower duration of movement, suggesting a shorter healthspan ($p < 0.0001$, one-way ANOVA followed by Tukey's HSD test) compared to either OD 5 or OD 2.5 populations.

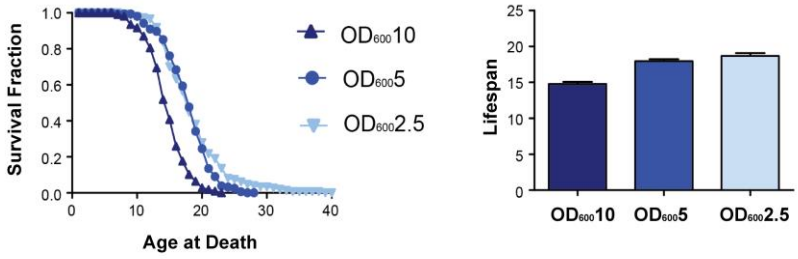

Figure 2.7. Longevity across different food levels. *(left)* Lifespan curves for wild-type N2 populations cultured at food levels of $OD_{600}2.5$ (18.67 ± 0.40, n=147 individuals), $OD_{600}5$ (18.00 ± 0.23, n=245), and $OD_{600}10$ (14.78 ± 0.29, n=108). *(right)* Bar graph of average lifespan at different food levels ($OD_{600}10$, $OD_{600}5$, and $OD_{600}2.5$) (error bars show SEM, $OD_{600}10$ v. $OD_{600}5$/ $OD_{600}2.5$: $p < 0.0001$, log-rank test. $OD_{600}5$ v. $OD_{600}2.5$: $p = 0.0854$, log-rank test).

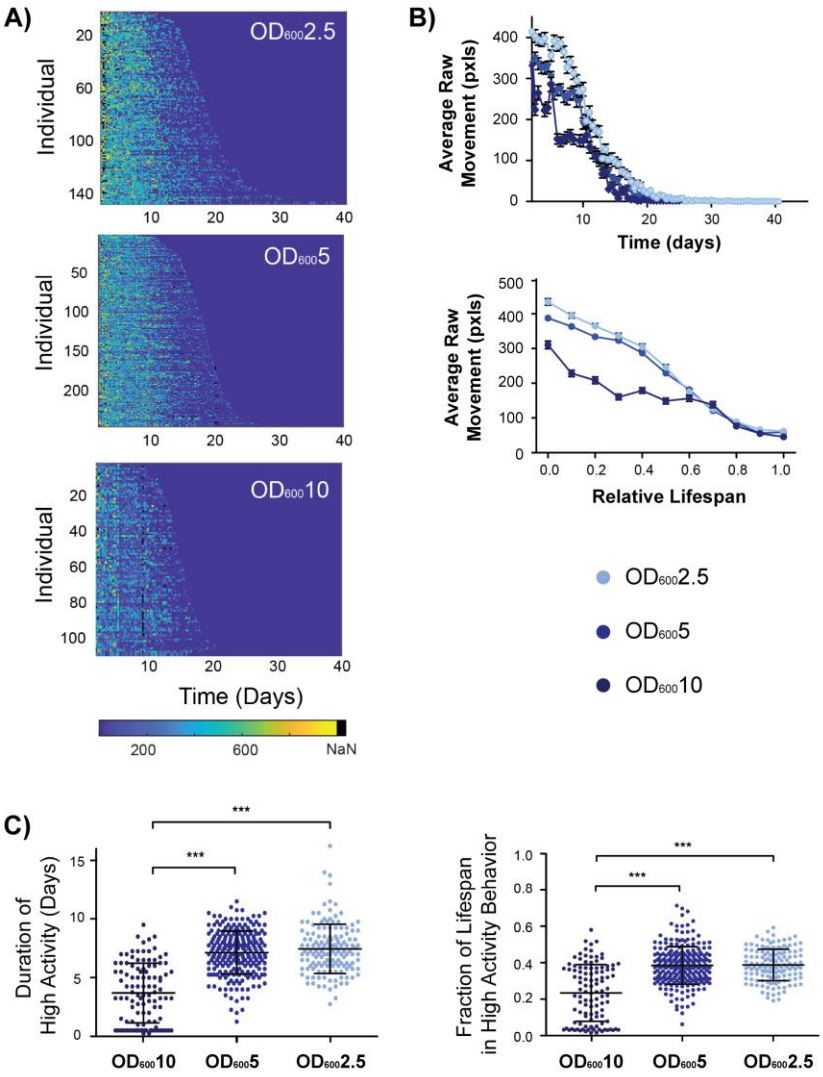

Figure 2.8. Movement decline across different food levels. A) Heatmaps showing individual decline in raw movement across food levels over time. B) (*top)* Population averaged raw movement for the food conditions (error bars are SEM). (*bottom)* Relative population average activity for raw movement normalized to lifespan across food conditions (error bars are SEM). C) *(left)* Duration of high activity for raw movement across food levels (*right)* Relative fraction of life in high activity for raw movement across food levels. (Error bars are SD, *** $p < 0.0001$, via one-way ANOVA followed by Tukey's HSD test. Non-significant differences are not marked).

2.4.4 Effects of thermal perturbations on longevity and behavior

Given that *C. elegans* is a poikilotherm and our system can easily vary temperature, we examined the effects of thermal fluctuations on aging. We took inspiration from the natural diurnal temperature cycle *C. elegans* experience in the wild and explored whether dynamic thermal cycling influences their lifespan and healthspan. We measured the lifespan of worms that were switched every 12 hours between 15°C and 20°C, along with worms cultured at constant temperatures (15°C, 17.5°C, and 20°C) (**Figure 2.9**). Average lifespan decreases with increased temperature under static conditions, following known trends.[41,42] Animals undergoing temperature oscillations had an average lifespan similar to worms reared at 20°C, showing no beneficial extension in lifespan from their time at 15°C. However, the range of lifespans under the cycling condition was much larger than that of animals reared at the static 20°C condition, hinting that variability in temperature contributes to the variability in longevity within a population.

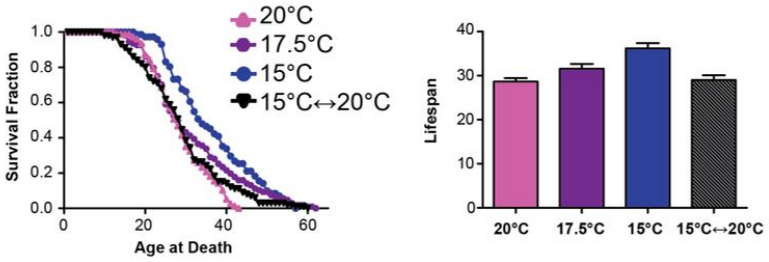

Figure 2.9. Longevity across thermal perturbations. (*left)* Lifespan curves for wild-type cultured at constant 15°C (36.21 ± 1.19, n = 71), 17.5°C (31.60 ± 1.09, n = 107), and 20°C (28.65 ± 0.80, n = 77), and population under oscillatory temperature conditions, changing from 15°C to 20°C every 12 hours (29.10 ± 1.04, n= 99). (*right)* Bar graph of average lifespan for worms cultured at static 20°C, 17.5°C, 15°C, and an oscillatory condition that switched from 15°C to 20°C every 12 hours. (Error bars show SEM. 20°C v. 17.5°C p = 0.0094. 20°C v. 15°C p < 0.001, 20°C v. 15°C↔ 20°C p = 0.2082. 17.5°C v. 15°C p = 0.0574, 17.5°C v. 15°C↔ 20°C p = 0.1371, 15°C v. 15°C↔ 20°C p = 0.0004 via log-rank test).

When examining behavior across the constant temperature conditions, all populations appeared to have a high level of activity for approximately half of their lifespan followed by a period of decline (**Figure 2.10a,b**). Populations at lower temperatures had a slight increase in the duration of high activity movement. However, when normalized by lifespan, the proportion of time spent in the high activity period is not significantly different across conditions (**Figure 2.10c**). This suggests temperature has a similar scaling effect on both the period of high activity behavior and lifespan.

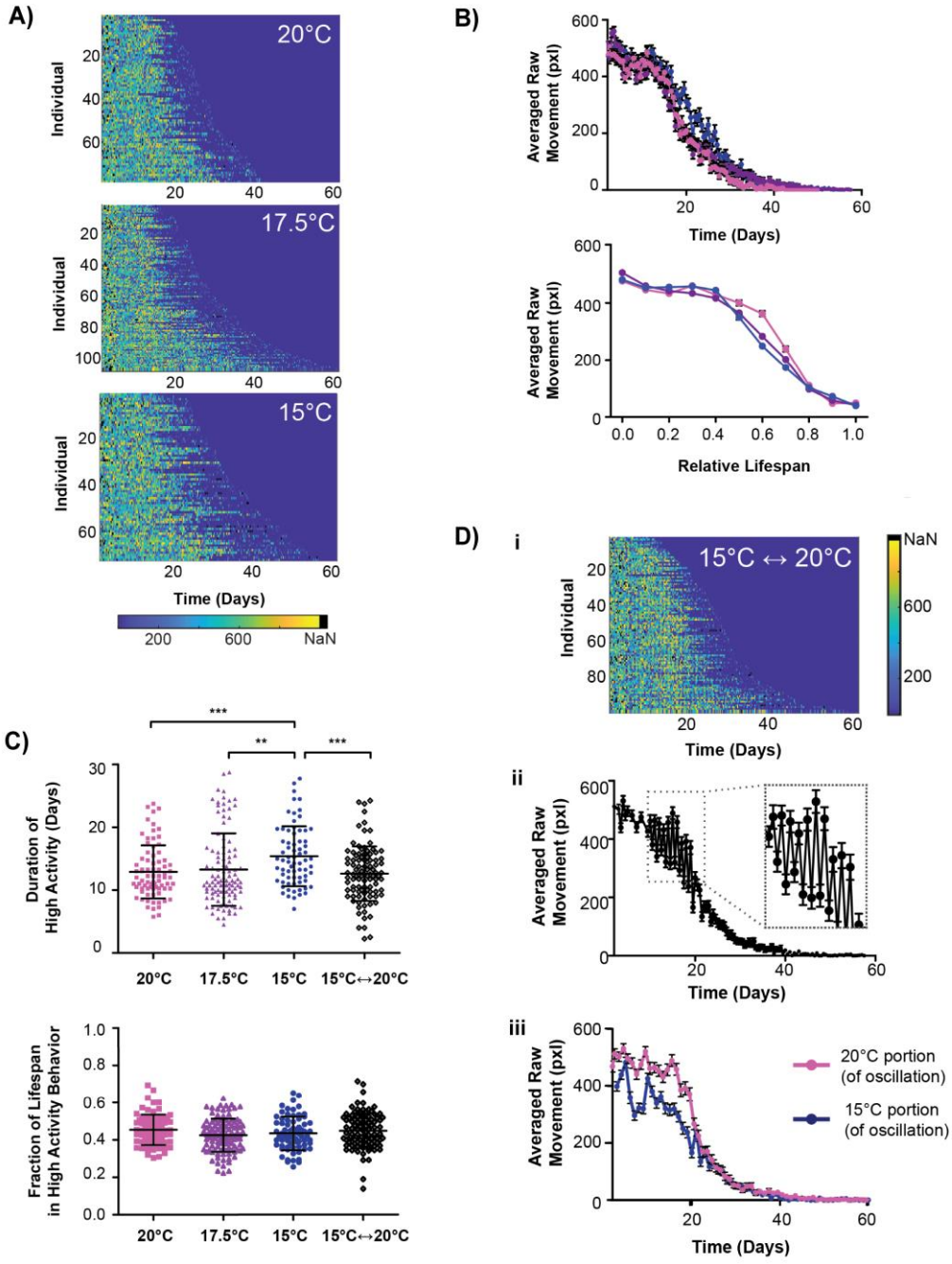

Figure 2.10. Movement decline across thermal perturbations. A) Heatmaps showing individual decline in raw movement across static temperature conditions over time. B) (*top)* Population averaged raw movement for the static temperature conditions (error bars are SEM). (*bottom)* Relative population average activity for raw movement normalized to lifespan across static temperature conditions (error bars are SEM). C) *(top)* Duration of high activity for raw movement across temperatures (error bars are SD, *** $p < 0.0001$, via one-way ANOVA followed by Tukey's HSD test) (*bottom)* Relative fraction of life in

high activity for raw movement across temperature conditions (error bars are SD). No statistically significant difference from each other ($p > 0.0001$, via one-way ANOVA followed by Tukey's HSD test. Non-significant differences are not marked). D) *(i)* Heatmap showing individual decline in raw movement across oscillatory temperature condition over time. (*ii)* Population averaged raw movement activity for the oscillatory temperature condition (error bars are SEM). (*iii*) Average raw movement in oscillatory condition separated by temperature the population was experiencing at the time (error bars are SEM).

Mirroring the trends in lifespan, the population undergoing temperature oscillations had the duration and fraction of life in high activity behavior similar to that of the static 20°C condition (**Figure 2.10c)**. However, when examining averaged raw movement we observed large fluctuations in average activity (**Figure 2.10d**), with the magnitude of movement corresponding to the temperature at the time (**Figure 2.10dii**). Interestingly, under oscillatory conditions, the average movement at 15°C was reduced compared to movement across all other thermal conditions, including the static 15°C control (**Figure 2.10diii).** Due to the ability of our system to obtain frequent behavioral recordings, we were able to subsample a portion of the population with greater temporal resolution and observed a dramatic decrease in movement immediately after the temperature downshift (**Appendix A.2.5**). Over the course of the 12-hour cyclical period there was a steady increase in the average movement approaching the levels observed during the static 15°C control. Literature has demonstrated the presence of noxious cold receptors in *C. elegans* with an activation threshold around 18°C.[104] The drastic decrease in movement could be an initial noxious response to the 15°C transition, with subsequent increases in movement indicating eventual habituation to the colder thermal condition. This response to downshifted temperatures illustrates interesting activity that would otherwise be difficult to obtain with existing methods.

2.4.5 Intrapopulation differences and variability in movement decline

In addition to examining population trends, we examined the effects of variability on aging in an isogenic population. Similar to previous work, we are able to compare behavioral decline across the shortest- and longest-lived cohorts within a population and demonstrate different decline patterns across cohorts (**Figure 2.11, Appendix A.2.6)**.[59,60] As previously reported, the shortest-lived cohort generally exhibited higher levels of activity throughout its relative lifespan compared to the long-lived cohort across all genetic or environmental perturbations. Across thermal conditions, all individuals had similar average decline patterns **(Appendix A.2.6).** Food concentration appears to have a role in the variability of a population's behavioral decline. Shorter-lived cohorts experience higher levels of activity later in life; interestingly, higher food concentrations appear to reduce the differences in decline between the two subpopulations, with little apparent difference between the cohorts (**Figure 2.11a,c**).

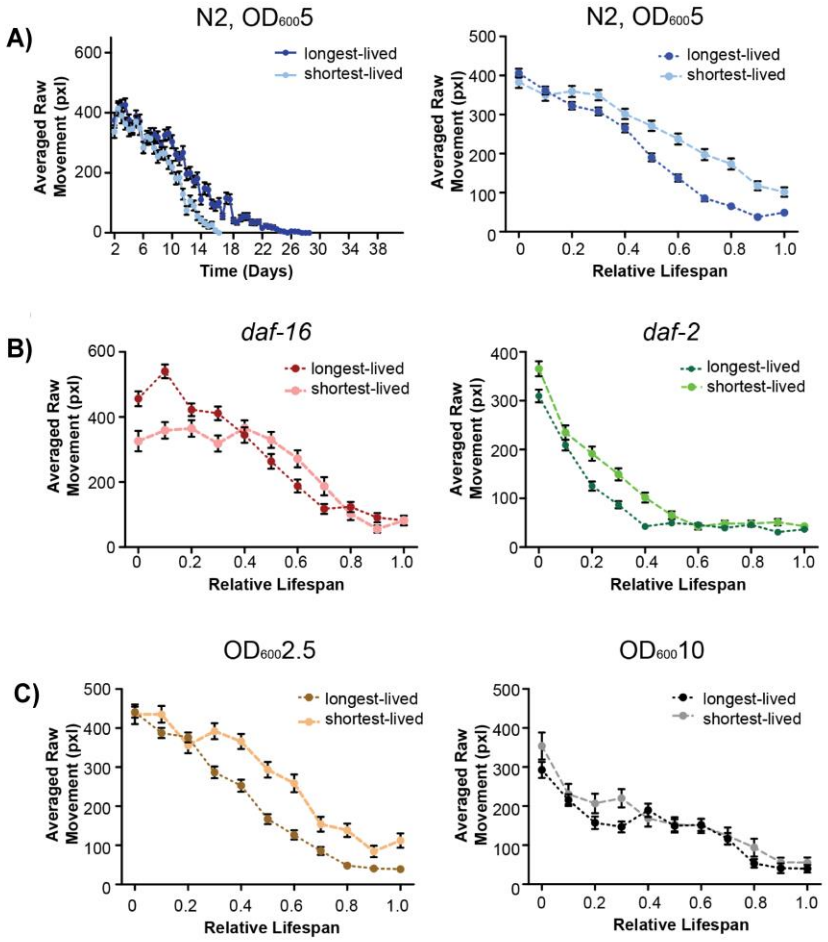

Figure 2.11. Intrapopulation variation across genetic and environmental perturbations. A) (*left)* Averaged raw movement over time of the short- (n = 62 individuals) and long-lived (n = 55 individuals) subpopulations within the wild-type population culture at 25°C at $OD_{600}5$ food level (error bars are SEM). (*right)* Averaged raw movement over normalized relative lifespan of short- and long-lived WT populations cultured at 25°C at $OD_{600}5$ food level (error bars are SEM). B) Averaged raw movement over the normalized, relative lifespan of the short- and long-lived subpopulations across different genotypes at 25°C at $OD_{600}5$ food level. *(left) daf-16* short- (n = 23 individuals) and long-lived (n = 21 individuals) subpopulations. *(right) daf-2* short- (n = 22 individuals) and long-lived (n = 23 individuals) subpopulations (error bars are SEM). C) Averaged raw movement over the normalized, relative lifespan of the short- and long-lived subpopulations across wild-type populations at 25°C across different food levels. *(left)* $OD_{600}2.5$ short- (n = 45 individuals) and long-lived (n = 37 individuals) subpopulations. *(right)* $OD_{600}10$ short- (n = 22 individuals) and long-lived (n = 26 individuals) subpopulations (error bars are SEM).

In addition to examining averaged decline within subpopulations, our system enables us to directly track an individual's behavior throughout its relative lifespan. To easily compare individuals throughout their lifespan we performed dimensional reduction, projecting every individual's relative behavioral trajectory into a shared principal component space (**Figure 2.12, Appendix A.2.7, Appendix A.2.8)**. We directly compare an individual's relative behavioral decline across not only the same population, but also with individuals under different genetic or environmental perturbations. On a population-level, we see how certain perturbations, such as *daf-2* mutation or high food conditions (OD 10), appear to shift in phenospace, indicating a distinct effect on behavioral decline in comparison to other genetic mutations (*daf-16*) or thermal perturbations. With HeALTH's ability to perform individual behavioral tracking and monitoring, we can observe the spread of the population and examine whether certain perturbations result in increased biological noise for relative behavioral decline. For example, temperature has a more variable behavioral space within the population, indicating increased variability in decline. Furthermore, we can examine the separation between subpopulations (i.e. the short- and long-lived cohorts) and how it varies across perturbations, giving us insight into how stereotyped relative behavioral decline is within a population (**Appendix A.2.8)**. For example, *daf-2* shortest- and longest-lived cohorts were separated largely by the first principal component (PC), while *daf-16* relied on the second PC to distinguish between differently aged cohorts. In contrast, wild-type used a combination of the two PCs to separate the sub-populations.

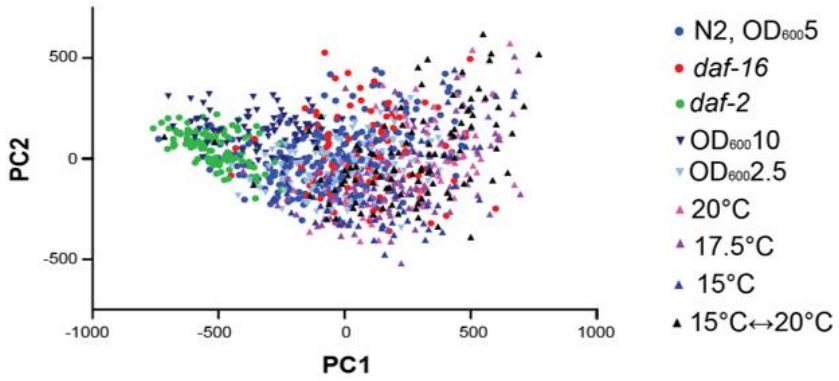

Figure 2.12. Comparing individuals across genetic and environmental perturbations. All individuals (n = 981 individuals) plotted in a shared principal component space.

2.5 Conclusions

In **Chapter 2** I developed HeALTH, which allows for automated and robust longitudinal culture of *C. elegans* throughout their lifespan under precise spatiotemporal environmental conditions. The system's inherent modularity and flexibility can accommodate a variety of experimental conditions. It could easily be adapted to monitor different microfluidic devices or environmental perturbations. Furthermore, the overall cost and physical footprint makes it feasible to create replicates of the system and expand experimental capacity without dramatically increasing space or large equipment requirements. As a result, it could be used for a wide array of high-throughput aging and longevity studies, providing high-content behavioral data with fine spatial and temporal resolution.

We demonstrated the power and versatility of HeALTH by examining both population-level and individual decline across different genotypes and environmental perturbations. Controlled, diurnal temperature shifts resulted in a wider range of lifespans, suggesting at the potential of increased variability caused by environmental perturbations.

DR altered the level of activity and relative behavioral decline across populations in a non-linear way. Furthermore, the decreased lifespan at higher bacterial concentrations (OD 10) raises the possibility that existing microfluidic lifespan devices inadvertently enact some form of DR or hormetic stress on their cultured populations, due to the lower bacterial concentrations used by these systems on-chip. This in turn could potentially result in confounding effects on longevity. Both environmental conditions would be extremely difficult, if not impossible, to study on a large-scale with existing methods, but can be performed using HeALTH.

The inherent modularity and flexibility of HeALTH can enable a variety of different assays to examine different facets of the aging process. Due to the liquid culture environment, our system could explore the effects pheromone concentration on behavior and aging. We could also examine the effects of intermittent fasting, perform drug screens, or examine the effect of stressors (such as heat shock, oxidative stress, or osmotic stress). The system may also be applied to behavioral neuroscience, examining how sensory response and cognitive aging change over time. HeALTH could be expanded for any behavioral study that requires precise environmental control with longitudinal tracking. For example, it could be used for immunology or toxicology applications to examine the impact of pathogens or different microbiome interactions at the whole organism scale. By simply rescaling the microfluidic device, this system could be directly used for a variety of small model organisms for similar applications. Thus, this platform could be easily adaptable and extendable to a variety of different behavioral assays and aging studies, providing insights into behavior changes influenced by any genetic, environmental, or stochastic perturbations over time.

CHAPTER 3. DEEP LEARNING FOR THE FLEXIBLE ANALYSIS OF *C. ELEGANS* BEHAVIOR IN HETERGENOUS ENVIRONMENTS

Portions of this chapter are adapted from a research article entitled "Deep learning for robust and flexible tracking in behavioral studies for *C. elegans*", in principle accepted to PLOS Computational Biology on October 13, 2021 (https://doi.org/10.1101/2021.02.08.430359).[105] This article was co-authored in collaboration with Dr. Kathleen Bates.

3.1 Introduction

In this chapter, I discuss the development of a deep-learning based analysis pipeline that allows for the robust and scalable segmentation and pose extraction of individual *C. elegans* in complex, heterogenous environments. I detail the steps of the pipeline, along with the corresponding characterization and validation of its performance. In parallel, I also display alternative applications for portions of this pipeline, highlighting the ability for object detection to be used as a quick and accurate alternative for commonly used behavioral metrics of interest.

3.2 Background

Ethology has been crucial in the fields of neuroscience, genetics, and aging.[106–109] This rings true even in the simplified *C. elegans* model, which has been used to probe a variety of ethological questions.[110–115] In these experiments, it is extremely valuable to

robustly and accurately measure the behavior of *C. elegans* on a large scale. While technological advancements have enhanced the capability to collect large and complex behavioral datasets relevant to neuroscience and aging, the increase in the quantity of recordings and data shifts the scientific bottleneck to the analysis of large-scale image datasets. Traditional methods reliant on manual annotation are infeasible and impractical to perform on a large scale. Thus, there is a substantial need for methodologies to address this technical limitation.

One of the major challenges in analyzing behavioral data is the detection and subsequent segmentation of the object of interest, particularly across a variety of imaging and experimental conditions. There are a variety of existing image processing tools and software designed to aid in the automated segmentation of objects of interest.[83–85,116–118] Many rely on basic image processing methods, such as background subtraction, thresholding based on the color or intensity of the object, or the use of morphological operations or features, to detect and identify the object of interest.[83–85,87,118] For example, in the popular worm tracker Tierpsy Tracker, users manually optimize parameters based on experimental conditions and are subsequently able to extract behavioral data from their dataset.[83] With these existing segmentation and tracking tools, users can extract a variety of informative behavioral phenotypes, such as size, speed of movement, and the posture of individuals.

However, with the advent of more complex experimental setups that introduce more heterogeneous experimental or environmental conditions, it is not straightforward to adapt these methods to robustly and accurately detect objects of interest (**Figure 3.1**). In conditions with low or uneven imaging contrast, basic thresholding based on intensity

values may not be accurate. If animals or the objects of interest display slight movement, or if there are alternative moving objects in the frame, background subtraction cannot be used to easily differentiate between the object of interest and the background of the image. Even with advanced tools, which rely on machine learning for more accurate predictions, these challenges still require a large accurate initial training set, making it difficult to resolve complex postures (**Figure 3.1**). Additionally, if there is a wide range in morphological properties, such as the dramatic size change of animals during development, it is difficult to rely on morphological features such as size as a method of identifying objects of interest. Coupled with the increased scale of behavioral datasets,[119] there is a need for a robust, flexible, and facile method to detect and identify worms that would be able to work across a variety of different experimental conditions.

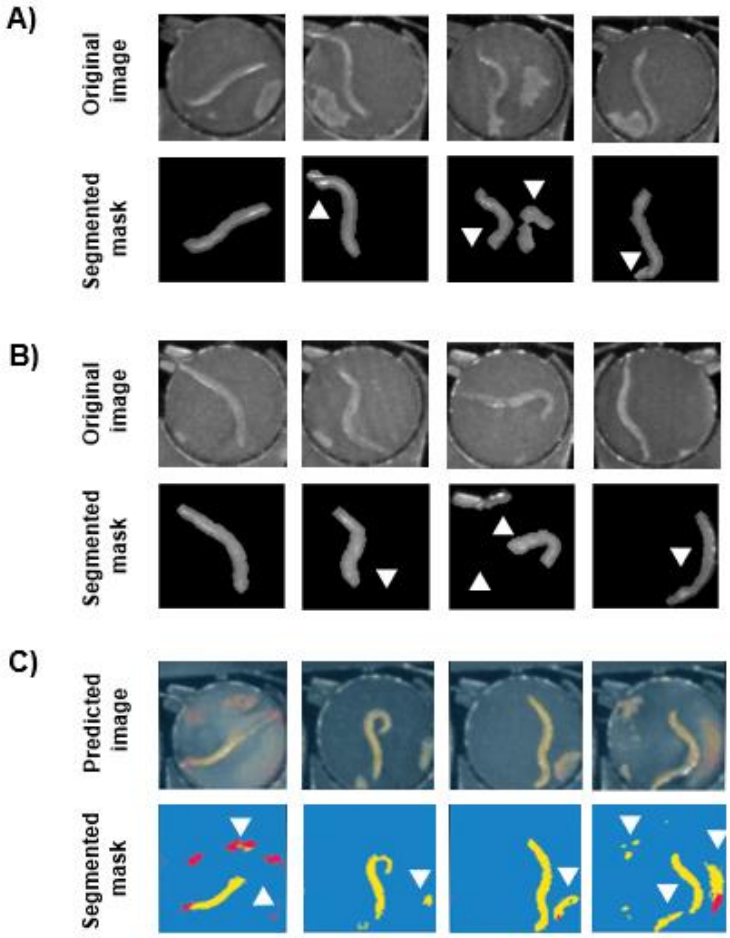

Figure 3.1. Existing techniques for segmentation are unable to be easily generalized across behavioral recordings. A) Detection of a young worm using Tierpsy Tracker.[83] Parameters were tuned for a video, with a representative frame shown on the left. The three other frames are detections of worms of the same age and contrast conditions using the tuned parameters. Detection errors are marked by white arrows. B) Detection of old, slow moving worms using Tierpsy Tracker.[83] Segmentation parameters were tuned for a video, with a representative frame shown on the left. The three other frames are detections of worms of the same age and contrast conditions using the tuned parameters. Detection errors are marked by white arrows. C) Representative example frames of issues with segmentation using Ilastik across similar videos.[117] All frames were taken under the same imaging condition. *(top)* Prediction of pixel classification using the trained model. The model was trained with at least 50 images prior. Blue denotes background, yellow marks the worm, and red marks the egg objects. *(bottom)* Segmentation of objects based on the predictions. Note the truncation of worms and the misclassification of eggs as worms.

3.3 Materials and Methods

3.3.1 C. elegans culture

The strain used in this work was N2. Synchronized L4-stage wildtype animals were loaded into a worm chamber array microfluidic device described in **Chapter 2**. Worms were cultured at 20°C in *E. coli* (HB101) spiked with Pluronic F-127 (0.005%), carbenicillin (50µg/ml), and kanamycin (50µg/ml) to prevent the risk of bacterial aggregation and contamination during long-term culture. The bacteria also contained 5uM of C22. At Day 2 of adulthood, worms were then shifted to 25°C and to the desired food level. Individuals were maintained at OD_{600} 10 unless otherwise stated. See **Chapter 2** for more details.

3.3.2 Behavioral recordings

Recordings were taken under the same imaging conditions as detailed in **Chapter 2**. In brief, videos were taken at an acquisition rate of 14 fps using a CMOS camera coupled with a 10X close focus zoom lens. The videos were 1280 x 1024 pixels. Illumination was provided by a set of concentric red LED rings. Videos were sampled evenly throughout the lifespan of individuals in food levels of OD_{600}10 and OD_{600}2.5.

3.3.3 Model training

3.3.3.1 Mask R-CNN model training

Due to the high performance of existing Mask R-CNN models, we used an existing pre-trained model on the COCO 2017 dataset

('mask_rcnn_inception_resnet_v2_1024x1024') and tuned the model using the behavioral dataset of interest. We manually annotated 113 frames of worms and, if present, eggs using the Labelme Python package. Images were randomly split into training and testing sets using a rough 90/10 split (99 images for training, 14 test images). The model was trained using TensorFlow GPU (v 2) on a system with an Intel(R) Xeon(R) CPU E5-1620 v4 processor and a NVIDIA Quadro M4000 GPU.

3.3.3.2 Faster R-CNN model training

Due to the high performance of existing Faster R-CNN models, we used an existing pre-trained model on the COCO dataset ('Faster_rcnn_inception_v2' model from the TensorFlow 1 model zoo) and tuned the model using the behavioral dataset of interest. We manually annotated 5,176 frames of worms and, if present, eggs using the labelImg Python package. Images were randomly split into training and testing sets using a rough 90/10 split (4658 images for training, 518 test images). The model was trained using TensorFlow GPU (v 1.14) on a system with an Intel(R) Xeon(R) CPU E5-1620 v4 processor and a NVIDIA Quadro M4000 GPU.

3.3.4 Model characterization

The performance of the Mask R-CNN and Faster R-CNN models were evaluated by using average precision (AP) and average recall (AR). These are standard detection metrics used by the Microsoft Common Objects in Context (MS COCO) Object Detection Challenge, which is the benchmark set of images used to characterized the performance of deep learning algorithms.[120]

To determine whether detections by the models were true positives (TP), false positives (FP), or false negatives (FN), we used a measure of the overlap of detections and ground truth known as intersection over union (IoU).

$$IoU = \frac{|GT \cap P|}{|GT \cup P|} \tag{1}$$

GT (ground truth) is the annotated mask or bounding box of the ground truth and P is the annotated mask or bounding box of the prediction. An IoU greater than or equal to the IoU threshold is categorized as a TP and an IoU less than the IoU threshold as a FP for the detections. From these scores, we were able to calculate the precision and recall across the set of evaluated images using the equations below.

$$precision = \frac{TP}{TP + FP} \tag{2}$$

$$recall = \frac{TP}{TP + FN} \tag{3}$$

Precision is a measure of the false positive rate, while recall is a measure of the false negative rate. The precision and recall values were evaluated across a range of confidence thresholds (the probability the predicted object is present in the detected area as predicted by the model), which is summarized in precision-recall curves (**Appendix B.1**). The AP is the integral of the precision-recall curve, capturing the average precision across the recall values. Higher AP values indicate higher accuracy in detection. The AP was evaluated across a range of IoU threshold values (from 0.5 to 0.9) with the mean average precision (mAP) being an average of the AP values. In addition to the precision-

recall curves, we also examined recall-IoU curves, which plots the recall of the model across a range of IoU thresholds (ranging from 0.5 to 1.0) and captures the detection effectiveness. This curve can be summarized through AR, which is the recall averaged over all the IoU thresholds.

3.3.5 Evaluating movement decline in aging

To obtain the ground truth of how movement declines with age, we measured raw movement across frames. Unlike prior measurements, in where we computed the pixel difference across the entire frame, we hand annotated images of worms using Ilastik and examined the difference across the segmented bodies. The equation below was used to calculate the pixel differences across worms with age.

$$pixel\ difference = \frac{\sum|img1 - img2|}{(img1 + img2)/2} \tag{4}$$

Where img1 was the initial segmented frame of the video and img2 was the final segmented frame of the video. To gauge movement decline using the bounding boxes, we examined the IoU across the boxes, which were calculated using the built-in MATLAB function bboxOverlapRatio. The 1-IoU metric was found by looking at the overlap between the bounding box found in the first frame and the bounding box found in the last frame of the video.

3.3.6 WormPose model training

The WormPose convolutional neural network (CNN) model was trained on 500,000 synthetic images with a batch size of 128 and evaluated on 10,000 real

preprocessed images. The synthetic images were generated from 335,239 frames taken from 31 different individuals, from Day 2 to 13 of adulthood, capturing the reproductive period of the worm. Representative synthetic images are shown in **Appendix B.2** alongside the frames inputted into the model for reference. The model was trained for 75 epochs. This was done using TensorFlow GPU (v 1.14) on a system with an Intel(R) Xeon(R) CPU E5-1620 v4 processor and a NVIDIA Quadro M4000 GPU.

3.4 Results and Discussion

To address the limitations of previous methods it was crucial to develop an algorithm that was able to extract out features of interest across complex conditions - throughout a range of sizes, contrast levels, and regardless of the presence of other confounding objects - while being scalable for datasets on the order of terabytes.

To develop this pipeline, we focused on a specific dataset which captures all of these complexities – behavioral recordings of worms cultured on the HeALTH platform from the L4-stage to death. The pipeline consists of four stages: 1) preprocessing, 2) segmentation, 3) postural extraction, and 4) tracking the orientation of the worm and post-processing to mitigate potential errors from the prior stages (**Figure 3.2**). The following sections detail the design and characterization of these stages.

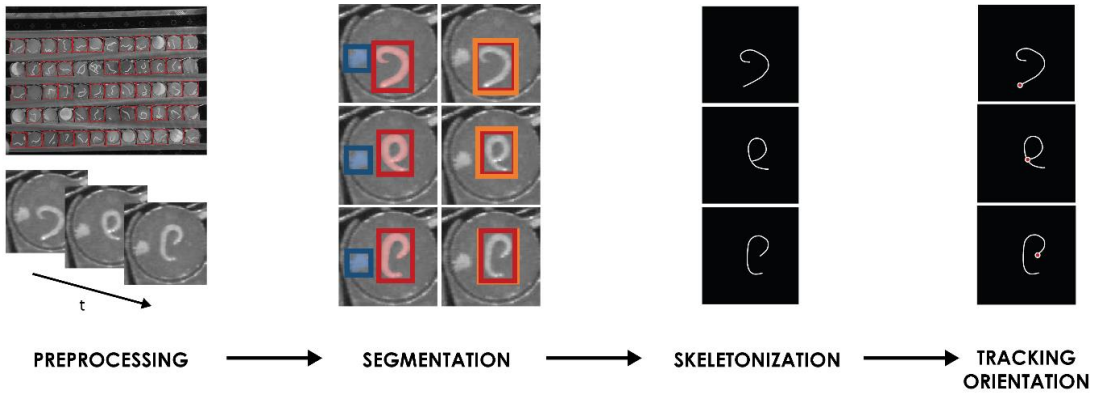

Figure 3.2. Overview of the deep learning analysis pipeline.

3.4.1 Video preprocessing

A major objective of this pipeline is to be scalable for large behavioral datasets. Oftentimes, a large portion of the area recorded for behavioral studies is not of interest, with no individuals present in the region. This area offers no behavioral information while increasing the size of the recording file, thereby increasing the computational time and difficulty in file handling. To reduce file size and ease file handling, the pipeline finds and crops regions of interest within the ROI to separate video files.

Using a custom MALAB code, the user is presented with a background-subtracted frame of the device and selects the center locations of the four corner chambers of the device, along with the specific chambers of interest containing isolated worms. The center locations of all the chambers within the device are then interpolated and recorded. Potential shifts in the device placement over time were measured and adjusted with image registration using cross-correlation for a static patterned feature for each video, similar to what was described in **Chapter 2**. The modified ROIs for each worm of interest in each behavioral recording were cropped and saved as an independent file. This preprocessing

step downsizes a 2GB video (with an ROI of 1280 x 1024 pixels) to 60 7MB videos (with ROIs of 91 x 91 pixels), an almost 5x reduction in file size. This step is personalized to this particular dataset; however, this concept can easily be generalized to other videos of interest.

3.4.2 Image segmentation via deep learning

As previously mentioned, traditional image processing techniques for segmenting frames require user-defined parameters. For more complex datasets with heterogeneity in the contrast levels, intensity values, size of the object of interest, and conflicting objects within the field of view with similar intensity values, these basic techniques can fail to be applicable across datasets.

This is particularly apparent in the case of the behavioral recordings of worms cultured in the HeALTH system (see **Chapter 2** for additional details on HeALTH). Since the worm is cultured from L4 stage to death, it undergoes a substantial change in body size. Contrast against the background greatly varies depending on the experimental condition of interest. Furthermore, due to the use of C22, the individual worms still lay eggs during the reproductive period of their life, with the chamber containing clusters of eggs for a significant period of the worm's lifespan. This presents a few major challenges. The image intensity values of the eggs and worm are comparable, making it difficult to utilize thresholding to separate the two objects, particularly during moments of intersection between the two objects (**Figure 3.3a**). At times the size of the egg cluster is comparable to the area of the worm (**Figure 3.3b**). Also, while the eggs are not actively moving, the movement of the worm and the constant flow of bacteria within the chambers at times

move the egg clusters, preventing the use of background subtraction from eliminating these objects. Lastly, a single device within the experiment could generate over 150 videos of the microfluidic chamber array, resulting in potentially 9,000 videos of individual worms totaling 63 GB in size, making it difficult to adjust manual parameters and account for experimental differences over time in a scalable manner.

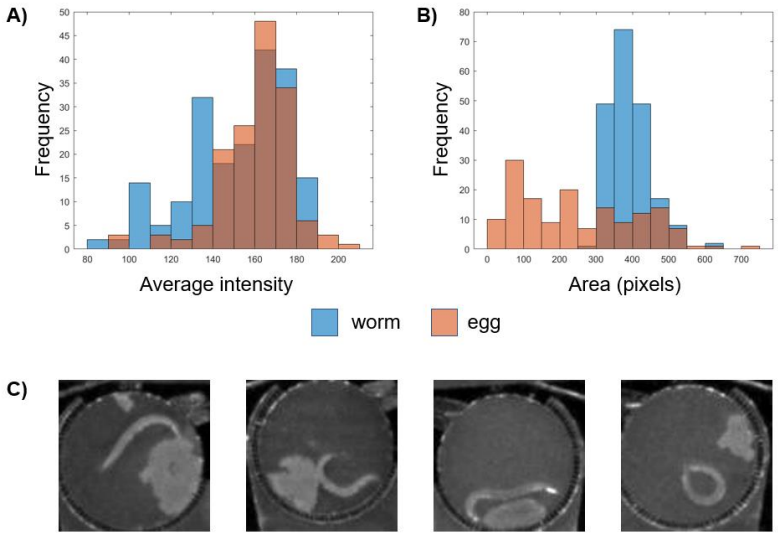

Figure 3.3. Worms and clusters of eggs have similar morphological features. A) Histogram of the average intensity of the worm (n = 200 frames) and eggs (n = 127 frames), demonstrating an almost complete overlap in intensity values across the two objects. B) Histogram of the area of the worm and eggs, demonstrating a substantial overlap in size across the two groups of objects. C) Representative images of worms and egg clusters within the microfluidic chamber.

As such, there is a need for a flexible method to segment and extract objects of interest across different imaging conditions. To achieve this objective, we turn to deep learning, which has emerged as a powerful data-driven tool for object detection and segmentation. Deep learning is a class of machine learning algorithms that utilize neural network architectures with multiple layers.[121,122] It requires significant amounts of labeled data and is able to automatically learn and identify features of interest, in contrast to other

machine learning algorithms that require manual feature extraction. As such, these algorithms are highly accurate in computer vision applications, albeit with the drawback of needing significant computing power to train the model. This pipeline takes advantage of its strength in computer vision applications and uses a consensus approach between two convolutional neural networks (CNNs). It performs instance segmentation coupled with an independent validation of the objection's location to allow for the highly accurate detection, identification, and segmentation of the worm.

For the scope of this thesis, the segmentation is trained for a specific application – examining aging worms within a constrained microfluidic chamber (the behavioral recordings generated by the HeALTH system). However, by design it is flexible and easily adaptable to other experimental conditions where worm tracking across a range of conditions is required. Examples of its generalizability are detailed in the manuscript "Deep learning for robust and flexible tracking in behavioral studies for *C. elegans*" (https://doi.org/10.1101/2021.02.08.430359) and also noted below in 3.4.4.1.[105]

3.4.2.1 Instance segmentation via Mask R-CNN

Mask R-CNN is a highly accurate, robust algorithm for performing instance segmentation. It couples region proposal networks (RPN) with convolutional neural networks (CNNs) to extract the location (in the form of bounding boxes) and binary mask for each object, along with the corresponding estimated likelihood for each detection.[123] It is relatively simple to train and has shown to be generalizable across different training sets using the same framework. Crucially, it is computationally efficient compared to other instance segmentation methods, ideal for large-scale datasets, and most importantly one of

the highest performing segmentation methods as measured by the mean average precision (mAP) of detections on the standardized COCO dataset.[123] As such, we considered it to be a promising method for segmentation.

After the initial training period, the model was able to accurately detect and segment both worms and egg objects, even in instances where multiple objects intersect (**Table 1, Figure 3.4**).

Table 1. Detection results for the trained Mask R-CNN model

mAP	$AP_{IoU=0.5}$	$AP_{IoU=0.75}$	$AR_{IoU=0.5:0.95}$	mAP_{worm}	mAP_{egg}
0.683	0.977	0.732	0.700	0.818	0.653

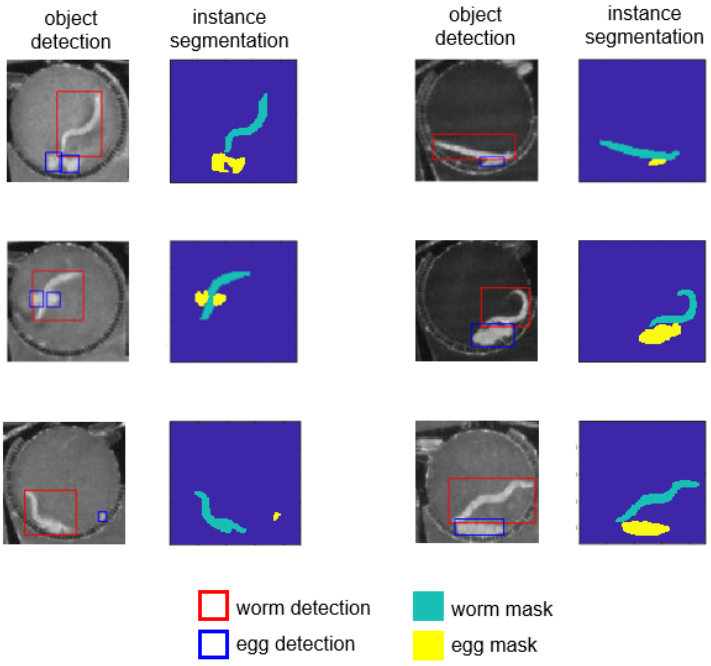

Figure 3.4. Representative examples of object detection and instance segmentation using Mask R-CNN.

In addition to examining the COCO evaluation metrics to compare the inferenced masks to the annotated ground truth masks, it is important to compare the performance of Mask R-CNN to existing image processing techniques. The prior iteration of the segmentation code for this set of data was a custom MATLAB script.[88] It used background subtraction coupled with a user selected Niblack thresholding to obtain the binarized frame of the worm and post-processing morphological filters to eliminate features based on parameters, such as the area or length of the object. It also relied on prior frames to iteratively adjust parameters across the dataset. Although this was quick and computationally low-cost, it was difficult to scale and unable to segment out the worm in either low contrast conditions or in recordings with large, moving egg clusters.

To compare the two methods, we examined the IoU score for frames with a hand annotated segmented ground truth compared to the computed segmented worm. We examined frames from recordings of the highest food level (i.e. with the lowest contrast between the worm and the background) across the lifespan of the population. The Mask R-CNN segmentation significantly outperformed the prior method (with an average IoU score and standard deviation of 0.89 ± 0.22 compared to 0.44 ± 0.34 respectively), as shown in **Figure 3.5**. To ensure that this improvement was unbiased across the different conditions and error cases, we categorized the frames based on the age of the worm, since different segmentation challenges are associated with different stages of life. For instance, the reproductive period of the worm that results in the presence of eggs within the chamber holds different challenges compare to aged, non-moving worms in low-contrast conditions. We then subsequently compared the IoU scores throughout the age groups across the two methods (**Figure 3.5**). As the worm age, the accuracy of the initial segmentation code

decreases dramatically (0.58 ± 0.33 average IoU for the young individuals to 0.29 ± 0.32 for the old individuals). In contrast, the accuracy of the Mask R-CNN segmentation remained relatively consistent across the age groups. This underscores both consistency of Mask R-CNN across the different error cases, along with the large improvement in segmentation accuracy compared to the prior segmentation method. Although there was a significant improvement in accuracy, there were a few instances, particularly within the young age group, where Mask R-CNN failed to properly identify the location of the worm. Not only did it fail to identify the location of the worm, it also resulted in a FP detection, predicting with high likelihood estimates. Thus, there is still a need to have a validation step to reduce the likelihood of false positives in identifying and segmenting the worm.

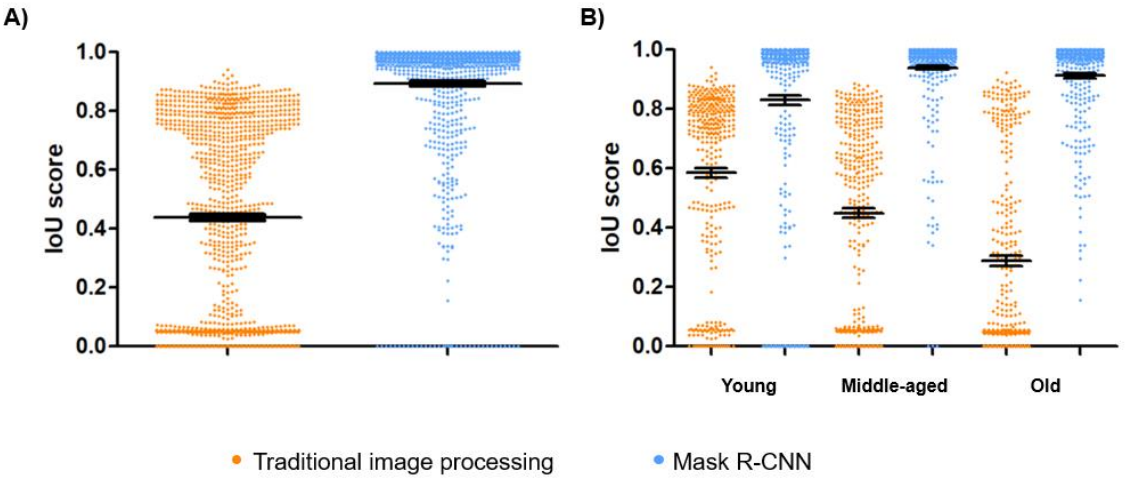

Figure 3.5. Mask R-CNN segmentation consistently outperforms traditional image processing-based techniques. A) The IoU score of annotated frames (n = 1057) segmented using traditional image processing techniques (0.44 ± 0.34) compared to Mask R-CNN (0.89 ± 0.22) across all ages (error bars are SEM, $p < 0.001$ via t-test). B) The IoU score of frames segmented using traditional image processing techniques compared to Mask R-CNN separated by age (error bars are SEM): young worms (0.58 ± 0.30 vs. 0.83 ± 0.31, n = 338 frames, $p < 0.001$ via t-test), middle-aged worms (0.45 ± 0.32 vs. 0.94 ± 0.14, n = 380 frames, $p < 0.001$ via t-test), old worms (0.29 ± 0.32 vs. 0.91 ± 0.15, n = 380 frames, $p < 0.001$ via t-test).

Mask R-CNN has been shown to be a quick deep learning method for performing instance segmentation. However, due to the computational complexity, the average inference time for a frame (0.421 ± 0.023 seconds) is approximately one order of magnitude longer than the prior segmentation method (0.088 ± 0.018 seconds), which relied on basic image processing techniques. As a result, it is difficult to perform Mask R-CNN locally on a large scale, with a single 4 minute long, 7MB video taking approximately 24 minutes to analyze. To address this processing bottleneck, we take advantage of the non-serialized nature of instance segmentation along with the availability of parallel computing capabilities. Using PACE computing clusters, we run tens of jobs simultaneously, drastically reducing active computational wait times. Although this resource is not widely available, this could be broadly generalized and performed using Amazon AWS ParallelCluster services, or even through online resources such as Google Colab. As a result, it is feasible to analyze terabyte scale data sets without unreasonable computational time.

3.4.2.2 Faster R-CNN

To improve the overall accuracy of Mask R-CNN, we implemented an additional validation step in the form of an independent object detection algorithm. Faster R-CNN is a top performing object detection method.[124] A precursor to Mask R-CNN, Faster R-CNN is built off the same network architecture, albeit without the mask prediction of each object. Compared to other CNN methods with equivalent or higher mAP, the Faster R-CNN architecture is less computationally costly and advantageous for large volumes of data.[125] Further, the Faster R-CNN architecture has been tested in a wide range of applications,

ranging from vehicle and pedestrian detection to malarial detection via cell classification.[124,126]

As such, we considered it to be a powerful method for object detection and promising in identifying regions of interest where the worm is within the complex environment. After the initial training period, the model was able to accurately detect objects, across the different age ranges and contrast levels (**Table 2, Figure 3.6, Appendix B.1**). This model has higher accuracy in mAP, AP, and AR values across conditions in comparison to the Mask R-CNN model, likely due to significantly larger training set. As a result, this model could be reliably used as a validation step post the initial segmentation stage. In addition to the high accuracy of detection, the inference time for each image is short (~131 ms/frame) making it a highly feasible method of performing object detection on a large scale. Since this is insignificant in comparison to the computational time associated with Mask R-CNN, it can be easily run on a large scale using the pre-existing parallel computing framework.

Table 2. Detection results for the trained Faster R-CNN model

mAP	$AP_{IoU=0.5}$	$AP_{IoU=0.75}$	$AR_{IoU=0.5:0.95}$	mAP_{worm}	mAP_{egg}
0.777	0.980	0.914	0.795	0.834	0.751

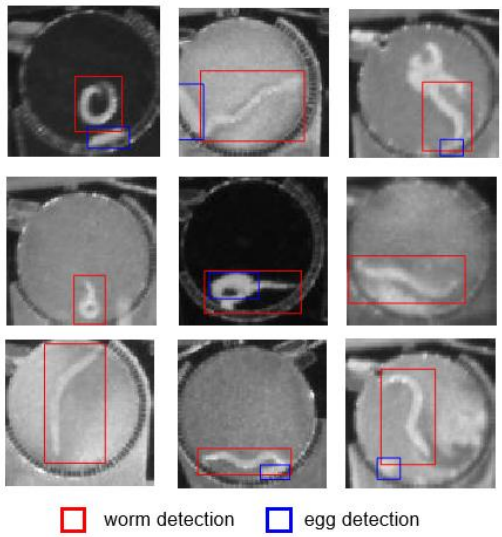

Figure 3.6. Representative examples of object detection using Mask R-CNN across a variety of object sizes and contrast levels.

By coupling the outputted detections from the independently trained Mask R-CNN model and the Faster R-CNN model, and censoring frames in where there is less than a 0.8 intersection between the two detection bounding boxes, we improved the average overall IoU score from 0.89 to 0.93, with minor computational cost.

3.4.3 Skeletonization

After obtaining the segmented mask of the worm, it is crucial to accurately extract the centerline or skeleton of the individual for accurate subsequent behavioral analysis. For most postures it is relatively trivial to use simple morphological operations to extract the skeleton - such as the built-in MATLAB function bwmorph 'thin' - and iteratively prune small extraneous branches based on the length of the branch. The coordinates of the remaining pixels are then smoothed to return the skeleton of the posture. This technique is widely used across existing worm trackers and is computationally low-cost.[83,118,127]

However, for more complex postures, such as when the worm is occluded onto itself, this technique is often unable to accurately resolve the underlying backbone, resulting in censoring these poses from subsequent analysis.

3.4.3.1 Resolving coiled structures

Occluded postures often carry biological significance, often occurring during foraging, chemotaxis, or as an escape behavior in response to noxious stimuli.[114,128,129] As a result, it is crucial to be able to capture and resolve these behaviors in a robust manner. One common solution aside from censoring those instances is manually annotating frames where occlusions occur. Although there are tools that aid in manual annotation and tracing the skeleton, this method becomes increasingly difficult, labor intensive, and infeasible with increasingly large sets of behavioral recordings.[130] There are some existing statistical models and optimization based algorithms that have demonstrated the ability to resolve occluded postures.[131–134] However, they either rely on additional image features making them susceptible to changes in imaging conditions and difficult to scale across experiments, or are computationally intensive, making them prohibitive to use on a large-scale.

To address the issue of resolving coiled centerlines on a large-scale I used WormPose, an open-source Python package designed for pose estimation for *C. elegans*.[135] This algorithm creates realistic, synthetic worm postures with known, generated centerlines, mirroring the examined data of interest. It then uses a CNN trained with these synthetic images to predict an accurate centerline skeleton from the unresolved experimental image, validating the model based on real labeled (non-occluded) images. Additionally, it generates an image similarity score to compare the predicted synthetic

image with the actual frame of interest for further quality control of the predictions. This avoids the requirement of needing large, hand-annotated training sets of coiled or occluded postures and is flexible enough to be applied to recordings across a wide range of conditions. Furthermore, after the initial training period, it is computationally quick and theoretically able to perform real-time pose estimation making it feasible for applying to large-scale data sets without extensive computational time.

After training WormPose on *C. elegans* cultured on-chip across a variety of ages, I was able to resolve ~70% of coiled or occluded frames (n = 1840) across a range of different image contrast levels, as shown in **Figure 3.7**. Its quick computational time for inferences (~3.37 seconds per frame) and ability to be robustly applied across the data makes WormPose a useful tool to incorporate into the overall analysis pipeline to address the occurrence of coiled or unresolved postures. Instances of occlusion are automatically flagged and subsequently resolved using the trained CNN model.

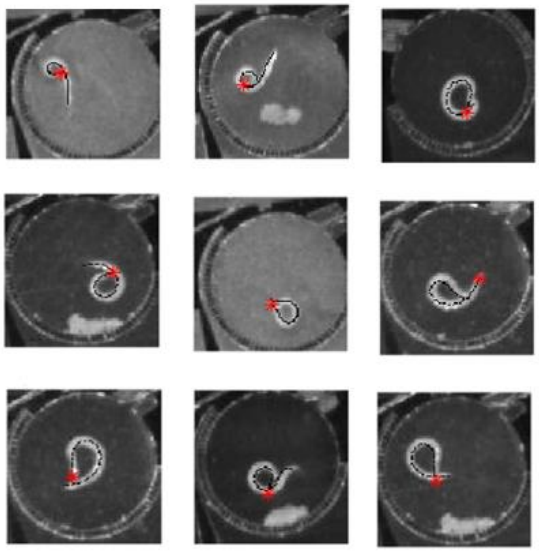

Figure 3.7. WormPose is able to resolve occluded poses of worms cultured on-chip. Representative frames of coiled worms and the backbone (the black centerline) as predicted by WormPose. The head is noted by the red star.

3.4.4 Post-processing: Tracking worm orientation throughout time

In addition to accurately extracting the centerline of the segmented individual, it is also crucial to correctly identify and track the head and tail locations for an individual throughout the recording. Inaccurate identification can lead to different centerlines, potentially resulting in inaccurate behavioral classifications. As a result, there is a need to accurately identify and track the location of the head, regardless of missing frames or coiled postures.

Prior methods utilize morphological features, such as body width, the angle of the corner of the curvature of segmented worms, or image intensity, to differentiate between the two endpoints.[83,87,118,127] However, due to the imaging condition, low-magnification, and at times low imaging contrast, it can be challenging to reliably and consistently extract the features previously used to distinguish between the head or tail of the posture.

For the purposes of this pipeline, the head is defined with the underlying assumption of movement of the head curvature having higher amplitude relative to the tail curvature.[118] The head is defined as the 1st tenth of the worm centerline, while the tail is defined as the last tenth of the worm centerline. The endpoint with the greatest average curvature was designated as the head, with the assumption that worms would move more in the forward direction; however, it is important to note that this technique may be work for highly moving, swimming individuals, this may not be the most accurate, particularly in cases with extremely low to no movement for aged individuals.

Prior tracking algorithms use nearest neighbor tracking to ensure the consistent identification of endpoint identities. However, this can fail in instances of either missing frames, issues with segmentation, or instances during coiled postures, omega bends, or occlusions. Thus, it was necessary to have a method to ensure the consistent tracking of the head endpoint throughout the duration of the recording.

To address this concern, I created a MATLAB-based graphical user interface (GUI) (**Appendix B.3**) that allows users to view frames of the video of interest, with the initially assumed head endpoint highlighted, and allow the user to traverse through the frames of the video and manually correct any misclassifications or – in instances with errors in obtaining the backbone of the individual – censor the frame from subsequent analysis. For frames with potential errors in tracking the head location the user is able to run through the videos of interest and correct the head locations throughout the video as needed.

3.4.4.1 Alternative applications of the Faster R-CNN model

Although the Faster R-CNN model was trained to validate the Mask R-CNN model to ultimately segment and obtain postural information, object detection can be used to independently extract coarse level behavioral information. By utilizing the dynamic location of the detected object's bounding box and tracking it over time, one could use Faster R-CNN to measure commonly used behavioral phenotypes, such as the distance traveled by an individual or its linear velocity. This could be useful in cases where complex behavioral phenotyping is not needed, and there is a need for a computational simplicity.

As a proof of concept, we examined the centroids of detected bounding boxes obtained from the model to the centroids of hand-annotated postures at 9 time points. These worms range from L4 stage to Day 16 of adulthood, encapsulating the behavior from late development to late in adulthood. The bounding box detected by the model had centroids that were comparable to the centroids of the hand-annotated postures (with an average of 3.05±3.03μm absolute distance ± standard deviation between the two points), demonstrating that the centroid of the bounding box could be used as an accurate proxy for the centroid of the segmented individual. To test whether we could also measure motion accurately with this method, we calculated motion between the bounding box centroids and hand-annotated worm shape centroids every 10 seconds. There was no significant difference between these two measurements across time (3.69±4.03μm, mean absolute difference ± standard deviation), and the motion trends were clearly replicated between the hand-annotated shape centroids and the bounding box centroids (**Figure 3.8**). This highlights the potential for Faster R-CNN to track behavior and movement during development as an insight into their behavioral state.[105]

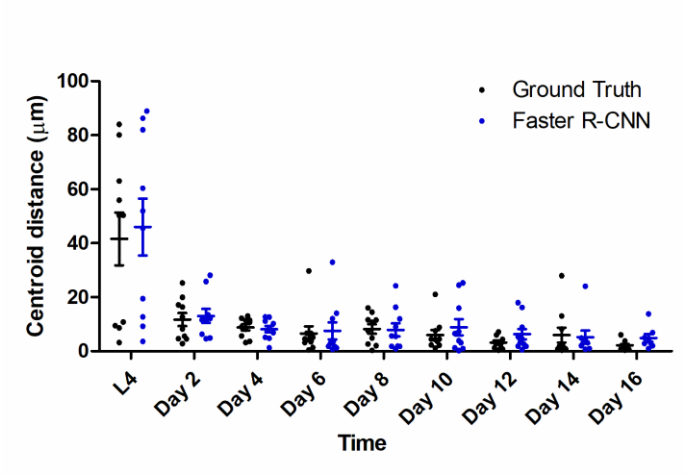

Figure 3.8. Faster R-CNN is an accurate estimate of the centroid of the segmented object of interest. The centroid distance traveled in 10 seconds is plotted across ages for the annotated ground truth segmented worm and the bounding box detected using Faster R-CNN (n = 10). None of the ground truth and Faster R-CNN detections were significantly different across any of the timepoints ($p < 0.001$, ANOVA with Bonferroni correction).

Faster R-CNN can also serve as a quick and accurate alternative to gauge behavioral decline with aging across a population. By tracking the bounding box locations of the worm detected by the Faster R-CNN model and measuring the IoU of the detection bounding boxes across the video, we can get a rough metric of movement. Although this method is more complex then examining the pixel difference across frames, similar to the previous metric in **Chapter 2**, it is more robust against potential sources of noise in the video. For example, in instances with extremely heterogenous environments within the period of interest, examining the raw movement in the form of pixel differences could erroneously capture differences in the background across time points instead of just the movement of the worm.

To examine how movement changed with age we tracked 31 individual worms from L4 stage to Day 16 of adulthood, comparing the IoU of the bounding boxes within

the first and last frame of a 10 second recording. We calculated a movement score (1 – IoU), and observed individual decline in movement, as well as a population-level behavioral declines with age (**Figure 3.9a,b**). This decline mirrored the pattern observed when measuring the pixel difference across the first and last hand annotated segmented frames of a video taken across the same timepoints (**Figure 3.9c**, n = 15 individuals), illustrating its ability to capture behavioral decline with age.

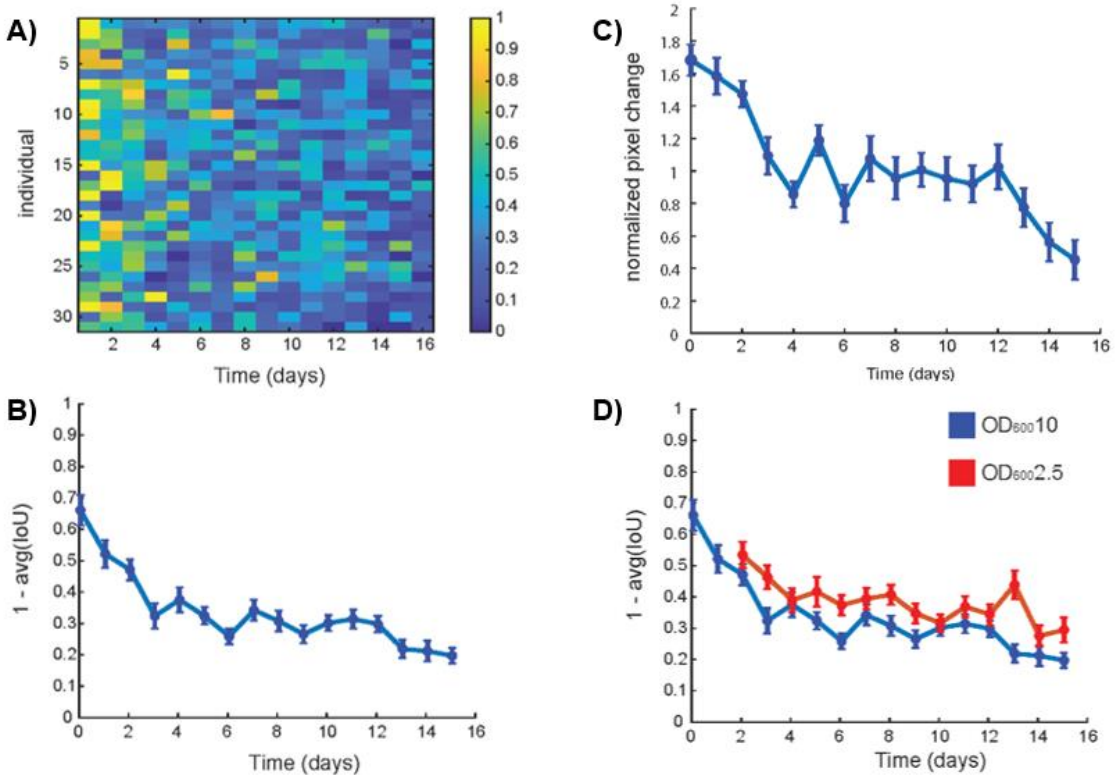

Figure 3.9. Tracking movement decline in aging using Faster R-CNN. A) Heatmap of individual movement (1-IoU) from L4 to Day 15 of adulthood (n = 31). Individuals are cultured at OD_{600}10. B) Average movement decline over time (error is plotted as SEM). C) Average pixel change values of segmented worms over time from L4 to Day 15 of adulthood (n = 15, error is plotted as SEM). D) Average movement decline over time for individuals cultured in high levels of food (OD10) or DR (OD2.5) (error is plotted as SEM, movement for OD10 and OD2.5 is significantly different via Kolmogorov-Smirnov 2-sample test (p = 0.03)).

This measurement can also be used to differentiate between movement across different experimental conditions. We examined the movement score of worms cultured under DR (OD_{600}2.5) starting at Day 2 of adulthood and were able to demonstrate that the worms under lower food levels had a statistically significant difference in behavioral decline compared to worms cultured at higher food levels (OD_{600}10). This mirrored the trends observed in **Chapter 2** (**Figure 3.9d**). In addition, to verify the performance of the model on the dataset, we also validated that the detected bounding boxes from the model were comparable to the bounding box of the hand annotated, segmented worms (**Appendix B.4**). This demonstrates that motion quantitatively estimated by Faster R-CNN can be used as a quick metric to track and examine behavioral decline within an aging population.

3.5 Conclusions

In **Chapter 3**, I demonstrate a flexible, robust deep-learning based platform to extract worm postures from heterogeneous, complex environments. In comparison to basic image processing techniques, we showed an improved segmentation accuracy (from 0.89 to 0.93 average IoU score) using a consensus approach from both the Mask R-CNN and Faster R-CNN models across various ages of individual. We also demonstrate the ability to track and extract accurate worms centerlines in complex instances, such as in occluded or coiled postures, using a combination of WormPose and an user-annotation tool to correctly track the head endpoint.

Although this pipeline requires training the deep-learning models for the accurate segmentation of the worm, which is not an insignificant investment in terms of creating an appropriate training and evaluation set, this is designed for large data sets in where methods

of using user-defined parameters for optimizing traditional image processing methods would falter. Not only is this pipeline accurate and flexible across conditions post training, it is easily scalable, being designed for parallel computing, allowing us to apply this on large datasets, as exemplified later in **Chapter 4**.

Lastly, we demonstrate how portions of this pipeline, such as the objection detection from the Faster R-CNN model, can be used to obtain coarse, yet useful, behavioral information that may be useful for a variety of ethological behavioral studies. We illustrated its use in examining commonly used behavioral phenotypes, such as distance traveled over time and raw movement, and highlighted its ability to recapitulate known biological trends in behavioral decline under different dietary conditions. This model could also be applied to detect other phenotypes of interest, such as detecting and counting eggs as a measure of an individual's fecundity over time, as shown in "Deep learning for robust and flexible tracking in behavioral studies for *C. elegans*" (https://doi.org/10.1101/2021.02.08.430359). By creating a robust and scalable tool for extracting posture, this will enable researchers to extract and subsequently analyze behavioral results, providing greater insights into the fields of aging and ethology.

CHAPTER 4. MEASURING THE IMPACT OF DIET AND DYNAMIC PERTURBATIONS ON THE BEHAVIORAL REPERTOIRE AND AGE-RELATED BEHAVIORAL CHANGES IN *C. ELEGANS*

4.1 Introduction

In this chapter, I characterize age-related changes in the behavior in *C. elegans* using a data-driven, unbiased behavioral mapping approach. I demonstrate that this method can be used to uncover subtle behavioral differences not captured with traditional, heuristically defined movement-based measurements. I define and characterize the overall behavioral repertoire of the worm and examine how different behaviors are temporally connected to one another. I then examine how the frequency of these behaviors change with age and examine how this differs across individuals in response to stimuli and within the same isogenic population. Finally, I explore how known environmental modulators of aging in the form of different dietary restriction regimes – chronic caloric restriction (CR) and intermittent fasting (IF) – influence behavior and age-related behavioral changes to better understand how behavior can be used as a measure to provide insight into the underlying physiological health and aging process in individuals.

4.2 Background

C. elegans display a surprisingly large behavioral repertoire, ranging from crawling, to swimming, to pirouettes and turns as a culmination of their internal state and perceived surroundings. Despite the fact that worms exhibit a wide array of behaviors, aging studies

examine basic movement metrics, such as the extent of movement after a strong stimulus, to gauge the extent of sarcopenia and health of the individual.[50,51,59,60] These measurements are often coupled with additional metrics, such as the worm's morphology, reproductive capability, and tissue integrity, to assess the overall health and physiological age of the individual.[50,51,59,102] Thus, it is unknown whether the complete behavioral repertoire of the worm is sufficient to indicate its underlying state of health and physiological age.

In classical ethology and neuroscience studies, a common strategy to measure behavior is to identify preselected, user-defined behaviors, such as a forward crawl or an omega turn, and count the frequency and or duration of these behaviors over a set observational period.[109] This type of approach is generally high-throughput, easily interpretable, and is generalizable across a we range of model organisms, ranging from worms, fish, and mice.[83–85,87,118,136–138] However, it is limited by the human-defined behavioral categories, being prone to user bias, and often cannot capture subtle behavioral differences across groups of interest. As a result, there is a need for an unbiased, data-driven quantitative method to identify compare behavioral patterns across populations of interest.

There are several methods that aim to quantitatively capture the wide array of behaviors in an unbiased manner. For instance, *C. elegans* behavior has been shown to be compressed into repeatable behavioral motifs that describe differences in the locomotion across mutants, in response to optogenetic stimuli, and across different environments.[111,112,139] Another technique, applied to *Drosophila melanogaster*, uses t-distributed stochastic neighbor embedding (t-SNE) to map the spatial and dynamic temporal elements of behavioral time series data in a 2-D space.[140] Areas of high density

on the map represent stereotyped behaviors, allowing researchers to identify commonly performed behaviors in a data-driven manner. This has been shown to uncover subtle behavioral differences across gender, in response to stimuli, and across aged cohorts.[140–143] However, this technique has not been applied to examine behavior in *C. elegans* in an aging context.

4.3 Materials and Experimental Methods

4.3.1 C. elegans *culture* on-chip

The strain used in this work was N2. To obtain large-scale longitudinal behavioral recordings across the entire lifespan, we used the HeALTH platform, described in **Chapter 2**. In brief, synchronized L4-stage wildtype animals were loaded into a worm chamber array microfluidic device. Worms were cultured at 20°C in *E. coli* (HB101) spiked with Pluronic F-127 (0.005%), carbenicillin (50µg/ml), kanamycin (50µg/ml, and 5uM of C22. At Day 2 of adulthood, worms were then shifted to 25°C and to the desired food level.

Individuals cultured at the constant high food level (n = 134 individuals) were maintained at bacterial food levels of OD_{600} 10 throughout their lifespan. Individuals that underwent constant caloric restriction (CR) (n = 103 individuals) were maintained at OD_{600} 2.5, which was created from the OD_{600} 10 stock was diluted with S Medium with Pluronic, carbenicillin, and kanamycin. Individuals cultured under the intermittent fasting (IF) condition (n = 110 individuals) were cultured in buffer (S Medium with Pluronic, carbenicillin, and kanamycin) for 2 days and then switched to the high food condition of OD_{600} 10 for 2 days. This four day cycle repeated until death. See **Chapter 2** for more details on the culture method.

4.3.2 Lifespan and behavioral analysis

Lifespans for individuals were obtained by manual annotation, with individuals being marked as dead if no movement was detected past two days. The lifespans of the individuals cultured on the HeALTH platform followed expected trends.[63] Individuals under either form of DR had extended lifespan, as shown in **Figure 4.1**. Following prior literature, individuals under IF had significantly longer lifespans than those under CR.[63]

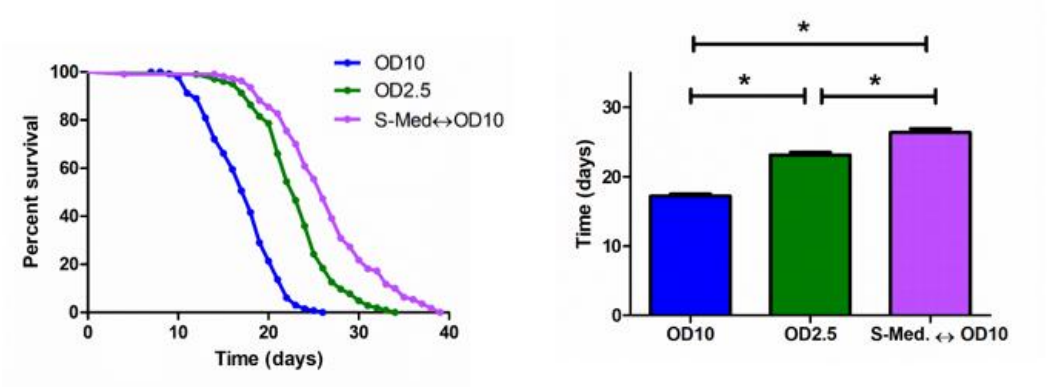

Figure 4.1. DR extends longevity in *C. elegans* on-chip. *(left)* Lifespan curves for wild-type N2 populations cultured under no DR (OD10, 17.19 ± 0.32, n = 134 individuals), CR (OD2.5, 23.11 ± 0.41, n = 103 individuals), and IF (S-Med ↔ OD10, 26.35 ± 0.56, n = 110 individuals). *(right)* Bar graph of average lifespan under different DR regimes (error bars show SEM, $p < 0.0001$, log-rank test).

Behavioral recordings of the microfluidic devices were taken every 6 hours under the HeALTH imaging conditions, as detailed in **Chapter 2**. The videos were 4 minutes in length, with the last two minutes of the video capturing evoked behavior after a mechanical pulse stimulus. The recordings were analyzed using the deep-learning pipeline developed in **Chapter 3**. Due to the large volume of behavioral recordings, we examined a subset of our data, looking at behavior every 12 hours. The videos were segmented using 4 cores of a Dual Intel Xeon Gold 6226 CPU @ 2.7 GHz as part of a parallel computer cluster. The

remaining portions of the pipeline were processed on a system with an Intel(R) Xeon(R) CPU E5-1620 v4 processor and a NVIDIA Quadro M4000 GPU.

Using the pipeline, we resolved 26,470,580 frames from the available 41,734,363 frames. The number of resolved frames was dependent on the imaging conditions and the age of the worm, with increased contrast and greater age resulting in a greater fraction of resolved frames (**Appendix C.2.1**).

4.3.3 t-SNE embedding

Common to all the data-driven techniques used to characterize behavior is the need to quantitatively define the posture. Due to the morphological simplicity of the worm, it is straightforward to measure and describe its pose. Prior work has shown that the space of shapes occupied by *C. elegans* undergoing spontaneous behavior on agar is able to be represented in a lower, four-dimensional space.[110] Any pose can be reconstructed using a combination of a small number of eigenvectors (termed eigenworms), providing a simplistic basis of posture for behavioral studies.

To represent the postures displayed by the worms in the microfluidic environment, it was necessary to convert the posture into an independent representation unbound from the recorded coordinate locations. Similar to previous work, the skeleton was divided into 100 evenly spaced segments, and the tangent angles of the segments were taken from the head to the tail of the individual.[110] To align the postures, the mean angle was subtracted from each of the tangent values, resulting in a 100 length vector that describes the shape of the worm without reference to the individual's position or orientation. To extract postural dynamics from this angled representation, we then examine the covariance matrix of angles

across the behavioral recordings and perform eigendecomposition to undercover the underlying dimensionality of the shape.

This was done across recordings from all food conditions and time points (n = 37,881 frames). The worms cultured within the microfluidic device had distinct eigenworms from the worms crawling unrestricted on an agar plate. Only five eigenvalues were significant, and they accounted for 82.9% of the variance in angle along the worm body **(Figure 4.2**).

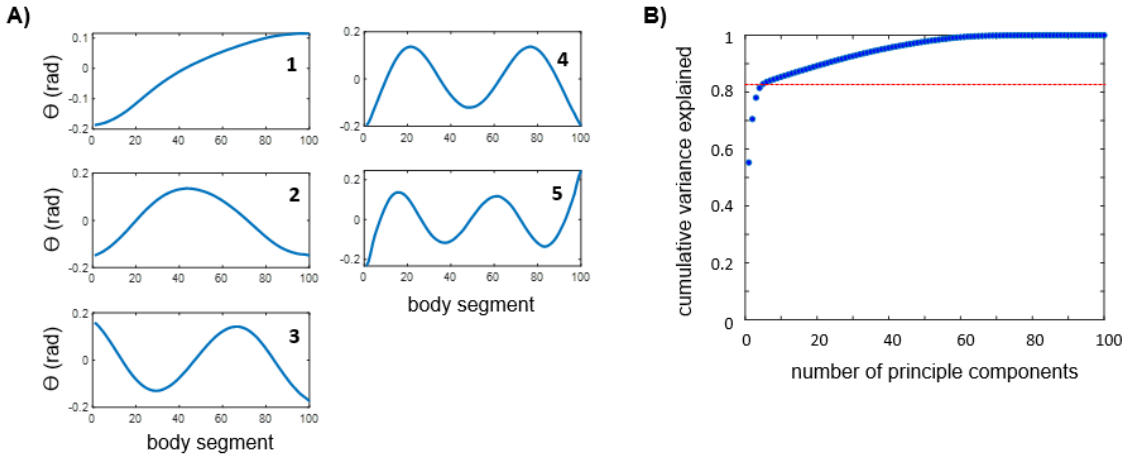

Figure 4.2. Eigenworms for *C. elegans* cultured on-chip. A) The first five eigenworms for worms cultured on-chip throughout their lifespan. B) The first five modes capture ~83% of postural variance.

We also examined whether the eigenworms varied across age. Although there were slight differences in the head and tail portions of the body length (**Appendix C.2.2**), no major differences were noted in the overall shape of each respective eigenworm, allowing us to represent all the collected recordings using the same, underlying basis set and within the same representative embedding map. Moving forward, we represented the postural dynamics as a time series of five amplitude values.

Similar to previous work,[140] to account for the underlying dynamics of behavior, we then performed a Morlet continuous wavelet transform for the time series values ranging from 7 Hz (limited by the Nyquist sampling) to 0.1 Hz. The resulting spectrograms were then further dimensionally reduced via t-SNE, creating a 2-D probability density function (PDF) across the map of the postural dynamics. Due to the shared basis set, all conditions, across age and food condition, were embedded within the same map. When comparing across subsets of data video recordings we performed hierarchical bootstrap sampling until reaching roughly the equivalent number of frames across comparisons.

4.3.4 Examining the time scale of behavioral transitions

To examine how individuals moved across different behavioral regions within the map, we measured the transition probability (T) that an individual would travel from region i to region j after a set time (τ); compiling all the transition probabilities across the regions results in a behavioral transition matrix $T_M(\tau)$. To examine whether $T_M(\tau)$ contained non-Markovian time scales, we examined the transition matrix at longer time scales ($\tau > 1$ frame). Following existing work,[141] the decay time (t_2) in a Markovian system can be estimated by the equation below.

$$t_2 = -\frac{1}{\log\ |\lambda_2(1)|} \tag{5}$$

where $\lambda_2(1)$ is the second largest eigenvalue describing $T_M(\tau)$. The average across all individual worms is $|\lambda_2(1)| = 0.849 \pm 0.031$. Thus, the presence of structure within $T_M(\tau)$ past $t_2 = 6.19 \pm 1.14$ transitions (i.e. 7 frames or 0.5 seconds) indicates that the

behavioral transitions are non-Markovian and in fact have an underlying memory and dependence on prior states.

4.3.5 Measuring the extent of movement

To gauge the performance of conventional methods of analyzing behavior decline, we measured the extent of movement for the obtained behavioral recordings. We examined two different metrics based on the detected location of the worm: examining the distance traveled by the centroid location and the raw movement of the individual over time. We chose to use metrics based on the bounding box locations, obtained using the analysis pipeline detailed in **Chapter 3** due to quick computational cost, time, and ease of accessing the information.

The first metric measures the distance between the centroid location of the bounding box over a set duration. We previously demonstrated how the centroid of the bounding box is an accurate estimate of the centroid of the segmented worm (**Figure 3.8**). For these measurements, we took the 90^{th} percentile distance traveled by the centroid of the bounding boxes every 10 seconds in the behavioral recordings for the food and time point of interest. The second is an analogue to measuring the raw movement of the individual. Similar to previous work in **Chapter 3**, we compared the IoU of the bounding boxes within the first and last frame of a every 10 seconds in the behavioral recordings of the food and time point of interest. We calculated a movement score (1 – IoU) and measured the average of the movement scores over time.

4.3.6 Statistical Analysis

4.3.6.1 Lifespan studies

For each experimental condition, we performed at least three different biological replicates. Raw lifespan data for each analyzed individual, along with corresponding experimental conditions and trial information, is included in **Appendix C.1**. Lifespans were analyzed via the log-rank test in JMP Pro14.

4.3.6.2 Comparing behavioral probability density functions (PDFs)

This behavioral dataset is hierarchical in nature. As a result, traditional strategies for statistical comparisons, such as Student's t-test or ANOVA, are not accurate due to the lack of independence across data points. To address this limitation, we perform hierarchical bootstrap to compare across the PDF of the different experimental conditions, which has been demonstrated on similar datasets.[144] We chose this approach due to its ease of implementation and few required assumptions on the underlying structure of the data. In addition, it has been shown to have comparable false-positive and false-negative rates compared to LMM results.[144]

Drawing from prior work,[144] we created Gaussian mixture models (GMM) for the bootstrap sampled data (n=1000) for each point on the discretized map for the experimental conditions of interest. To compare across conditions and across the same spatial area in the embedding map, we compute a joint probability distribution of the two GMMs from the different experimental conditions of interest. A symmetric Gaussian indicates no significant difference between the two groups. Asymmetric distributions, such as if the summed density of the joint probability distribution on one side of the diagonal was greater than $1 - \alpha/2$ or less than $\alpha/2$, indicate significant differences between the groups. Multiple

experimental groups are compared via pairwise-comparisons between groups, with significance value ($\alpha = 0.05$) adjusted with the Bonferroni correction.

4.3.6.3 Quantitatively comparing changes in behavior over time

To directly compare how behavior changes with age, we chose to examine the behavioral covariance matrix across the different food and age groups. Similar to existing work,[142] we found the average probability each individual would be in one of the 24 defined discretize behavioral regions for each timepoint. We then found the mean behavioral vector ($\mu_k^{(z)}$) for the individuals within each food condition and age group of interest, where z is the food condition of interest and k is the age group. We divided the age groups into two-day long cohorts. The mean behavioral vectors are then combined to create the behavioral matrix M, where $M = [\mu_{Day\ 2-4}^{OD10} \cdots \mu_{Day\ 18-20}^{OD10}, \mu_{Day\ 2-4}^{OD2.5} \cdots \mu_{Day\ 24-26}^{OD2.5}, \mu_{Day\ 2-4}^{IF} \cdots \mu_{Day28-30}^{IF}] \in \mathcal{R}^{24x35}$, with 24 behavior regions and 35 different age and food grouped populations. We then found the covariance of this behavior matrix to observe the relationship between behaviors across the time and food conditions.

To assess the structure of the covariance matrix and test for the number of significant modes to describe the covariance matrix, we independently shuffled the covariance matrix and performed eigendecomposition on the resulting structure. Eigenvalues higher than those from the shuffled matrix indicate significance, as shown in **Figure 4.9**.

To compare across populations, the average projection plot was smoothed using a gaussian filter, with a window of 10. The error was generated using bootstrapping, with

1000 samples. The standard deviation across the bootstrapped samples are plotted as the region of error for each timepoint.

4.4 Results and Discussion

4.4.1 Defining the behavioral repertoire of C. elegans *on-chip*

Using the t-SNE behavioral mapping method we obtained a PDF map that captures the behavioral repertoire of *C. elegans* (**Figure 4.3**). This map contains 26,470,580 frames with behaviors ranging from Day 2 of adulthood to 12 hours prior to death. The behaviors span across three different food regimes as well: high amounts of food, CR, and IF. The peaks on the plot correspond with stereotyped behaviors. To better characterize the detected behaviors, the plot was discretized using a watershed algorithm. This resulted in a map with 24 distinct behavioral regions (**Figure 4.3b**).

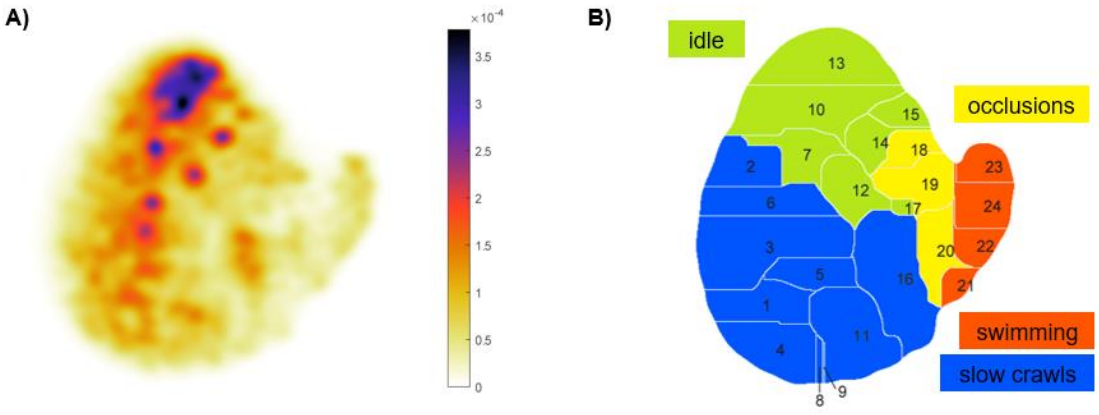

Figure 4.3. Behavioral map of *C. elegans* cultured on-chip capturing the entire adult lifespan and under various food conditions. A) PDF of stereotyped behavior B) Discretized behavioral map.

After qualitatively examining the behaviors within each region, we identified four main sections. The first (Regions 21-24) encompasses highly active swimming or thrashing movements, with regions having different swimming frequencies and body bend amplitudes (**Appendix C.2.3**). Although previous work had identified distinct regions for forward and reverse movement on agar, [143] both movements were found in the same region. This clustering could be attributed to the frequency of reversal behavior. Unlike worms on agar, reversals in liquid are rare, making up ~1-2% of swimming behavior.[87] Since swimming itself is not a dominant behavior within this dataset, with much larger density peaks occurring in other parts of the map, it is likely that the rarity of the behavior made it not frequent enough to form its own distinct region.

The second area (Regions 18-20) has worms undergoing deep body bends; one region in this section (Region 20) has coiling behaviors. The third area (Region 1-6, 8,9,11, and 16) has slow crawling behavior. Regions 3, 4, 8, and 9 have deeper body bends, while regions closer to the top of the map, such as Region 2, tend to have straighter postures. Additionally, there is heterogeneity in the frequency of movement, with the regions to the left having slower behaviors. There are some behaviors that appear to be slower than the 10 second window of behavior examined, indicating a potential need to examine longer-term dynamics within the behavioral recordings. The last area (Regions 7, 10, 12-15, and 17) consists of behaviors with little to no movement. The postures captured here vary; however, similar to previous trends, the regions closer to the top of the map, such as Region 13, tend to have straighter postures. For more information regarding the characterization of behaviors across the regions, see **Appendix C.2.3**.

After characterizing the behaviors of the regions on the map, we examined their temporal relation with one another, to observe how individuals travel across different behavioral regions within the map (**Figure 4.4**). We measured the transition probability (T) that an individual would travel from Region i to Region j after a set time (τ = 1 frame) throughout the recordings, ignoring instances where the worm performs a 'static' behavior, staying in the same region. We also observed how the flux across regions changes, defined as $f = \rho_i \times T(\tau)_{i,j}$, where ρ_i is the stationary probability density for Region i, accounting for the likelihood that the initial behavioral state would occur.

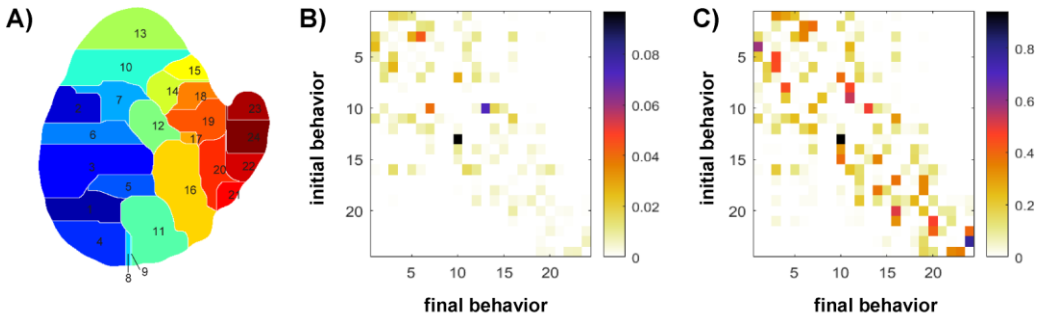

Figure 4.4. Worms travel to similar behaviors throughout the behavioral map. A) Labeled discretized behavior map (24 regions). B) Flux matrix across the 24 regions across all recordings. C) Transition probability matrix (τ = 1 frame) across the 24 regions across all recordings.

The transitions across regions are largely limited to similar types of behaviors. For instance, Regions 21-24 almost exclusively transition to one another, with a few transitions to neighboring regions (such as Regions 19-20). This is apparent in the block-like, clustered structure within T_M, and follows known trends in literature.[141] The transitions across two regions are also often asymmetric, implying a preference or directionality of transition. For example, the probability of transitioning from Region 13 to 10 is much higher than Region

10 to 13, while the probability of transitioning from Region 23 to 24 is much higher than Region 24 to 23. Lastly, we are able to pick out that the most common transitions appear between Region 10 and 13, due to their high probability density (i.e. frequency of occurrence) within the overall behavior map.

Previous studies have demonstrated that behavioral transitions are non-Markovian, retaining a structure, or memory, across long times scales indicative of an internal behavioral state.[141] Similarly, the transitions across behaviors in worms is non-Markovian, with a persistent underlying structure within the transitional matrix remaining past the expected decay found in a Markovian system (**Appendix C.2.4**). This points at the worm having a short behavioral 'memory', with the transition matrix losing structure past 10 seconds (τ = 140 frames). Thus, although the behavioral transitions are not completely random and are influenced by prior behaviors, within this cultured environment, these spontaneous behaviors do not appear to capture long-term memory on the scale of minutes or hours within these recordings.

4.4.2 Behavioral changes in response to mechanical stimulation

Prior studies have examined the differences between spontaneous and stimulated behavior, with stimulated behavior providing a more accurate measure of the physiological health of an individual in comparison to spontaneous movement.[51,60,102] Traditional movement metrics, such as raw movement, were not able to capture significant difference between stimulated and non-stimulated movement under the HeALTH system in microfluidic culture (**Appendix A.2.5**). However, we were curious as to whether subtle differences in behavior could be detected within the PDF maps. The maps appear to have

the similar stereotyped behaviors; however, the stimulated map has significantly greater density in areas of movement, such as the swimming region of the map, in comparison to the spontaneous map, which had a significantly greater density in idle, non-moving regions (**Figure 4.5**). This mirrors known trends and underscores the ability of the behavioral mapping to detect slight behavioral differences across recordings.

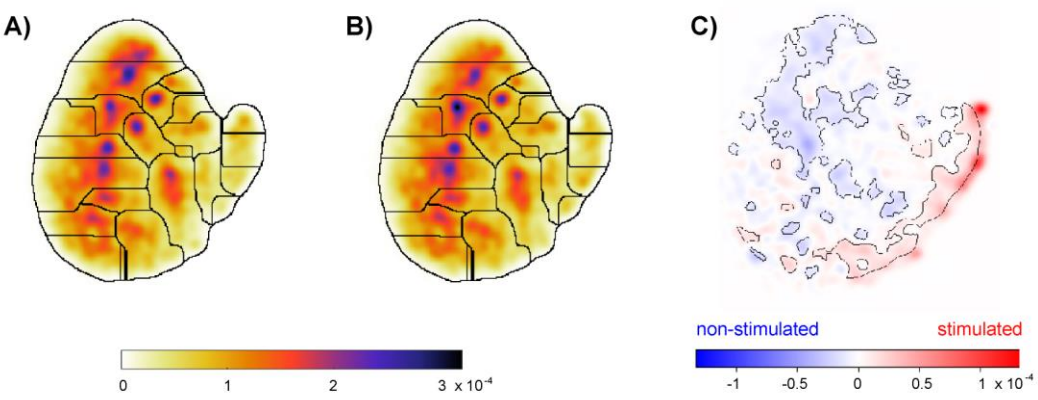

Figure 4.5. Differences in spontaneous and stimulated behavior. A) Behavioral PDF map of recordings prior to a mechanical pulse, across all timepoints and food conditions. B) Behavioral PDF map of recordings after a mechanical pulse, across all timepoints and food conditions. C) Difference between the two PDFs in A) and B). Outlined areas are statistically significantly different regions across the two maps.

4.4.3 Behavioral changes due to age

To observe how age impacts the behavior repertoire we examined changes in the condition without dietary perturbations. Behavioral recordings were grouped into two-day cohorts, and we performed hierarchical bootstrap sampling within groups to ensure even sampling across time and plotted the respective PDF within the behavior space (**Figure 4.6, Appendix C.2.5**). Following expected trends, as the population ages, their respective

behavior changes as well. In early adulthood (Day 2–4) the worms are highly active, largely residing in high movement, swimming region of the map. This aligns with the peak reproductive period of the worm's lifespan. As they age, they become increasingly less active (Day 4-10) residing in the slower moving, crawling activity behaviors, and once past the reproductive period and close to death (Day 10-18) they inhabit the idle regions. This qualitatively matches behavioral decline patterns found using commonly used movement metrics (**Figure 2.8b**, **Figure 3.9c**).

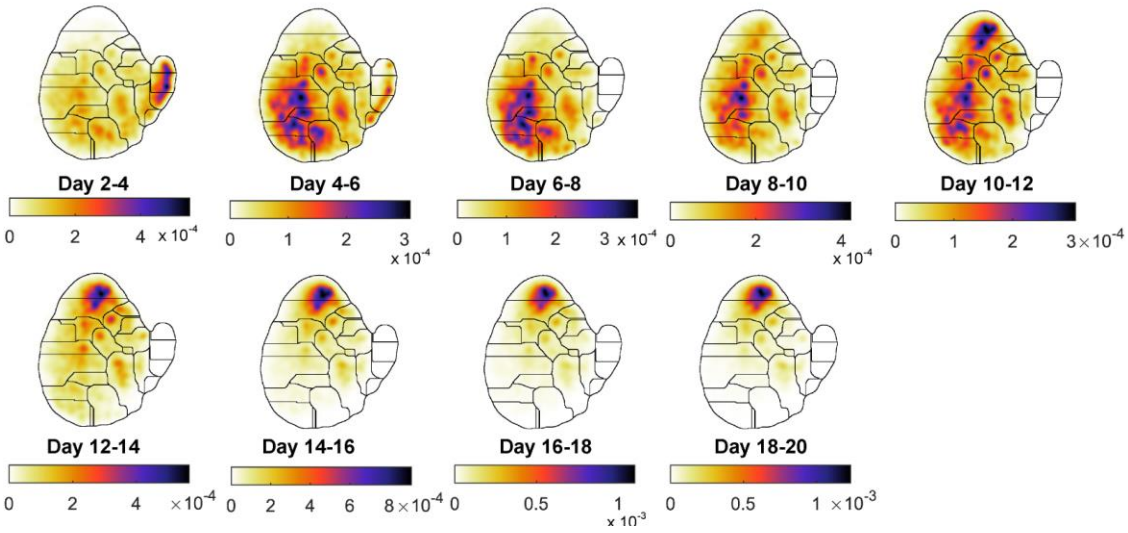

Figure 4.6. Differences in behavior across age. Behavioral PDF maps individuals cultured with no DR across their lifespan.

In addition to comparing the PDF maps with age, the behavioral transitions across regions were also compared across age groups (**Appendix C.2.6**). The structure is largely maintained across the different age groups, with regions transitioning to nearby or similar behaviors. However, one notable difference is that as the worms get into old age, certain transitions, such as the ones in the swimming area of the map, become much less frequent.

This is likely attributed to the significant drop in performing these behaviors during this age, which is underscored in the corresponding flux matrices.

4.4.4 Observing intrapopulation differences in aging

It is known that there is variation in the aging process within an isogenic population.[48,145] In **Chapter 2** we examined behavioral differences within the same population using basic movement-based metrics (**Figure 2.11**). Although there were identifiable differences for short- and long-lived individuals within populations across different genetic and thermal conditions in this earlier work, there was no significant difference in the movement levels for individuals cultured in high food conditions, a trend that was recapitulated in this independent set of experiments (**Figure 4.10b,d, Appendix C.2.7**). To take advantage of the depth of behavioral information captured using the t-SNE embedding method, and to parse out potential subtle differences in behavior, we examined the behavioral maps for the shortest- and longest-lived cohort within the population (**Figure 4.7).**

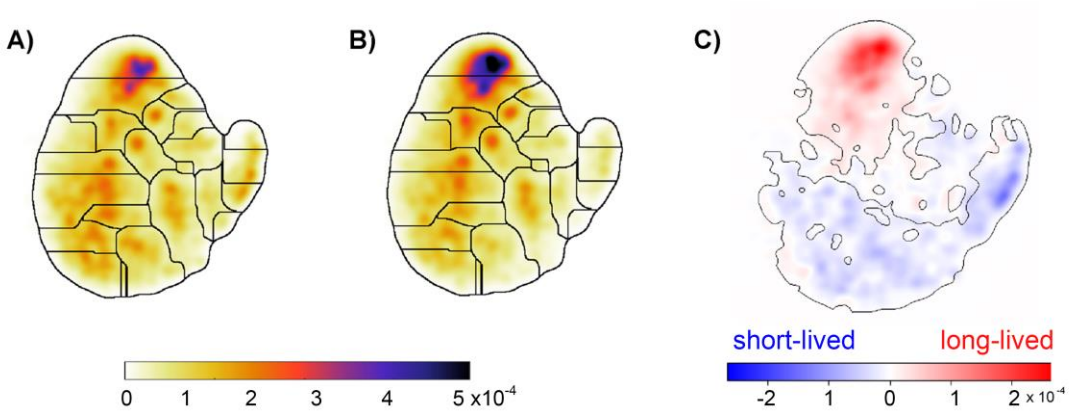

Figure 4.7. Differences in short- and long-lived individuals within an isogenic population. Short-lived individuals consist of the bottom 20th percentile in lifespan while long-lived

individuals consist of the top 20th percentile in lifespan. A) Behavioral PDF map of recordings of short-lived individuals, across all timepoints under no DR. B) Behavioral PDF map of recordings of long-lived individuals, across all timepoints under no DR. C) Difference between the two PDFs in A) and B). Outlined areas are statistically significantly different regions across the two maps.

Unlike traditional methods, there is a statistically significant difference between the PDF maps across the two cohorts (**Figure 4.7c**). Long-lived individuals had a higher likelihood of occupying the low moving, idle areas of the map, while short-lived individuals had a greater probability of subsiding in the high-movement, swimming area of the map. This difference across the cohorts is further underscored when examining the PDF maps across age groups (**Figure 4.8**). Both populations follow the same spatial trend within the map seen in **Figure 4.6**, but the relative amount of time spent in each region varies, with the short-lived individuals spending less time in the idle regions of the map. This is mirrored while comparing across their relative age (**Appendix C.2.8**), and qualitatively hints at a different aging path or trajectory across the two groups.

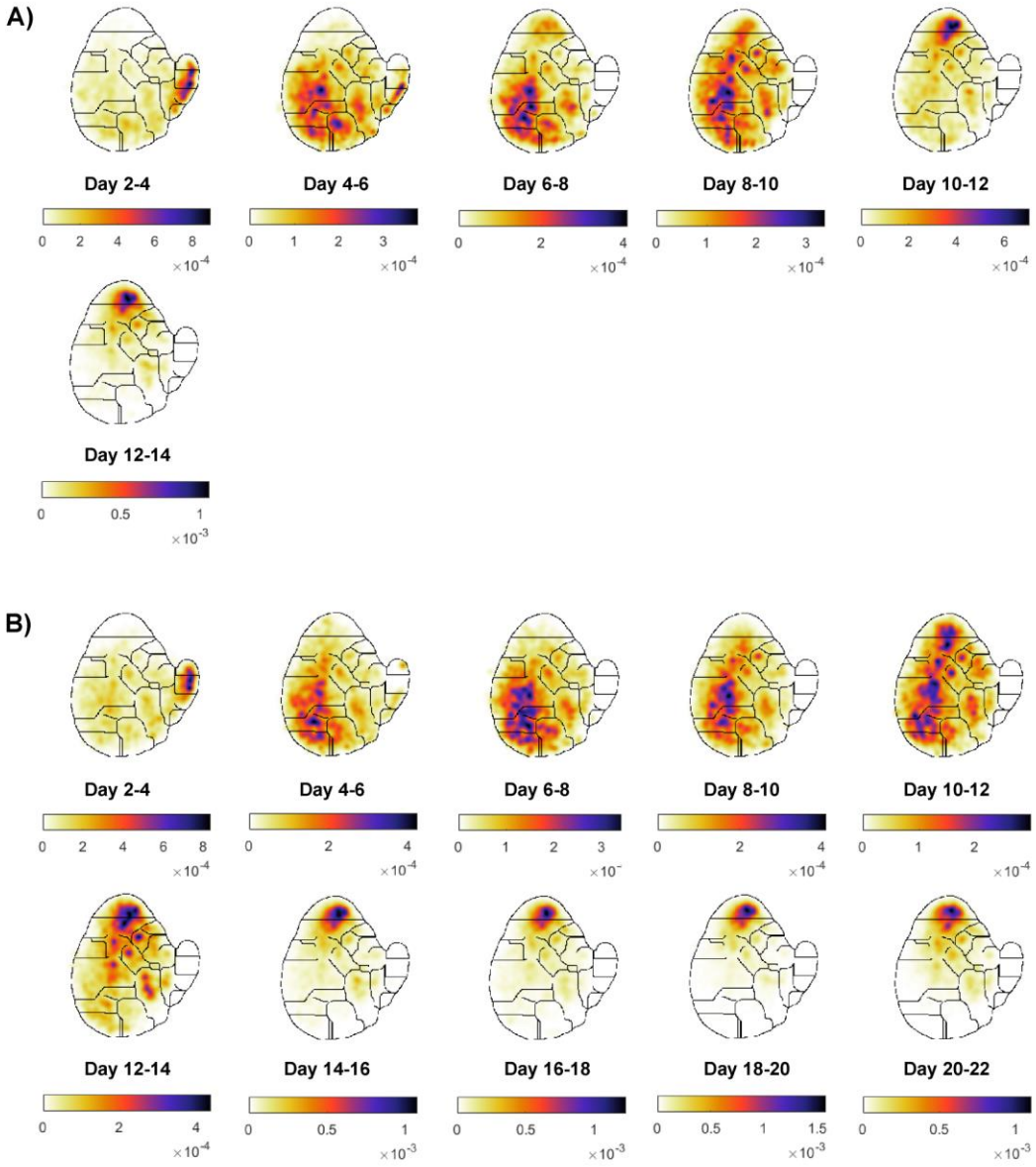

Figure 4.8 Differences in behavior of short-lived and long-lived isogenic individuals across age. A) Behavioral PDF maps of short-lived individuals cultured with no DR across their lifespan. B) Behavioral PDF maps of long-lived individuals cultured with no DR across their lifespan.

In addition to comparing the PDF maps within the behavioral space, we also wanted to quantitatively compare age-related behavioral changes. Similar to previous work,[142] we examined the behavioral covariance across time and food conditions and performed

eigendecomposition to extract the underlying structure (**Figure 4.9a**). From this, we found only one significant mode (**Figure 4.9b**), which delineates between the idle and moving regions on the map (**Figure 4.9c**). In addition, it also seems to capture some of the amplitude differences, with distinctions between the slower moving regions on the bottom left and the high movement, swimming behaviors on the map.

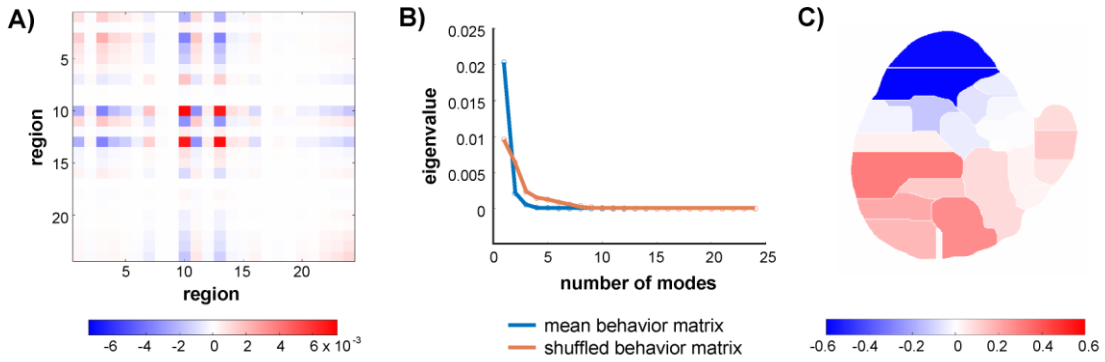

Figure 4.9. Behavioral covariance with age. A) Covariance matrix of behavior. B) Eigenvalues of the covariance matrix. Only 1 mode is significantly larger than the shuffled dataset. C) Eigenvectors of the first eigenvalue.

We then plotted the projection of each worm's individual behavior over time onto the significant eigenvector. When examining the shortest- and longest-lived individuals for the high food condition there was a distinct difference in their average behavioral dynamics with age (**Figure 4.10a,c**). Similar to previous literature, the short-lived individuals tend to remain active and experience a precipitous decline immediately prior to their death.[59,60,88] In contrast, older individuals have an extended period of low-movement in the last portion of their lifespan, apart from a slight increase of movement near the end of their life. This mirrors the trends qualitatively seen in the PDFs of the two populations, and further validates the idea of having distinct aging 'trajectories' within the same population, demonstrating this trend across different culture environments. Furthermore, this

underscores the potential for the t-SNE behavioral mapping technique to detect behavioral differences that are otherwise hidden using traditional, basic behavioral metrics**. (Figure 4.10b,d, Appendix C.2.7**).

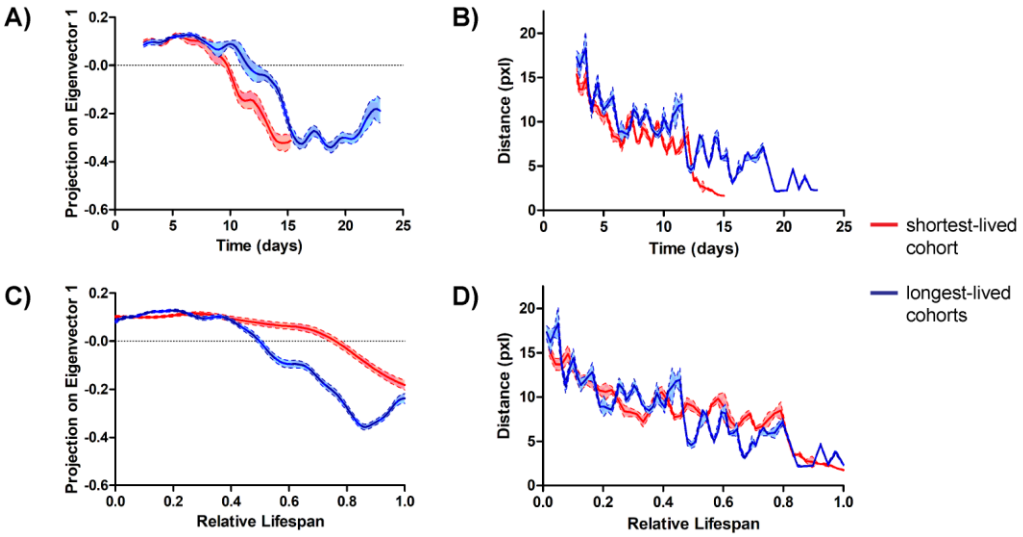

Figure 4.10. Differences in behavior for short- and long-lived individuals within an isogenic population with age. A) Projection onto the first eigenvector from the behavioral covariance matrix across time (error bars are the standard deviation from bootstrapped sampling). B) Maximum distance traveled by the centroid of the bounding box of the worm across time (error bars are SEM). C) Projection onto the first eigenvector from the behavioral covariance matrix across the normalized lifespan (error bars are the standard deviation from bootstrapped sampling). B) Maximum distance traveled by the centroid of the bounding box of the worm across the normalized lifespan (error bars are SEM).

4.4.5 Changes in behavior as a result of DR

In addition to examining the overall behavioral repertoire of worms, we examined how behavior changed in response to controlled environment perturbations, in the forms of caloric restriction (CR) and intermittent fasting (IF). To compare their respective behaviors, the behavioral recordings were plotted within a shared postural space (**Figure 4.11a-c**). The overall distribution patterns across the food conditions appear similar, with

large, stereotyped peaks occurring in the idle areas of Regions 7,10 and 13, and smaller peaks distributed in similar locations throughout the map, such as in the slower crawling areas. No behavioral region defined in the map is specific to a particular food condition. Additionally, the behavioral transitions across the food conditions are also conserved, with similar transition probabilities and structure across the different behavioral regions (**Appendix C.2.9**).

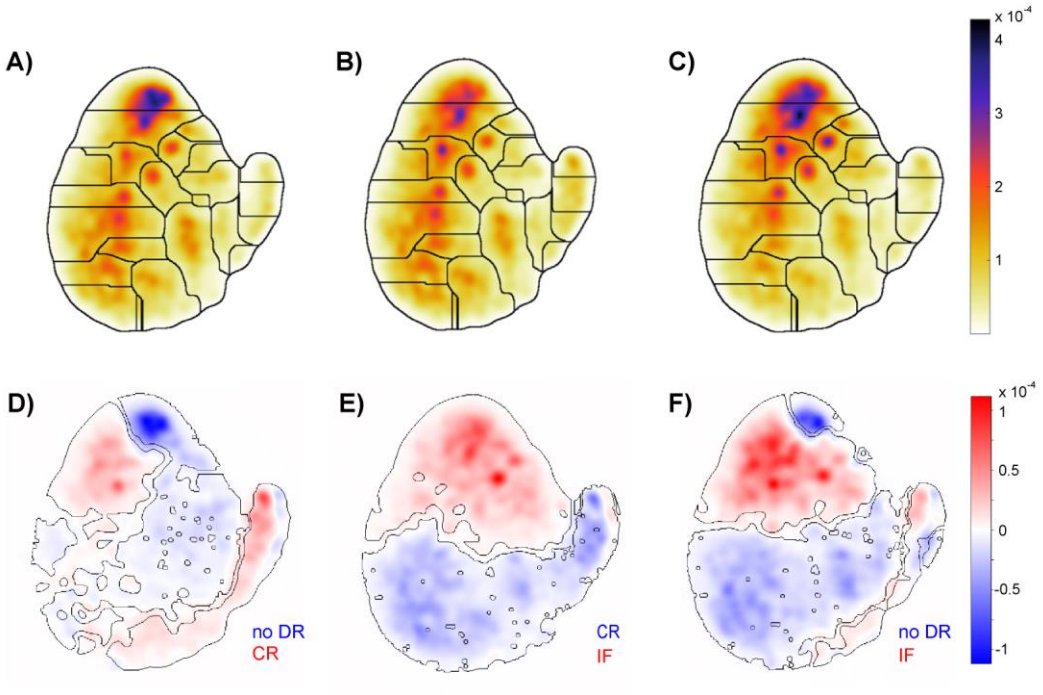

Figure 4.11. Differences in food conditions. A) Behavioral PDF of recordings of individuals cultured under no DR, across all timepoints. B) Behavioral PDF of recordings of individuals cultured under CR, across all timepoints. C) Behavioral PDF of recordings of individuals cultured under IF, across all timepoints. D) Difference between the PDFs of no DR and CR populations. Outlined areas are statistically significantly different regions across the two maps. E) Difference between the PDFs of CR and IF populations. Outlined areas are statistically significantly different regions across the two maps. F) Difference between the PDFs of no DR and IF populations. Outlined areas are statistically significantly different regions across the two maps.

Although the overall behavioral repertoires across the food conditions appear similar, there are subtle differences (**Figure 4.11d-f**). When comparing the different DR regimes, the worms under IF appear to be more idle, while the worms under CR more heavily reside in the active swimming and crawling portions of the map (**Figure 4.11e**). When compared to the population without DR, the two DR regimes appear to have similar trends (**Figure 4.11d,f**). The slower moving, crawling portions of the map are largely occupied by the cohort with no DR. While DR conditions appear to be more idle, a small subregion in Region 13 is highly popular for the high food conditions. Similarly, there appears to be subdivisions within the swimming areas of the worm, with the DR and non-DR conditions residing in distinct subregions within each region. This hints at further potential behavioral subdivisions not shown with the current level of categorization.

In addition to highlighting differences in behaviors across food conditions, there are distinct differences within the same dietary regime (**Figure 4.12**). The behavior of worms under IF significantly differs based on the currently experienced food level. While cultured in buffer, the preferred behavior of the worm is divided into two distinct groups, clustering either in the idle region of the map or in the region capturing active swimming. This follows known trends of swimming behavior in *C. elegans*, in where if cultured in liquid for long-time scales individuals have been shown to oscillate between active swimming and a stationary, quiescent stage, a potentially adaptive behavior.[146,147] Although this has been examined on the order of hours, this has not been a commonly reported phenomena on the timescale of days. In contrast, while under high food conditions, the worms are more likely to undergo the slow, crawling behaviors captured in

the bottom left portion of the map, mirroring the PDF of worms constantly cultured in constant food conditions.

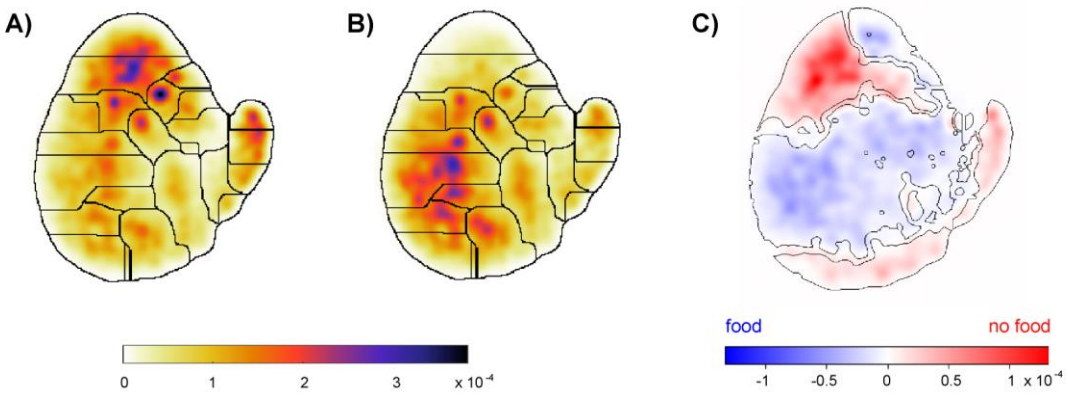

Figure 4.12. Differences in behavior during IF. A) Behavioral PDF of recordings of individuals cultured under IF with no food present, across all timepoints. B) Behavioral PDF of recordings of individuals cultured under IF with food present, across all timepoints. C) Difference between the PDFs of food and no food present for the IF population. Outlined areas are statistically significantly different regions across the two maps.

4.4.6 Changes in behavior with age across DR regimes

In addition to observing how different forms of DR influence both the longevity and behavior of the worm, we are interested in how external modulators alter behaviors and behavioral preferences change with age. These changes could give insight into the internal state of individuals and potentially link their behavior with their physiological age. Similar to the previous examination into the single-food condition, the behaviors for each food condition were grouped into two-day cohorts and plotted the PDFs within the same behavioral space **(Figure 4.13**).

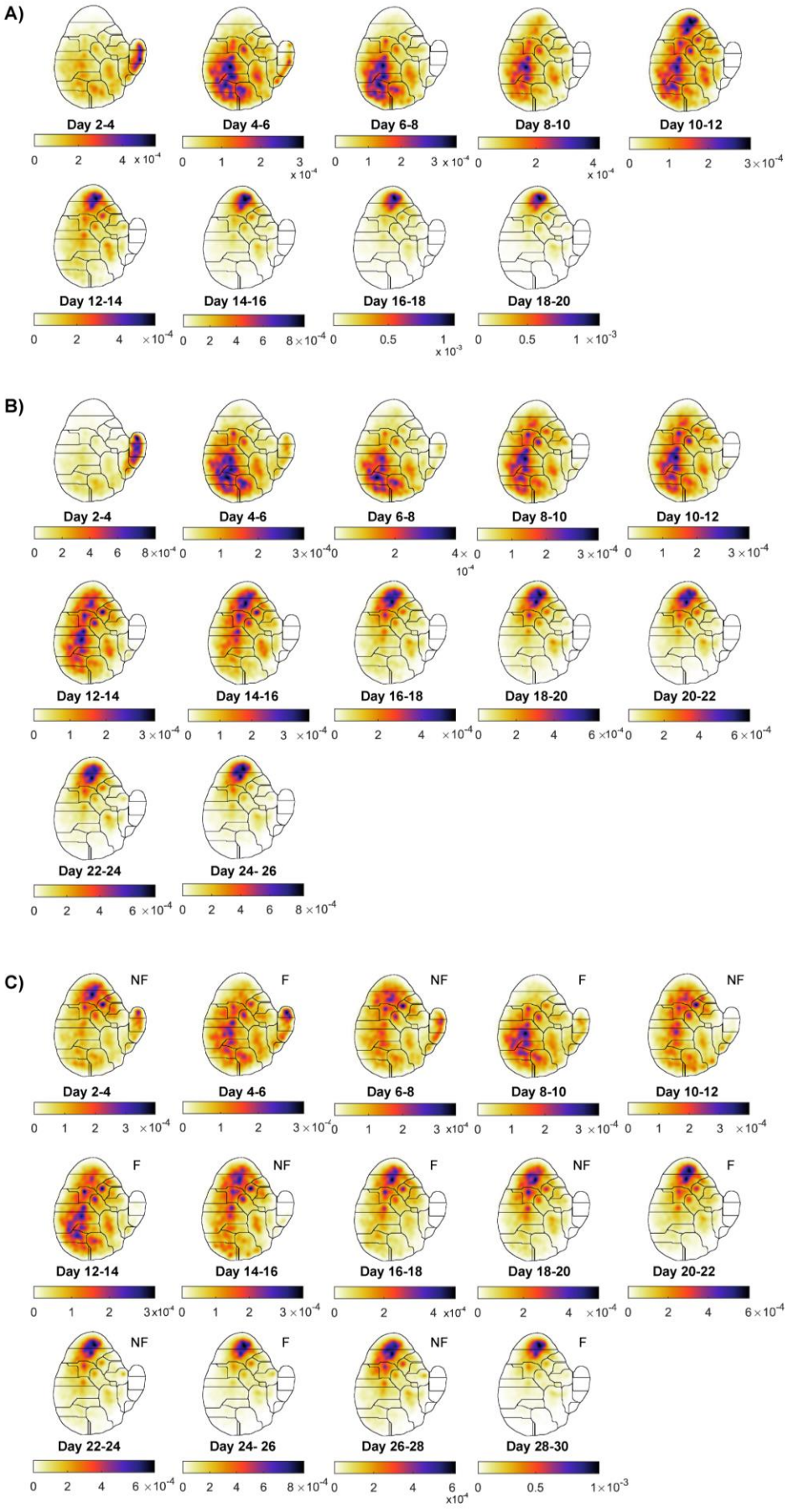
A)
Day 2-4
Day 4-6
Day 6-8
Day 8-10
Day 10-12
Day 12-14
Day 14-16
Day 16-18
Day 18-20
B)
Day 2-4
Day 4-6
Day 6-8
Day 8-10
Day 10-12
Day 12-14
Day 14-16
Day 16-18
Day 18-20
Day 20-22
Day 22-24
Day 24- 26
C)
NF
F
Day 2-4
Day 4-6
Day 6-8
Day 8-10
Day 10-12
Day 12-14
Day 14-16
Day 16-18
Day 18-20
Day 20-22
Day 22-24
Day 24- 26
Day 26-28
Day 28-30

Figure 4.13. Differences in behavior across food conditions across age. A) Behavioral PDF maps of individuals cultured with no DR across their lifespan. B) Behavioral PDF maps of individuals cultured under CR across their lifespan. C) Behavioral PDF maps of individuals cultured under IF across their lifespan.

The behavioral changes for the low food condition resemble the aging trajectory seen in the high food condition; during early adulthood (Day 2-4) the worms are largely active, in the swimming region of the map. With age, (Day 4-12) they increasingly occupy the bottom intermediate areas, eventually residing in the upper idle regions of the map for the second half of their lifespan (Day 12-26). In contrast to the high food condition, the worms under CR perform swimming behaviors more frequently early in life (**Figure 4.13a,b, Appendix C.2.10**). This follows expected trends,[88] with individuals in lower food levels having increased activity, likely searching for greater food concentrations. In addition, the CR population appears to spend more time in a transitionary period from the lower, active regions to the upper idle regions on the map (Day 10-16) and spends more time in its life within the idle regions (Day 16 – 26), seemingly scaling the time spent in the areas of the map based on lifespan (**Appendix C.2.10**).

Dietary restriction has been shown to influence the reproductive peak and period of individuals, reducing the number of progeny but extending the period of reproduction.[148] Similar to the high food condition, we qualitatively observed a peak period of fecundity in early adulthood (Day 2-4); however, we did observe an extended period of reproduction, with an absence of large egg cluster and with many chambers no longer having eggs around Day 7- 8 of adulthood, mirroring the decline in swimming, active movement during that age.

In contrast to the similar behavioral patterns across the high food and CR populations, the IF population displayed distinct behavioral preferences in early to mid-adulthood. In early adulthood under no exposure to food condition, they were largely centered around the high frequency swimming behavior along with the idle regions near the top of the map, mirroring the dichotomy seen in **Figure 4.12a**. In contrast, from Day 4-6, under the high food condition, the worms were spread out throughout the map, with large peaks in the swimming regions and the active, slower moving bottom regions of the map. The dichotomy between the two food conditions within the IF regime is largely apparent early in life; this oscillation between states begins to lessen during mid adulthood (Day 10 onwards), with the worms eventually mainly occupying the idle regions in mid- to late adulthood (Day 16-30). Similar to prior food conditions, the IF condition occupies mainly the idle regions in the latter half of the lifespan.

In addition to exhibiting distinct density functions dependent on the food currently exposed to the worm, there were striking similarities in the density functions of the worms cultured under IF experiencing high food levels, and those under no DR (**Figure 4.14**). This is apparent through the majority of the lifespan of the IF condition, with plots generally mirroring earlier timepoints seen in the constant high food condition. Although there are statistically significant differences in the maps across the food conditions (**Appendix C.2.11**), this similarity hints at the possibility that aging and age-related behavioral changes can be attenuated or even temporally delayed in response to DR. Previous studies have shown a similar link between changes in mortality rates in response to the instigation of DR at different ages.[29] This phenomenon could potentially be modulated by the presented food levels, timing of DR, and frequency of food switching.

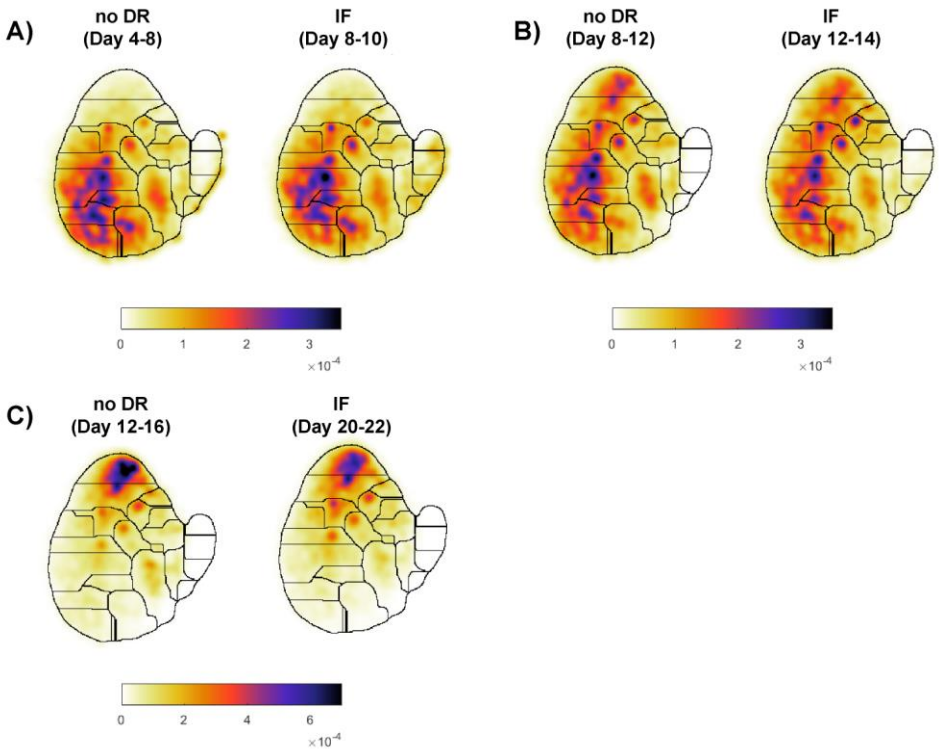

Figure 4.14. Differences in behavior across no DR and IF conditions across age. A) Behavioral PDF maps of individuals cultured with no DR from Day 4-8 of adulthood and individuals cultured with IF, in the presence of food, from Day 8-10. B) Behavioral PDF maps of individuals cultured with no DR from Day 8-12 of adulthood and individuals cultured with IF, in the presence of food, from Day 12-14. C) Behavioral PDF maps of individuals cultured with no DR from Day 12-16 of adulthood and individuals cultured with IF, in the presence of food, from Day 20-22.

In addition to examining the spatial and temporal relationships of the behavioral regions over time across food conditions, we also wanted to quantitatively compare age-related behavioral changes. Similar to examining the shortest- and longest-lived cohorts within an isogenic population, we compared the time series projections on the first eigenvector for the behavioral covariance across time and food conditions (**Figure 4.15**). The average projection of the high food and CR conditions appears similar early in life; however, at around Day 8 the average of high food condition appears to diverge from the average CR condition. This sudden downward trajectory also occurs for the CR condition

at a delayed timepoint, at around Day 10, with the rate of decline similar to the condition under no DR. Interestingly, this point of inflection occurs at the same time in where the worms on the PDF begin to increasingly occupy the idle regions on the map, potentially hinting at the end of the period of life in where worms reliably are able or willing to perform active spontaneous movement. Near the end of the very end of their life, both populations have a slight positive slope in the average projection. Qualitatively we have often observed a bout of spontaneous movement immediately prior to death, which, though masked in the PDF plots, is recapitulated through the projections.

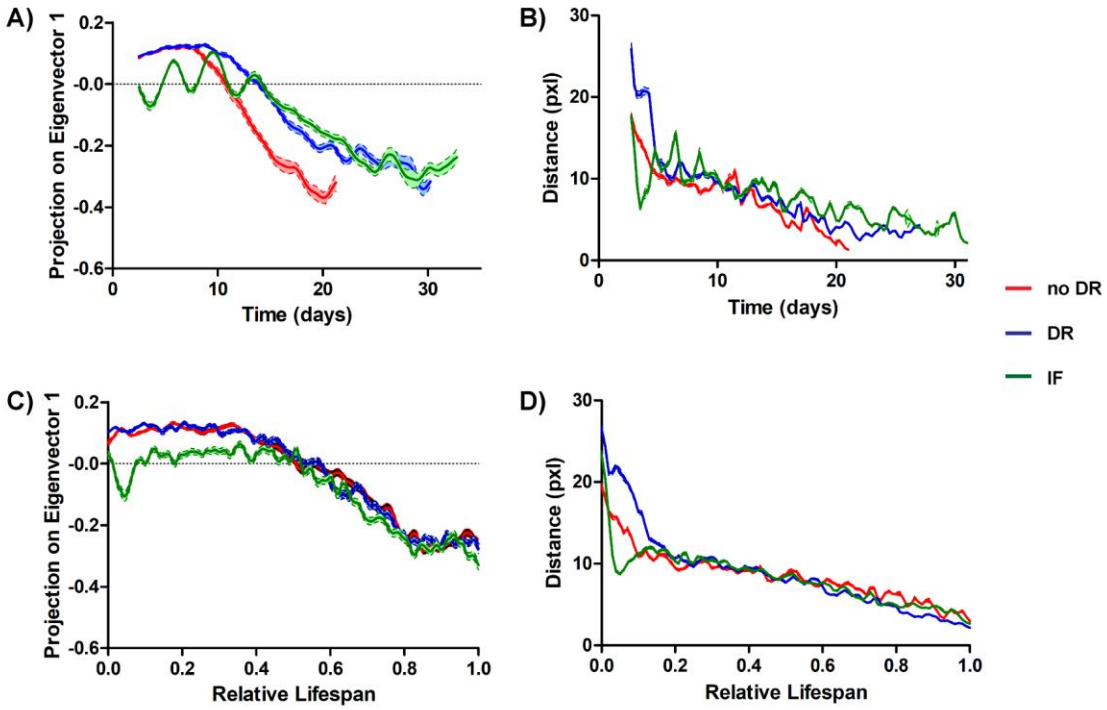

Figure 4.15. Differences in behavior across different food conditions with age. A) Projection onto the first eigenvector from the behavioral covariance matrix across time (error bars are the standard deviation from bootstrapped sampling). B) Maximum distance traveled by the centroid of the bounding box of the worm across time (error bars are SEM). C) Projection onto the first eigenvector from the behavioral covariance matrix across the normalized lifespan (error bars are the standard deviation from bootstrapped sampling). B)

Maximum distance traveled by the centroid of the bounding box of the worm across the normalized lifespan (error bars are SEM).

In contrast to the constant food conditions, the projections of the IF condition appear to oscillate in early to mid-adulthood (Day 2-10), with the periodicity correlating with the food switching frequency (**Appendix C.2.13**). Although there were differences in the PDFs (**Appendix C.2.11**), the average projection of the periods under the high food condition in IF are comparable to the projection values seen in earlier time points under the constant high food conditions (**Appendix C.2.12**), mirroring the qualitative trends seen in the density plots in **Figure 4.14**. With age, after Day 10, the average projection also appears to decline, albeit at a smaller slope than seen in the constant food conditions.

Both the projections and traditional metrics capture differences in behavior with age across food conditions; however, they highlight distinct aspects of behavior. For the IF condition, while traditional methods appear to capture the environmental oscillations throughout the lifespan, the projections and PDFs illustrate a dampening of environmental influence on behavior with age, with worms performing similar types of behaviors later in life, regardless of environmental condition. For the static food conditions, traditional metrics are able capture early in life differences, with worms in CR having higher levels of movement, likely attributed to increased food searching behavior, while the projections from the t-SNE analysis show no discernable difference. However, as they age the levels of movement are comparable, while the average projections and corresponding demonstrate a stark difference. Previous metrics demonstrate a non-linear scaling of movement decline across high food and DR conditions. In contrast, t-SNE analysis illustrates that worms under CR follow the same aging ‘path’ on the behavioral map,

performing the same types of behaviors with age linearly scaled to the individual's lifespan. Thus, though the extent of absolute movement does not linearly scale with age, the types of behaviors performed with age over time does, illustrating how this method of analysis could give complementary insights into the behavior and overall health of the individual.

4.5 Conclusions

In **Chapter 4**, I demonstrate the use of t-SNE behavioral analysis to explore age-related changes in *C. elegans*. I defined the entire behavioral repertoire of the worm within the microfluidic environment throughout its entire adult life, across over 515 hours of behavioral recordings. From this, I extracted stereotyped behaviors in an unbiased manner and characterized the temporal relationship between the different behaviors. I explored how known environmental modulators of longevity – CR and IF – influenced both the behavioral repertoire of the animal, along with age-related behavioral changes.

Although this approach is computationally intensive and requires large amounts of behavioral recordings, it is also able to highlight subtle behavioral differences that are not otherwise captured using traditional movement metrics. This was demonstrated in two distinct cases. The first was in observing the differences within an isogenic population. The shortest- and longest-lived cohorts in the high food condition had distinct behavioral 'trajectories' during the aging process, which was not apparent using basic movement metrics. The second was seen in the case of DR, in where we demonstrated that the average behavioral 'trajectory' scales linearly with age, in contrast to the non-linear of movement decline under high food and CR conditions.

Overall, the work performed in this chapter establishes a novel way of examining aging and age-related behavioral changes in *C. elegans*. This can be used to create valuable insights into how different genetic or environmental modulators of aging influence behavior in previously undetected ways, and better characterize how behavior is linked to the internal state and physiological age of the individual.

CHAPTER 5. CONCLUSIONS AND FUTURE DIRECTIONS

5.1 Thesis Contributions

The objective of this thesis was to develop tools and analytical techniques to investigate aging and longevity in *C. elegans*. The work addresses several technological gaps associated with existing methodologies, on both the data collection and on the subsequent behavioral analysis front. Current aging assays and culture systems are not able to provide robust, long-term culture and behavioral monitoring with single worm level resolution and precise spatiotemporal control. In terms of data analysis, existing tools lack the flexibility and scalability to accurately segment or extract features of interest within large, heterogenous datasets. Furthermore, conventional behavioral metrics used in aging studies are low-content and are unable to detect subtle behavioral differences between groups of interest. The platform, segmentation pipeline, and alternative approach to behavioral analysis overcome these limitations, to help better investigate modulators of aging and their impact on the health and age-related changes in behavior in a high-throughput manner.

In **Chapter 2**, in collaboration with Dr. Mei Zhan and Dr. Yongmin Cho, I developed HeALTH, an automated microfluidic-based platform designed for the long-term culture and behavioral recordings of *C. elegans* throughout their lifespan. The system allows for single-animal, longitudinal behavioral recordings, along with precise spatiotemporal environmental control. I improved both the design and culture protocol of the initial system for increased experimental viability and usability. This experimental robustness was demonstrated in three separate examples of large-scale aging studies. We

examined how mutations in the IIS pathway influence changes in movement with age. We explored how DR, in the form of CR, altered the level of activity and relative movement decline across populations. Lastly, we explored how temperature, and controlled diurnal temperature oscillations, influence the aging process. This underscores the power and versatility of the system to be used for a wide array of high-throughput aging and longevity studies, providing high-content behavioral data with fine spatial and temporal resolution.

In **Chapter 3** I designed a flexible, deep-learning based pipeline to extract worm postures from complex, heterogenous conditions and environments. It uses Mask R-CNN and Faster R-CNN to perform and confirm instance segmentation of the worm of interest, significantly outperforming conventional image processing techniques and existing, machine learning based image processing packages. It is also able to accurately track and extract the centerline in complex poses, allowing the user to observe and analyze occluded or coiled postures. Although this pipeline requires training the deep-learning models for the accurate segmentation of the worm, it is accurate and flexible across conditions post training, and easily scalable, designed for parallel computing, making it a powerful method for analyzing large-scale recordings (on the order of terabytes). In addition, in collaboration with Dr. Kathleen Bates, I demonstrate how object detection using Faster R-CNN can be used to obtain coarse behavioral information in the context of ethological behavioral studies. It is able to recapitulate commonly used metrics, such as distance traveled over a set period of time or the movement of an individual and was able to separate two distinct behavioral phenotypes. By creating a robust and scalable tool for extracting both basic behavioral metrics and complex pose information, this will enable researchers to extract

and subsequently analyze behavior in a wide variety of contexts, providing greater insights into the fields of aging and ethology.

In **Chapter 4** I investigated the impact of two distinct forms of dietary restriction – caloric restriction and intermittent fasting – on longevity and age-related behavioral changes in *C. elegans.* In contrast to conventional behavioral metrics, I used an unbiased, data-driven approach to identify stereotyped behaviors and defined the entire behavioral repertoire of the worm throughout its entire lifespan using a large-scale behavioral dataset (with over 515 hours of recordings). Using this untraditional approach, I identified differences in aging behaviors within an isogenic population under the same culture conditions, and in worms under CR and IF, changes that were otherwise undetected using traditional movement measurements. This provides insight into a complementary approach of examining aging and age-related behavioral changes in *C. elegans*, which could potentially detect the influence of subtle genetic or environmental modulators of aging.

5.2 Future Directions

The work presented in this thesis illustrates the capabilities of the tools and analysis techniques developed to facilitate the study of aging and age-related changes in behavior in *C. elegans.* In this section, I discuss a few possible applications for these tools along with opportunities for further development.

5.2.1 Sex-specific changes in healthspan and longevity

There are known sex specific differences in aging.[19,149–151] A stark example of the dimorphism between the two sexes in *C. elegans* is DR - while DR extends lifespan in

hermaphrodites, it has little to no impact on the longevity of male *C. elegans*.[152] However, the vast majority of aging studies in *C. elegans* are performed using hermaphrodites. This is in large part due to the difficultly of performing traditional lifespan assays with male worms. The deleterious impact of male pheromone on longevity prevents large population assays with males, and it is extremely difficult to scale studies that examine isolated, individually cultured males.[153,154] These handling and scalability challenges makes it difficult to examine how different genetic or environmental perturbations have sex specific influences.

Using the HeALTH platform, we could individually culture male worms on a large-scale and observe how their lifespan and behavior changes in response to a variety of stimuli. The constant fluid flow would eliminate the presence of the male pheromone in the environment, preventing confounding, premature causes of death. Using this high-throughput, versatile tool, we could observe and compare the sex specific response to ascaroside pheromones, genetic perturbations in the IIS pathway, and even perform drugs screens to observe whether the mechanism for lifespan extension are preserved across the different sexes. In addition, this could also be used in a non-aging specific context, to better capture and characterize the behavior of the male worm outside the context of mating.

5.2.2 Increasing the phenotypes obtained with HeALTH

Currently, the HeALTH platform captures whole-body behavior on an individual level. In this thesis (**Chapters 2 & 4**), I have demonstrated how behavior can be used as an insightful phenotype to observe aging and the health of an individual. However, additional metrics – either physiological or behavioral – have been shown to add a greater

depth and accuracy in gauging the internal state and underlying health of individuals.[50,51,59,102] By modifying the recording scheme along with the imaging and illumination hardware, we may be able to increase the breadth of collected information.

For instance, by increasing the temporal resolution of recordings we would be able to better track the fecundity of individuals, a known metric for measuring the health of individuals.[59,77,155] Due to the use of C22, the worms lay progeny, which are trapped in the microfluidic chamber until being pushed out of the outlet channel. This often does not occur until a strong mechanical pulse, resulting in a higher flow rate, due to the small size of the channel (30μm height) and comparable size of an embryo (~30μm in diameter). If the platform captured images immediately prior to the mechanical pulsing, which occurs on an hourly basis, we would likely be able to accurately track the trends in the accumulation of eggs for each worm and estimate its relative fecundity over time. The measurement of the accumulation of eggs could easily be automated using the analysis pipeline developed in **Chapter 3**; the Mask R-CNN model is already trained to segment eggs within the chamber. Basic morphological metrics, such as the area of the egg clusters, could be used to estimate egg count.

By adding a fluorescent imaging module to the platform, we would be able to measure coarse autofluorescence in the worm's entire body, as a proxy for lipofuscin accumulation, which has shown to have a strong correlation with lifespan and physiological health.[49,52] Furthermore, the depending on the resolution of the camera, it may be able to detect and capture localized fluorescent expression within the worm. This opens the door to a multitude of options, ranging from measuring gene expression levels for genes of interest to examining neuronal activity using GCaMP and tracking changes over the

lifespan of the individual. Not only would this give substantial insight into how specific gene expression or neural activity changes with age, but we could also link expression with the behaviors performed by the individual. This would give us substantial insight into how internal states result in behavioral outputs, and how that impacts long-term outcomes in longevity and health.

5.2.3 Expanding the defined behavioral repertoire and exploring age-related behavioral changes across genetic and environmental perturbations

In **Chapter 4** we explored an alternative method to examine and compare changes in behavior with age across different perturbations. Although we examined two distinct forms of DR, there are a plethora of different genetic and alternative environmental modulators of aging that have yet to be explored in terms of their impact on behavioral changes with age. A prime example would be the canonical IIS mutants – do *daf-2* mutants and *daf-16* mutants exhibit the same stereotyped behaviors, behavioral range, and changes with age? Another question would be whether known pharmaceutical interventions shown to extend lifespan in *C. elegans* delay behavioral changes, mirroring the impact of IF compared to individuals cultured in constant high food conditions (**Figure 4.14, Figure 4.15**). Lastly, could features from this analysis method be used as an accurate, predictive measure of physiological age and eventual lifespan, thus illustrating the full capabilities of behavior as a method for gauging the internal state of an individual?

Additionally, this behavioral space was obtained from videos of worms cultured in a very specific environment. Confined within the microfluidic chamber, the animals were unable to perform behaviors typically performed on agar plates. Another potential

continuation would be to perform similar analysis on aged worms on the conventional agar environment and compare the behavioral differences based on the context of the reared environment. Although the agar environment would not allow for as precise spatiotemporal environmental control, it would provide a more direct comparison to the majority of behavioral studies performed within the *C. elegans* neuroethology community.

APPENDIX A. CHAPTER 2 SUPPLEMENTARY MATERIAL

The figures below are adapted from a research article entitled "An automated platform to monitor long-term behavior and healthspan in *Caenorhabditis elegans* under precise environmental control" published in Nature Communications Biology in 2020.[88]

A.1 Raw Data for Survival Analysis

Table A.1.1. Lifespan data on HeALTH platform.

Censored idividuals are highlighted in grey. Temperature and food perturbations were implemented at Day 2 of adulthood.

Temperature (°C)	Strain	Food Level (OD600)	Date of L4	Device	Chamber	Age at Death
25	N2	OD5	9/21/2018	Exp29	4	18
25	N2	OD5	9/21/2018	Exp29	5	15
25	N2	OD5	9/21/2018	Exp29	9	21
25	N2	OD5	9/21/2018	Exp29	10	16
25	N2	OD5	9/21/2018	Exp29	11	17
25	N2	OD5	9/21/2018	Exp29	13	16
25	N2	OD5	9/21/2018	Exp29	14	14
25	N2	OD5	9/21/2018	Exp29	18	16
25	N2	OD5	9/21/2018	Exp29	19	17
25	N2	OD5	9/21/2018	Exp29	32	18
25	N2	OD5	9/21/2018	Exp29	34	14
25	N2	OD5	9/21/2018	Exp29	36	15
25	N2	OD5	9/21/2018	Exp29	37	15
25	N2	OD5	9/21/2018	Exp29	38	13
25	N2	OD5	9/21/2018	Exp29	41	18
25	N2	OD5	9/21/2018	Exp29	43	20
25	N2	OD5	9/21/2018	Exp29	45	18
25	N2	OD5	9/21/2018	Exp29	46	15
25	N2	OD5	9/21/2018	Exp29	47	18
25	N2	OD5	9/21/2018	Exp29	50	14
25	N2	OD5	9/21/2018	Exp29	55	18
25	N2	OD5	9/21/2018	Exp29	56	14
25	N2	OD5	9/21/2018	Exp29	58	15
25	N2	OD5	9/21/2018	Exp29	60	17

Table A.1.1 continued

25	N2	OD5	10/23/2018	Exp65	2	21
25	N2	OD5	10/23/2018	Exp65	3	17
25	N2	OD5	10/23/2018	Exp65	5	15
25	N2	OD5	10/23/2018	Exp65	7	16
25	N2	OD5	10/23/2018	Exp65	10	18
25	N2	OD5	10/23/2018	Exp65	11	21
25	N2	OD5	10/23/2018	Exp65	14	21
25	N2	OD5	10/23/2018	Exp65	16	21
25	N2	OD5	10/23/2018	Exp65	17	18
25	N2	OD5	10/23/2018	Exp65	20	18
25	N2	OD5	10/23/2018	Exp65	22	18
25	N2	OD5	10/23/2018	Exp65	24	24
25	N2	OD5	10/23/2018	Exp65	25	16
25	N2	OD5	10/23/2018	Exp65	26	21
25	N2	OD5	10/23/2018	Exp65	27	22
25	N2	OD5	10/23/2018	Exp65	28	7
25	N2	OD5	10/23/2018	Exp65	29	20
25	N2	OD5	10/23/2018	Exp65	30	26
25	N2	OD5	10/23/2018	Exp65	31	12
25	N2	OD5	10/23/2018	Exp65	32	16
25	N2	OD5	10/23/2018	Exp65	33	21
25	N2	OD5	10/23/2018	Exp65	34	14
25	N2	OD5	10/23/2018	Exp65	35	19
25	N2	OD5	10/23/2018	Exp65	39	23
25	N2	OD5	10/23/2018	Exp65	41	15
25	N2	OD5	10/23/2018	Exp65	43	12
25	N2	OD5	10/23/2018	Exp65	44	20
25	N2	OD5	10/23/2018	Exp65	45	15
25	N2	OD5	10/23/2018	Exp65	47	21
25	N2	OD5	10/23/2018	Exp65	48	23
25	N2	OD5	10/23/2018	Exp65	51	15
25	N2	OD5	10/23/2018	Exp65	52	18
25	N2	OD5	10/23/2018	Exp65	53	14
25	N2	OD5	10/23/2018	Exp65	54	20
25	N2	OD5	10/23/2018	Exp65	56	20
25	N2	OD5	10/23/2018	Exp65	57	23
25	N2	OD5	10/23/2018	Exp65	58	19
25	N2	OD5	10/23/2018	Exp65	59	19
25	N2	OD5	10/7/2018	Exp60	1	19
25	N2	OD5	10/7/2018	Exp60	2	20
25	N2	OD5	10/7/2018	Exp60	8	21
25	N2	OD5	10/7/2018	Exp60	20	15
25	N2	OD5	10/7/2018	Exp60	21	23
25	N2	OD5	10/7/2018	Exp60	22	27
25	N2	OD5	10/7/2018	Exp60	24	17

Table A.1.1 continued

25	N2	OD5	10/7/2018	Exp60	26	20
25	N2	OD5	10/7/2018	Exp60	27	19
25	N2	OD5	10/7/2018	Exp60	28	20
25	N2	OD5	10/7/2018	Exp60	29	19
25	N2	OD5	10/7/2018	Exp60	30	18
25	N2	OD5	10/7/2018	Exp60	33	26
25	N2	OD5	10/7/2018	Exp60	38	20
25	N2	OD5	10/7/2018	Exp60	40	14
25	N2	OD5	10/7/2018	Exp60	45	16
25	N2	OD5	10/7/2018	Exp60	46	21
25	N2	OD5	10/7/2018	Exp60	47	19
25	N2	OD5	10/7/2018	Exp60	48	19
25	N2	OD5	10/7/2018	Exp60	50	19
25	N2	OD5	10/7/2018	Exp60	52	16
25	N2	OD5	10/7/2018	Exp60	53	19
25	N2	OD5	10/7/2018	Exp60	54	18
25	N2	OD5	10/7/2018	Exp60	55	26
25	N2	OD5	10/7/2018	Exp60	57	21
25	N2	OD5	2/18/2019	Exp20	1	15
25	N2	OD5	2/18/2019	Exp20	3	19
25	N2	OD5	2/18/2019	Exp20	4	24
25	N2	OD5	2/18/2019	Exp20	5	16
25	N2	OD5	2/18/2019	Exp20	6	24
25	N2	OD5	2/18/2019	Exp20	7	19
25	N2	OD5	2/18/2019	Exp20	9	16
25	N2	OD5	2/18/2019	Exp20	13	14
25	N2	OD5	2/18/2019	Exp20	15	20
25	N2	OD5	2/18/2019	Exp20	16	10
25	N2	OD5	2/18/2019	Exp20	17	18
25	N2	OD5	2/18/2019	Exp20	19	22
25	N2	OD5	2/18/2019	Exp20	20	20
25	N2	OD5	2/18/2019	Exp20	21	19
25	N2	OD5	2/18/2019	Exp20	22	20
25	N2	OD5	2/18/2019	Exp20	24	19
25	N2	OD5	2/18/2019	Exp20	27	16
25	N2	OD5	2/18/2019	Exp20	28	22
25	N2	OD5	2/18/2019	Exp20	29	12
25	N2	OD5	2/18/2019	Exp20	30	13
25	N2	OD5	2/18/2019	Exp20	32	20
25	N2	OD5	2/18/2019	Exp20	35	17
25	N2	OD5	2/18/2019	Exp20	37	19
25	N2	OD5	2/18/2019	Exp20	39	20
25	N2	OD5	2/18/2019	Exp20	42	20
25	N2	OD5	2/18/2019	Exp20	43	17
25	N2	OD5	2/18/2019	Exp20	44	28

Table A.1.1 continued

25	N2	OD5	2/18/2019	Exp20	45	19
25	N2	OD5	2/18/2019	Exp20	47	24
25	N2	OD5	2/18/2019	Exp20	48	20
25	N2	OD5	2/18/2019	Exp20	50	17
25	N2	OD5	2/18/2019	Exp20	52	20
25	N2	OD5	2/18/2019	Exp20	53	18
25	N2	OD5	2/18/2019	Exp20	54	18
25	N2	OD5	2/18/2019	Exp20	55	17
25	N2	OD5	2/18/2019	Exp20	56	10
25	N2	OD5	2/18/2019	Exp21	3	22
25	N2	OD5	2/18/2019	Exp21	6	16
25	N2	OD5	2/18/2019	Exp21	10	16
25	N2	OD5	2/18/2019	Exp21	11	21
25	N2	OD5	2/18/2019	Exp21	14	19
25	N2	OD5	2/18/2019	Exp21	16	19
25	N2	OD5	2/18/2019	Exp21	17	21
25	N2	OD5	2/18/2019	Exp21	20	20
25	N2	OD5	2/18/2019	Exp21	23	24
25	N2	OD5	2/18/2019	Exp21	25	19
25	N2	OD5	2/18/2019	Exp21	27	23
25	N2	OD5	2/18/2019	Exp21	28	19
25	N2	OD5	2/18/2019	Exp21	29	18
25	N2	OD5	2/18/2019	Exp21	30	21
25	N2	OD5	2/18/2019	Exp21	31	10
25	N2	OD5	2/18/2019	Exp21	34	21
25	N2	OD5	2/18/2019	Exp21	40	23
25	N2	OD5	2/18/2019	Exp21	41	15
25	N2	OD5	2/18/2019	Exp21	44	20
25	N2	OD5	2/18/2019	Exp21	46	21
25	N2	OD5	2/18/2019	Exp21	50	16
25	N2	OD5	2/18/2019	Exp21	51	15
25	N2	OD5	2/18/2019	Exp21	52	19
25	N2	OD5	2/18/2019	Exp21	53	13
25	N2	OD5	2/18/2019	Exp21	54	22
25	N2	OD5	2/18/2019	Exp21	56	16
25	N2	OD5	2/18/2019	Exp21	57	24
25	N2	OD5	2/18/2019	Exp21	58	24
25	N2	OD5	2/18/2019	Exp21	59	20
25	*daf-2*	OD5	9/21/2018	Exp31	7	38
25	*daf-2*	OD5	9/21/2018	Exp31	8	42
25	*daf-2*	OD5	9/21/2018	Exp31	10	36
25	*daf-2*	OD5	9/21/2018	Exp31	17	41
25	*daf-2*	OD5	9/21/2018	Exp31	18	40
25	*daf-2*	OD5	9/21/2018	Exp31	19	34
25	*daf-2*	OD5	9/21/2018	Exp31	23	43

Table A.1.1 continued

25	*daf-2*	OD5	9/21/2018	Exp31	28	33
25	*daf-2*	OD5	9/21/2018	Exp31	29	41
25	*daf-2*	OD5	9/21/2018	Exp31	31	34
25	*daf-2*	OD5	9/21/2018	Exp31	33	36
25	*daf-2*	OD5	9/21/2018	Exp31	34	34
25	*daf-2*	OD5	9/21/2018	Exp31	38	38
25	*daf-2*	OD5	9/21/2018	Exp31	40	38
25	*daf-2*	OD5	9/21/2018	Exp31	45	34
25	*daf-2*	OD5	9/21/2018	Exp31	46	38
25	*daf-2*	OD5	9/21/2018	Exp31	48	41
25	*daf-2*	OD5	9/21/2018	Exp31	50	39
25	*daf-2*	OD5	9/21/2018	Exp31	51	41
25	*daf-2*	OD5	9/21/2018	Exp31	52	36
25	*daf-2*	OD5	9/21/2018	Exp31	53	42
25	*daf-2*	OD5	9/21/2018	Exp31	54	40
25	*daf-2*	OD5	10/23/2018	Exp63	5	30
25	*daf-2*	OD5	10/23/2018	Exp63	6	38
25	*daf-2*	OD5	10/23/2018	Exp63	7	34
25	*daf-2*	OD5	10/23/2018	Exp63	8	42
25	*daf-2*	OD5	10/23/2018	Exp63	10	24
25	*daf-2*	OD5	10/23/2018	Exp63	11	37
25	*daf-2*	OD5	10/23/2018	Exp63	13	34
25	*daf-2*	OD5	10/23/2018	Exp63	17	46
25	*daf-2*	OD5	10/23/2018	Exp63	18	40
25	*daf-2*	OD5	10/23/2018	Exp63	19	41
25	*daf-2*	OD5	10/23/2018	Exp63	23	48
25	*daf-2*	OD5	10/23/2018	Exp63	25	13
25	*daf-2*	OD5	10/23/2018	Exp63	26	42
25	*daf-2*	OD5	10/23/2018	Exp63	27	37
25	*daf-2*	OD5	10/23/2018	Exp63	28	44
25	*daf-2*	OD5	10/23/2018	Exp63	29	34
25	*daf-2*	OD5	10/23/2018	Exp63	31	53
25	*daf-2*	OD5	10/23/2018	Exp63	33	44
25	*daf-2*	OD5	10/23/2018	Exp63	34	30
25	*daf-2*	OD5	10/23/2018	Exp63	35	41
25	*daf-2*	OD5	10/23/2018	Exp63	36	46
25	*daf-2*	OD5	10/23/2018	Exp63	37	47
25	*daf-2*	OD5	10/23/2018	Exp63	39	51
25	*daf-2*	OD5	10/23/2018	Exp63	41	40
25	*daf-2*	OD5	10/23/2018	Exp63	43	41
25	*daf-2*	OD5	10/23/2018	Exp63	46	44
25	*daf-2*	OD5	10/23/2018	Exp63	47	55
25	*daf-2*	OD5	10/23/2018	Exp63	50	32
25	*daf-2*	OD5	10/23/2018	Exp63	53	44
25	*daf-2*	OD5	10/23/2018	Exp63	56	33

Table A.1.1 continued

25	*daf-2*	OD5	10/23/2018	Exp63	59	43
25	*daf-2*	OD5	10/23/2018	Exp63	60	50
25	*daf-2*	OD5	10/23/2018	Exp64	3	49
25	*daf-2*	OD5	10/23/2018	Exp64	6	49
25	*daf-2*	OD5	10/23/2018	Exp64	7	13
25	*daf-2*	OD5	10/23/2018	Exp64	9	30
25	*daf-2*	OD5	10/23/2018	Exp64	11	43
25	*daf-2*	OD5	10/23/2018	Exp64	24	42
25	*daf-2*	OD5	10/23/2018	Exp64	25	53
25	*daf-2*	OD5	10/23/2018	Exp64	28	51
25	*daf-2*	OD5	10/23/2018	Exp64	33	39
25	*daf-2*	OD5	10/23/2018	Exp64	34	47
25	*daf-2*	OD5	10/23/2018	Exp64	35	39
25	*daf-2*	OD5	10/23/2018	Exp64	39	52
25	*daf-2*	OD5	10/23/2018	Exp64	42	42
25	*daf-2*	OD5	10/23/2018	Exp64	44	45
25	*daf-2*	OD5	10/23/2018	Exp64	45	41
25	*daf-2*	OD5	10/23/2018	Exp64	50	50
25	*daf-2*	OD5	10/23/2018	Exp64	52	48
25	*daf-2*	OD5	10/23/2018	Exp64	55	33
25	*daf-2*	OD5	10/23/2018	Exp64	59	43
25	*daf-2*	OD5	2/18/2019	Exp18	3	36
25	*daf-2*	OD5	2/18/2019	Exp18	5	11
25	*daf-2*	OD5	2/18/2019	Exp18	8	41
25	*daf-2*	OD5	2/18/2019	Exp18	9	44
25	*daf-2*	OD5	2/18/2019	Exp18	10	47
25	*daf-2*	OD5	2/18/2019	Exp18	11	35
25	*daf-2*	OD5	2/18/2019	Exp18	14	33
25	*daf-2*	OD5	2/18/2019	Exp18	17	52
25	*daf-2*	OD5	2/18/2019	Exp18	19	44
25	*daf-2*	OD5	2/18/2019	Exp18	20	41
25	*daf-2*	OD5	2/18/2019	Exp18	21	47
25	*daf-2*	OD5	2/18/2019	Exp18	22	41
25	*daf-2*	OD5	2/18/2019	Exp18	23	50
25	*daf-2*	OD5	2/18/2019	Exp18	24	40
25	*daf-2*	OD5	2/18/2019	Exp18	25	25
25	*daf-2*	OD5	2/18/2019	Exp18	31	40
25	*daf-2*	OD5	2/18/2019	Exp18	32	41
25	*daf-2*	OD5	2/18/2019	Exp18	34	43
25	*daf-2*	OD5	2/18/2019	Exp18	39	28
25	*daf-2*	OD5	2/18/2019	Exp18	40	48
25	*daf-2*	OD5	2/18/2019	Exp18	45	44
25	*daf-2*	OD5	2/18/2019	Exp18	46	42
25	*daf-2*	OD5	2/18/2019	Exp18	48	39
25	*daf-2*	OD5	2/18/2019	Exp18	49	23

Table A.1.1 continued

25	*daf-2*	OD5	2/18/2019	Exp18	50	48
25	*daf-2*	OD5	2/18/2019	Exp18	51	43
25	*daf-2*	OD5	2/18/2019	Exp18	52	40
25	*daf-2*	OD5	2/18/2019	Exp18	53	40
25	*daf-2*	OD5	2/18/2019	Exp18	54	39
25	*daf-2*	OD5	2/18/2019	Exp18	55	40
25	*daf-2*	OD5	2/18/2019	Exp18	57	44
25	*daf-2*	OD5	2/18/2019	Exp18	59	56
25	*daf-2*	OD5	2/18/2019	Exp18	60	34
25	*daf-16*	OD5	9/21/2018	Exp32	3	10
25	*daf-16*	OD5	9/21/2018	Exp32	4	11
25	*daf-16*	OD5	9/21/2018	Exp32	5	12
25	*daf-16*	OD5	9/21/2018	Exp32	7	13
25	*daf-16*	OD5	9/21/2018	Exp32	8	11
25	*daf-16*	OD5	9/21/2018	Exp32	9	9
25	*daf-16*	OD5	9/21/2018	Exp32	10	9
25	*daf-16*	OD5	9/21/2018	Exp32	11	15
25	*daf-16*	OD5	9/21/2018	Exp32	13	11
25	*daf-16*	OD5	9/21/2018	Exp32	14	9
25	*daf-16*	OD5	9/21/2018	Exp32	15	10
25	*daf-16*	OD5	9/21/2018	Exp32	17	14
25	*daf-16*	OD5	9/21/2018	Exp32	18	14
25	*daf-16*	OD5	9/21/2018	Exp32	19	10
25	*daf-16*	OD5	9/21/2018	Exp32	20	16
25	*daf-16*	OD5	9/21/2018	Exp32	21	13
25	*daf-16*	OD5	9/21/2018	Exp32	23	11
25	*daf-16*	OD5	9/21/2018	Exp32	24	12
25	*daf-16*	OD5	9/21/2018	Exp32	26	10
25	*daf-16*	OD5	9/21/2018	Exp32	30	11
25	*daf-16*	OD5	9/21/2018	Exp32	34	9
25	*daf-16*	OD5	9/21/2018	Exp32	38	8
25	*daf-16*	OD5	9/21/2018	Exp32	40	11
25	*daf-16*	OD5	9/21/2018	Exp32	41	12
25	*daf-16*	OD5	9/21/2018	Exp32	42	12
25	*daf-16*	OD5	9/21/2018	Exp32	43	11
25	*daf-16*	OD5	9/21/2018	Exp32	44	15
25	*daf-16*	OD5	9/21/2018	Exp32	45	12
25	*daf-16*	OD5	9/21/2018	Exp32	50	10
25	*daf-16*	OD5	9/21/2018	Exp32	52	9
25	*daf-16*	OD5	9/21/2018	Exp32	53	11
25	*daf-16*	OD5	9/21/2018	Exp32	55	10
25	*daf-16*	OD5	9/21/2018	Exp32	56	9
25	*daf-16*	OD5	9/21/2018	Exp32	59	8
25	*daf-16*	OD5	9/21/2018	Exp32	60	10
25	*daf-16*	OD5	10/23/2018	Exp66	6	16

Table A.1.1 continued

25	*daf-16*	OD5	10/23/2018	Exp66	7	17
25	*daf-16*	OD5	10/23/2018	Exp66	9	6
25	*daf-16*	OD5	10/23/2018	Exp66	11	16
25	*daf-16*	OD5	10/23/2018	Exp66	13	9
25	*daf-16*	OD5	10/23/2018	Exp66	19	16
25	*daf-16*	OD5	10/23/2018	Exp66	23	13
25	*daf-16*	OD5	10/23/2018	Exp66	24	11
25	*daf-16*	OD5	10/23/2018	Exp66	26	10
25	*daf-16*	OD5	10/23/2018	Exp66	30	17
25	*daf-16*	OD5	10/23/2018	Exp66	31	15
25	*daf-16*	OD5	10/23/2018	Exp66	33	14
25	*daf-16*	OD5	10/23/2018	Exp66	37	7
25	*daf-16*	OD5	10/23/2018	Exp66	38	10
25	*daf-16*	OD5	10/23/2018	Exp66	40	15
25	*daf-16*	OD5	10/23/2018	Exp66	41	6
25	*daf-16*	OD5	10/23/2018	Exp66	42	13
25	*daf-16*	OD5	10/23/2018	Exp66	44	14
25	*daf-16*	OD5	10/23/2018	Exp66	50	15
25	*daf-16*	OD5	10/23/2018	Exp66	53	13
25	*daf-16*	OD5	10/23/2018	Exp66	56	12
25	*daf-16*	OD5	10/7/2018	Exp62	1	15
25	*daf-16*	OD5	10/7/2018	Exp62	2	14
25	*daf-16*	OD5	10/7/2018	Exp62	6	16
25	*daf-16*	OD5	10/7/2018	Exp62	8	15
25	*daf-16*	OD5	10/7/2018	Exp62	17	13
25	*daf-16*	OD5	10/7/2018	Exp62	19	17
25	*daf-16*	OD5	10/7/2018	Exp62	20	13
25	*daf-16*	OD5	10/7/2018	Exp62	21	15
25	*daf-16*	OD5	10/7/2018	Exp62	27	15
25	*daf-16*	OD5	10/7/2018	Exp62	28	16
25	*daf-16*	OD5	10/7/2018	Exp62	29	14
25	*daf-16*	OD5	10/7/2018	Exp62	30	13
25	*daf-16*	OD5	10/7/2018	Exp62	31	14
25	*daf-16*	OD5	10/7/2018	Exp62	43	12
25	*daf-16*	OD5	10/7/2018	Exp62	44	11
25	*daf-16*	OD5	10/7/2018	Exp62	50	14
25	*daf-16*	OD5	10/7/2018	Exp62	52	16
25	*daf-16*	OD5	10/7/2018	Exp62	55	15
25	*daf-16*	OD5	10/7/2018	Exp62	56	11
25	*daf-16*	OD5	10/7/2018	Exp62	57	11
25	*daf-16*	OD5	10/7/2018	Exp61	6	11
25	*daf-16*	OD5	10/7/2018	Exp61	9	13
25	*daf-16*	OD5	10/7/2018	Exp61	10	13
25	*daf-16*	OD5	10/7/2018	Exp61	12	13
25	*daf-16*	OD5	10/7/2018	Exp61	13	12

Table A.1.1 continued

25	*daf-16*	OD5	10/7/2018	Exp61	14	11
25	*daf-16*	OD5	10/7/2018	Exp61	17	14
25	*daf-16*	OD5	10/7/2018	Exp61	32	17
25	*daf-16*	OD5	10/7/2018	Exp61	33	14
25	*daf-16*	OD5	10/7/2018	Exp61	34	17
25	*daf-16*	OD5	10/7/2018	Exp61	35	10
25	*daf-16*	OD5	10/7/2018	Exp61	36	5
25	*daf-16*	OD5	10/7/2018	Exp61	38	12
25	*daf-16*	OD5	10/7/2018	Exp61	41	4
25	*daf-16*	OD5	10/7/2018	Exp61	42	14
25	*daf-16*	OD5	10/7/2018	Exp61	43	13
25	*daf-16*	OD5	10/7/2018	Exp61	44	4
25	*daf-16*	OD5	10/7/2018	Exp61	47	14
25	*daf-16*	OD5	10/7/2018	Exp61	48	14
25	*daf-16*	OD5	10/7/2018	Exp61	56	13
25	*daf-16*	OD5	10/7/2018	Exp61	57	14
25	*daf-16*	OD5	10/7/2018	Exp61	58	9
25	*daf-16*	OD5	10/7/2018	Exp61	59	11
25	N2	OD5	5/10/2018	Exp102/C	1	17
25	N2	OD5	5/10/2018	Exp102/C	2	14
25	N2	OD5	5/10/2018	Exp102/C	7	17
25	N2	OD5	5/10/2018	Exp102/C	8	19
25	N2	OD5	5/10/2018	Exp102/C	10	25
25	N2	OD5	5/10/2018	Exp102/C	11	18
25	N2	OD5	5/10/2018	Exp102/C	12	18
25	N2	OD5	5/10/2018	Exp102/C	14	18
25	N2	OD5	5/10/2018	Exp102/C	17	15
25	N2	OD5	5/10/2018	Exp102/C	24	21
25	N2	OD5	5/10/2018	Exp102/C	28	11
25	N2	OD5	5/10/2018	Exp102/C	29	20
25	N2	OD5	5/10/2018	Exp102/C	30	17
25	N2	OD5	5/10/2018	Exp102/C	31	11
25	N2	OD5	5/10/2018	Exp102/C	32	20
25	N2	OD5	5/10/2018	Exp102/C	34	19
25	N2	OD5	5/10/2018	Exp102/C	35	15
25	N2	OD5	5/10/2018	Exp102/C	39	18
25	N2	OD5	5/10/2018	Exp102/C	40	13
25	N2	OD5	5/10/2018	Exp102/C	41	22
25	N2	OD5	5/10/2018	Exp102/C	48	17
25	N2	OD5	5/10/2018	Exp102/C	49	20
25	N2	OD5	5/10/2018	Exp102/C	50	21
25	N2	OD5	5/10/2018	Exp102/C	51	21
25	N2	OD5	5/10/2018	Exp102/C	53	22
25	N2	OD5	5/10/2018	Exp102/C	55	15
25	N2	OD5	5/10/2018	Exp102/C	56	14

Table A.1.1 continued

25	N2	OD5	5/10/2018	Exp102/C	58	18
25	N2	OD5	5/10/2018	Exp102/C	59	19
25	N2	OD5	5/10/2018	Exp103/D	6	19
25	N2	OD5	5/10/2018	Exp103/D	7	16
25	N2	OD5	5/10/2018	Exp103/D	10	17
25	N2	OD5	5/10/2018	Exp103/D	15	19
25	N2	OD5	5/10/2018	Exp103/D	17	19
25	N2	OD5	5/10/2018	Exp103/D	22	22
25	N2	OD5	5/10/2018	Exp103/D	23	15
25	N2	OD5	5/10/2018	Exp103/D	25	19
25	N2	OD5	5/10/2018	Exp103/D	28	21
25	N2	OD5	5/10/2018	Exp103/D	32	12
25	N2	OD5	5/10/2018	Exp103/D	35	11
25	N2	OD5	5/10/2018	Exp103/D	39	21
25	N2	OD5	5/10/2018	Exp103/D	47	13
25	N2	OD5	5/10/2018	Exp103/D	48	16
25	N2	OD5	5/10/2018	Exp103/D	49	16
25	N2	OD5	5/10/2018	Exp103/D	51	14
25	N2	OD5	5/10/2018	Exp103/D	53	20
25	N2	OD5	5/10/2018	Exp103/D	55	10
25	N2	OD5	5/10/2018	Exp103/D	56	15
25	N2	OD5	5/10/2018	Exp103/D	57	12
25	N2	OD5	10/27/2018	Exp49	6	17
25	N2	OD5	10/27/2018	Exp49	7	15
25	N2	OD5	10/27/2018	Exp49	8	18
25	N2	OD5	10/27/2018	Exp49	9	19
25	N2	OD5	10/27/2018	Exp49	10	20
25	N2	OD5	10/27/2018	Exp49	16	10
25	N2	OD5	10/27/2018	Exp49	17	22
25	N2	OD5	10/27/2018	Exp49	18	11
25	N2	OD5	10/27/2018	Exp49	22	15
25	N2	OD5	10/27/2018	Exp49	28	18
25	N2	OD5	10/27/2018	Exp49	29	16
25	N2	OD5	10/27/2018	Exp49	30	17
25	N2	OD5	10/27/2018	Exp49	31	18
25	N2	OD5	10/27/2018	Exp49	35	18
25	N2	OD5	10/27/2018	Exp49	37	11
25	N2	OD5	10/27/2018	Exp49	44	12
25	N2	OD5	10/27/2018	Exp49	45	20
25	N2	OD5	10/27/2018	Exp49	46	23
25	N2	OD5	10/27/2018	Exp49	49	19
25	N2	OD5	10/27/2018	Exp49	54	19
25	N2	OD5	10/27/2018	Exp49	56	22
25	N2	OD5	10/27/2018	Exp49	58	11
25	N2	OD5	10/27/2018	Exp50	1	10

Table A.1.1 continued

25	N2	OD5	10/27/2018	Exp50	6	15
25	N2	OD5	10/27/2018	Exp50	7	17
25	N2	OD5	10/27/2018	Exp50	9	17
25	N2	OD5	10/27/2018	Exp50	10	17
25	N2	OD5	10/27/2018	Exp50	14	17
25	N2	OD5	10/27/2018	Exp50	15	19
25	N2	OD5	10/27/2018	Exp50	18	21
25	N2	OD5	10/27/2018	Exp50	24	16
25	N2	OD5	10/27/2018	Exp50	29	17
25	N2	OD5	10/27/2018	Exp50	33	18
25	N2	OD5	10/27/2018	Exp50	35	16
25	N2	OD5	10/27/2018	Exp50	37	14
25	N2	OD5	10/27/2018	Exp50	38	22
25	N2	OD5	10/27/2018	Exp50	40	15
25	N2	OD5	10/27/2018	Exp50	44	16
25	N2	OD5	10/27/2018	Exp50	46	23
25	N2	OD5	10/27/2018	Exp50	47	18
25	N2	OD5	10/27/2018	Exp50	51	23
25	N2	OD5	10/27/2018	Exp50	55	23
25	N2	OD5	10/27/2018	Exp50	56	21
25	N2	OD5	10/27/2018	Exp50	60	20
25	N2	OD2.5	10/23/2018	Exp47	3	18
25	N2	OD2.5	10/23/2018	Exp47	9	19
25	N2	OD2.5	10/23/2018	Exp47	11	14
25	N2	OD2.5	10/23/2018	Exp47	13	18
25	N2	OD2.5	10/23/2018	Exp47	21	16
25	N2	OD2.5	10/23/2018	Exp47	24	15
25	N2	OD2.5	10/23/2018	Exp47	33	15
25	N2	OD2.5	10/23/2018	Exp47	34	21
25	N2	OD2.5	10/23/2018	Exp47	35	15
25	N2	OD2.5	10/23/2018	Exp47	37	18
25	N2	OD2.5	10/23/2018	Exp47	40	18
25	N2	OD2.5	10/23/2018	Exp47	41	21
25	N2	OD2.5	10/23/2018	Exp47	42	23
25	N2	OD2.5	10/23/2018	Exp47	45	21
25	N2	OD2.5	10/23/2018	Exp47	47	24
25	N2	OD2.5	10/23/2018	Exp47	55	14
25	N2	OD2.5	10/23/2018	Exp47	56	19
25	N2	OD2.5	10/23/2018	Exp47	57	14
25	N2	OD2.5	10/23/2018	Exp47	58	18
25	N2	OD2.5	10/23/2018	Exp47	59	21
25	N2	OD2.5	10/23/2018	Exp48	8	21
25	N2	OD2.5	10/23/2018	Exp48	14	19
25	N2	OD2.5	10/23/2018	Exp48	15	19
25	N2	OD2.5	10/23/2018	Exp48	16	16

Table A.1.1 continued

25	N2	OD2.5	10/23/2018	Exp48	27	15
25	N2	OD2.5	10/23/2018	Exp48	28	18
25	N2	OD2.5	10/23/2018	Exp48	30	13
25	N2	OD2.5	10/23/2018	Exp48	32	18
25	N2	OD2.5	10/23/2018	Exp48	35	20
25	N2	OD2.5	10/23/2018	Exp48	36	15
25	N2	OD2.5	10/23/2018	Exp48	39	8
25	N2	OD2.5	10/23/2018	Exp48	40	19
25	N2	OD2.5	10/23/2018	Exp48	41	17
25	N2	OD2.5	10/23/2018	Exp48	42	20
25	N2	OD2.5	10/23/2018	Exp48	47	15
25	N2	OD2.5	10/23/2018	Exp48	53	21
25	N2	OD2.5	10/23/2018	Exp48	55	21
25	N2	OD2.5	10/23/2018	Exp48	56	17
25	N2	OD2.5	10/23/2018	Exp48	59	9
25	N2	OD2.5	5/10/2018	Exp104/E	1	17
25	N2	OD2.5	5/10/2018	Exp104/E	2	13
25	N2	OD2.5	5/10/2018	Exp104/E	3	33
25	N2	OD2.5	5/10/2018	Exp104/E	5	25
25	N2	OD2.5	5/10/2018	Exp104/E	9	34
25	N2	OD2.5	5/10/2018	Exp104/E	10	39
25	N2	OD2.5	5/10/2018	Exp104/E	11	22
25	N2	OD2.5	5/10/2018	Exp104/E	14	31
25	N2	OD2.5	5/10/2018	Exp104/E	19	32
25	N2	OD2.5	5/10/2018	Exp104/E	21	23
25	N2	OD2.5	5/10/2018	Exp104/E	23	20
25	N2	OD2.5	5/10/2018	Exp104/E	25	17
25	N2	OD2.5	5/10/2018	Exp104/E	29	23
25	N2	OD2.5	5/10/2018	Exp104/E	31	9
25	N2	OD2.5	5/10/2018	Exp104/E	34	20
25	N2	OD2.5	5/10/2018	Exp104/E	35	26
25	N2	OD2.5	5/10/2018	Exp104/E	39	20
25	N2	OD2.5	5/10/2018	Exp104/E	43	10
25	N2	OD2.5	5/10/2018	Exp104/E	44	23
25	N2	OD2.5	5/10/2018	Exp104/E	46	26
25	N2	OD2.5	5/10/2018	Exp104/E	49	19
25	N2	OD2.5	5/10/2018	Exp104/E	54	20
25	N2	OD2.5	5/10/2018	Exp104/E	55	14
25	N2	OD2.5	5/10/2018	Exp104/E	57	22
25	N2	OD2.5	5/10/2018	Exp104/E	58	20
25	N2	OD2.5	5/10/2018	Exp104/E	59	14
25	N2	OD2.5	5/10/2018	Exp105/F	3	24
25	N2	OD2.5	5/10/2018	Exp105/F	5	28
25	N2	OD2.5	5/10/2018	Exp105/F	6	24
25	N2	OD2.5	5/10/2018	Exp105/F	7	29

Table A.1.1 continued

25	N2	OD2.5	5/10/2018	Exp105/F	8	23
25	N2	OD2.5	5/10/2018	Exp105/F	10	20
25	N2	OD2.5	5/10/2018	Exp105/F	13	18
25	N2	OD2.5	5/10/2018	Exp105/F	14	19
25	N2	OD2.5	5/10/2018	Exp105/F	15	16
25	N2	OD2.5	5/10/2018	Exp105/F	23	24
25	N2	OD2.5	5/10/2018	Exp105/F	24	24
25	N2	OD2.5	5/10/2018	Exp105/F	25	14
25	N2	OD2.5	5/10/2018	Exp105/F	29	20
25	N2	OD2.5	5/10/2018	Exp105/F	30	15
25	N2	OD2.5	5/10/2018	Exp105/F	35	13
25	N2	OD2.5	5/10/2018	Exp105/F	37	18
25	N2	OD2.5	5/10/2018	Exp105/F	39	22
25	N2	OD2.5	5/10/2018	Exp105/F	40	24
25	N2	OD2.5	5/10/2018	Exp105/F	41	21
25	N2	OD2.5	5/10/2018	Exp105/F	44	24
25	N2	OD2.5	5/10/2018	Exp105/F	46	20
25	N2	OD2.5	5/10/2018	Exp105/F	47	23
25	N2	OD2.5	5/10/2018	Exp105/F	55	20
25	N2	OD2.5	5/10/2018	Exp105/F	56	16
25	N2	OD2.5	5/10/2018	Exp105/F	58	11
25	N2	OD2.5	10/27/2018	Exp53	3	21
25	N2	OD2.5	10/27/2018	Exp53	4	15
25	N2	OD2.5	10/27/2018	Exp53	5	14
25	N2	OD2.5	10/27/2018	Exp53	6	14
25	N2	OD2.5	10/27/2018	Exp53	8	18
25	N2	OD2.5	10/27/2018	Exp53	9	16
25	N2	OD2.5	10/27/2018	Exp53	11	12
25	N2	OD2.5	10/27/2018	Exp53	14	18
25	N2	OD2.5	10/27/2018	Exp53	15	16
25	N2	OD2.5	10/27/2018	Exp53	20	13
25	N2	OD2.5	10/27/2018	Exp53	22	14
25	N2	OD2.5	10/27/2018	Exp53	25	20
25	N2	OD2.5	10/27/2018	Exp53	28	23
25	N2	OD2.5	10/27/2018	Exp53	30	19
25	N2	OD2.5	10/27/2018	Exp53	31	15
25	N2	OD2.5	10/27/2018	Exp53	35	23
25	N2	OD2.5	10/27/2018	Exp53	38	18
25	N2	OD2.5	10/27/2018	Exp53	42	24
25	N2	OD2.5	10/27/2018	Exp53	43	18
25	N2	OD2.5	10/27/2018	Exp53	44	14
25	N2	OD2.5	10/27/2018	Exp53	45	15
25	N2	OD2.5	10/27/2018	Exp53	46	15
25	N2	OD2.5	10/27/2018	Exp53	48	17
25	N2	OD2.5	10/27/2018	Exp53	49	19

Table A.1.1 continued

25	N2	OD2.5	10/27/2018	Exp53	50	18
25	N2	OD2.5	10/27/2018	Exp53	51	17
25	N2	OD2.5	10/27/2018	Exp53	52	18
25	N2	OD2.5	10/27/2018	Exp53	55	15
25	N2	OD2.5	10/27/2018	Exp53	57	27
25	N2	OD2.5	10/27/2018	Exp54	1	15
25	N2	OD2.5	10/27/2018	Exp54	7	13
25	N2	OD2.5	10/27/2018	Exp54	8	17
25	N2	OD2.5	10/27/2018	Exp54	10	17
25	N2	OD2.5	10/27/2018	Exp54	11	6
25	N2	OD2.5	10/27/2018	Exp54	12	16
25	N2	OD2.5	10/27/2018	Exp54	15	15
25	N2	OD2.5	10/27/2018	Exp54	18	17
25	N2	OD2.5	10/27/2018	Exp54	19	13
25	N2	OD2.5	10/27/2018	Exp54	24	19
25	N2	OD2.5	10/27/2018	Exp54	25	27
25	N2	OD2.5	10/27/2018	Exp54	32	20
25	N2	OD2.5	10/27/2018	Exp54	35	15
25	N2	OD2.5	10/27/2018	Exp54	39	18
25	N2	OD2.5	10/27/2018	Exp54	40	17
25	N2	OD2.5	10/27/2018	Exp54	41	15
25	N2	OD2.5	10/27/2018	Exp54	42	15
25	N2	OD2.5	10/27/2018	Exp54	43	20
25	N2	OD2.5	10/27/2018	Exp54	44	14
25	N2	OD2.5	10/27/2018	Exp54	46	20
25	N2	OD2.5	10/27/2018	Exp54	47	22
25	N2	OD2.5	10/27/2018	Exp54	49	14
25	N2	OD2.5	10/27/2018	Exp54	51	15
25	N2	OD2.5	10/27/2018	Exp54	53	16
25	N2	OD2.5	10/27/2018	Exp54	54	15
25	N2	OD2.5	10/27/2018	Exp54	55	13
25	N2	OD2.5	10/27/2018	Exp54	56	16
25	N2	OD2.5	10/27/2018	Exp54	57	18
25	N2	OD2.5	10/27/2018	Exp54	59	16
25	N2	OD2.5	10/27/2018	Exp54	60	15
25	N2	OD10	5/10/2018	Exp100/A	4	22
25	N2	OD10	5/10/2018	Exp100/A	6	19
25	N2	OD10	5/10/2018	Exp100/A	7	17
25	N2	OD10	5/10/2018	Exp100/A	8	12
25	N2	OD10	5/10/2018	Exp100/A	10	17
25	N2	OD10	5/10/2018	Exp100/A	11	18
25	N2	OD10	5/10/2018	Exp100/A	14	15
25	N2	OD10	5/10/2018	Exp100/A	16	14
25	N2	OD10	5/10/2018	Exp100/A	18	18
25	N2	OD10	5/10/2018	Exp100/A	19	17

Table A.1.1 continued

25	N2	OD10	5/10/2018	Exp100/A	21	18
25	N2	OD10	5/10/2018	Exp100/A	26	14
25	N2	OD10	5/10/2018	Exp100/A	28	9
25	N2	OD10	5/10/2018	Exp100/A	29	16
25	N2	OD10	5/10/2018	Exp100/A	30	16
25	N2	OD10	5/10/2018	Exp100/A	32	17
25	N2	OD10	5/10/2018	Exp100/A	33	14
25	N2	OD10	5/10/2018	Exp100/A	35	10
25	N2	OD10	5/10/2018	Exp100/A	39	16
25	N2	OD10	5/10/2018	Exp100/A	40	14
25	N2	OD10	5/10/2018	Exp100/A	42	18
25	N2	OD10	5/10/2018	Exp100/A	43	16
25	N2	OD10	5/10/2018	Exp100/A	44	16
25	N2	OD10	5/10/2018	Exp100/A	45	15
25	N2	OD10	5/10/2018	Exp100/A	47	11
25	N2	OD10	5/10/2018	Exp100/A	50	18
25	N2	OD10	5/10/2018	Exp100/A	51	13
25	N2	OD10	5/10/2018	Exp100/A	53	18
25	N2	OD10	5/10/2018	Exp100/A	55	16
25	N2	OD10	5/10/2018	Exp100/A	56	13
25	N2	OD10	5/10/2018	Exp100/A	58	14
25	N2	OD10	5/10/2018	Exp100/A	59	13
25	N2	OD10	5/10/2018	Exp101/B	1	8
25	N2	OD10	5/10/2018	Exp101/B	11	11
25	N2	OD10	5/10/2018	Exp101/B	12	15
25	N2	OD10	5/10/2018	Exp101/B	19	23
25	N2	OD10	5/10/2018	Exp101/B	25	16
25	N2	OD10	5/10/2018	Exp101/B	35	17
25	N2	OD10	5/10/2018	Exp101/B	37	17
25	N2	OD10	5/10/2018	Exp101/B	38	19
25	N2	OD10	5/10/2018	Exp101/B	39	12
25	N2	OD10	5/10/2018	Exp101/B	40	9
25	N2	OD10	5/10/2018	Exp101/B	41	17
25	N2	OD10	5/10/2018	Exp101/B	43	15
25	N2	OD10	5/10/2018	Exp101/B	48	13
25	N2	OD10	5/10/2018	Exp101/B	58	13
25	N2	OD10	5/10/2018	Exp101/B	60	18
25	N2	OD10	10/27/2018	Exp51	1	14
25	N2	OD10	10/27/2018	Exp51	4	14
25	N2	OD10	10/27/2018	Exp51	5	13
25	N2	OD10	10/27/2018	Exp51	6	13
25	N2	OD10	10/27/2018	Exp51	10	16
25	N2	OD10	10/27/2018	Exp51	16	15
25	N2	OD10	10/27/2018	Exp51	22	14
25	N2	OD10	10/27/2018	Exp51	23	14

Table A.1.1 continued

25	N2	OD10	10/27/2018	Exp51	24	9
25	N2	OD10	10/27/2018	Exp51	25	20
25	N2	OD10	10/27/2018	Exp51	27	14
25	N2	OD10	10/27/2018	Exp51	28	14
25	N2	OD10	10/27/2018	Exp51	31	9
25	N2	OD10	10/27/2018	Exp51	33	14
25	N2	OD10	10/27/2018	Exp51	36	14
25	N2	OD10	10/27/2018	Exp51	41	17
25	N2	OD10	10/27/2018	Exp51	45	15
25	N2	OD10	10/27/2018	Exp51	46	14
25	N2	OD10	10/27/2018	Exp51	49	7
25	N2	OD10	10/27/2018	Exp51	50	12
25	N2	OD10	10/27/2018	Exp51	51	14
25	N2	OD10	10/27/2018	Exp51	52	16
25	N2	OD10	10/27/2018	Exp51	53	14
25	N2	OD10	10/27/2018	Exp51	55	12
25	N2	OD10	10/27/2018	Exp51	56	19
25	N2	OD10	10/27/2018	Exp51	57	15
25	N2	OD10	10/27/2018	Exp51	58	15
25	N2	OD10	10/7/2018	Exp45	2	20
25	N2	OD10	10/7/2018	Exp45	3	20
25	N2	OD10	10/7/2018	Exp45	4	12
25	N2	OD10	10/7/2018	Exp45	6	20
25	N2	OD10	10/7/2018	Exp45	8	19
25	N2	OD10	10/7/2018	Exp45	10	12
25	N2	OD10	10/7/2018	Exp45	15	13
25	N2	OD10	10/7/2018	Exp45	16	16
25	N2	OD10	10/7/2018	Exp45	17	11
25	N2	OD10	10/7/2018	Exp45	18	11
25	N2	OD10	10/7/2018	Exp45	23	16
25	N2	OD10	10/7/2018	Exp45	24	21
25	N2	OD10	10/7/2018	Exp45	25	14
25	N2	OD10	10/7/2018	Exp45	27	15
25	N2	OD10	10/7/2018	Exp45	29	11
25	N2	OD10	10/7/2018	Exp45	30	13
25	N2	OD10	10/7/2018	Exp45	31	13
25	N2	OD10	10/7/2018	Exp45	33	16
25	N2	OD10	10/7/2018	Exp45	34	15
25	N2	OD10	10/7/2018	Exp45	38	15
25	N2	OD10	10/7/2018	Exp45	39	13
25	N2	OD10	10/7/2018	Exp45	40	14
25	N2	OD10	10/7/2018	Exp45	41	17
25	N2	OD10	10/7/2018	Exp45	44	14
25	N2	OD10	10/7/2018	Exp45	45	16
25	N2	OD10	10/7/2018	Exp45	46	12

Table A.1.1 continued

25	N2	OD10	10/7/2018	Exp45	47	16
25	N2	OD10	10/7/2018	Exp45	49	9
25	N2	OD10	10/7/2018	Exp45	50	15
25	N2	OD10	10/7/2018	Exp45	54	18
25	N2	OD10	10/7/2018	Exp45	55	16
25	N2	OD10	10/7/2018	Exp45	56	13
25	N2	OD10	10/7/2018	Exp45	58	10
25	N2	OD10	10/7/2018	Exp45	59	16
20	N2	OD5	1/17/2019	Exp0	3	29
20	N2	OD5	1/17/2019	Exp0	6	34
20	N2	OD5	1/17/2019	Exp0	7	41
20	N2	OD5	1/17/2019	Exp0	10	21
20	N2	OD5	1/17/2019	Exp0	13	20
20	N2	OD5	1/17/2019	Exp0	15	23
20	N2	OD5	1/17/2019	Exp0	16	36
20	N2	OD5	1/17/2019	Exp0	19	43
20	N2	OD5	1/17/2019	Exp0	20	29
20	N2	OD5	1/17/2019	Exp0	31	38
20	N2	OD5	1/17/2019	Exp0	33	23
20	N2	OD5	1/17/2019	Exp0	34	29
20	N2	OD5	1/17/2019	Exp0	38	28
20	N2	OD5	1/17/2019	Exp0	41	25
20	N2	OD5	1/17/2019	Exp0	42	39
20	N2	OD5	1/17/2019	Exp0	43	39
20	N2	OD5	1/17/2019	Exp0	44	40
20	N2	OD5	1/17/2019	Exp0	47	41
20	N2	OD5	1/17/2019	Exp0	48	37
20	N2	OD5	1/17/2019	Exp0	53	20
20	N2	OD5	1/17/2019	Exp0	55	25
20	N2	OD5	1/17/2019	Exp0	56	19
20	N2	OD5	1/17/2019	Exp0	57	25
20	N2	OD5	1/17/2019	Exp0	59	35
20	N2	OD5	1/17/2019	Exp0	60	30
20	N2	OD5	1/21/2019	Exp6	2	31
20	N2	OD5	1/21/2019	Exp6	3	19
20	N2	OD5	1/21/2019	Exp6	10	25
20	N2	OD5	1/21/2019	Exp6	13	13
20	N2	OD5	1/21/2019	Exp6	14	20
20	N2	OD5	1/21/2019	Exp6	16	32
20	N2	OD5	1/21/2019	Exp6	17	24
20	N2	OD5	1/21/2019	Exp6	18	30
20	N2	OD5	1/21/2019	Exp6	20	32
20	N2	OD5	1/21/2019	Exp6	21	39
20	N2	OD5	1/21/2019	Exp6	22	22
20	N2	OD5	1/21/2019	Exp6	27	27

Table A.1.1 continued

20	N2	OD5	1/21/2019	Exp6	28	26
20	N2	OD5	1/21/2019	Exp6	29	31
20	N2	OD5	1/21/2019	Exp6	31	30
20	N2	OD5	1/21/2019	Exp6	32	20
20	N2	OD5	1/21/2019	Exp6	37	24
20	N2	OD5	1/21/2019	Exp6	39	22
20	N2	OD5	1/21/2019	Exp6	41	28
20	N2	OD5	1/21/2019	Exp6	43	25
20	N2	OD5	1/21/2019	Exp6	45	30
20	N2	OD5	1/21/2019	Exp6	51	22
20	N2	OD5	1/21/2019	Exp6	53	42
20	N2	OD5	1/21/2019	Exp6	56	20
20	N2	OD5	1/21/2019	Exp6	57	30
20	N2	OD5	1/21/2019	Exp6	59	32
20	N2	OD5	1/29/2019	Exp12	2	24
20	N2	OD5	1/29/2019	Exp12	3	26
20	N2	OD5	1/29/2019	Exp12	7	40
20	N2	OD5	1/29/2019	Exp12	8	27
20	N2	OD5	1/29/2019	Exp12	14	22
20	N2	OD5	1/29/2019	Exp12	15	32
20	N2	OD5	1/29/2019	Exp12	18	40
20	N2	OD5	1/29/2019	Exp12	23	40
20	N2	OD5	1/29/2019	Exp12	27	26
20	N2	OD5	1/29/2019	Exp12	28	29
20	N2	OD5	1/29/2019	Exp12	31	25
20	N2	OD5	1/29/2019	Exp12	34	37
20	N2	OD5	1/29/2019	Exp12	40	18
20	N2	OD5	1/29/2019	Exp12	41	24
20	N2	OD5	1/29/2019	Exp12	42	36
20	N2	OD5	1/29/2019	Exp12	44	35
20	N2	OD5	1/29/2019	Exp12	45	21
20	N2	OD5	1/29/2019	Exp12	49	23
20	N2	OD5	1/29/2019	Exp12	50	34
20	N2	OD5	1/29/2019	Exp12	52	23
20	N2	OD5	1/29/2019	Exp12	53	33
20	N2	OD5	1/29/2019	Exp12	54	27
20	N2	OD5	1/29/2019	Exp12	55	27
20	N2	OD5	1/29/2019	Exp12	56	27
20	N2	OD5	1/29/2019	Exp12	58	17
20	N2	OD5	1/29/2019	Exp12	60	28
15	N2	OD5	1/17/2019	Exp1	1	32
15	N2	OD5	1/17/2019	Exp1	3	30
15	N2	OD5	1/17/2019	Exp1	18	35
15	N2	OD5	1/17/2019	Exp1	33	38
15	N2	OD5	1/17/2019	Exp1	36	22

Table A.1.1 continued

15	N2	OD5	1/17/2019	Exp1	38	26
15	N2	OD5	1/17/2019	Exp1	39	29
15	N2	OD5	1/17/2019	Exp1	40	34
15	N2	OD5	1/17/2019	Exp1	41	25
15	N2	OD5	1/17/2019	Exp1	42	39
15	N2	OD5	1/17/2019	Exp1	44	33
15	N2	OD5	1/17/2019	Exp1	45	37
15	N2	OD5	1/17/2019	Exp1	46	45
15	N2	OD5	1/17/2019	Exp1	47	50
15	N2	OD5	1/17/2019	Exp1	49	25
15	N2	OD5	1/17/2019	Exp1	50	29
15	N2	OD5	1/17/2019	Exp1	51	31
15	N2	OD5	1/17/2019	Exp1	52	24
15	N2	OD5	1/17/2019	Exp1	53	45
15	N2	OD5	1/17/2019	Exp1	54	48
15	N2	OD5	1/17/2019	Exp1	55	26
15	N2	OD5	1/17/2019	Exp1	57	23
15	N2	OD5	1/17/2019	Exp1	58	37
15	N2	OD5	1/21/2019	Exp9	2	54
15	N2	OD5	1/21/2019	Exp9	6	32
15	N2	OD5	1/21/2019	Exp9	8	31
15	N2	OD5	1/21/2019	Exp9	9	39
15	N2	OD5	1/21/2019	Exp9	11	40
15	N2	OD5	1/21/2019	Exp9	13	47
15	N2	OD5	1/21/2019	Exp9	16	32
15	N2	OD5	1/21/2019	Exp9	17	25
15	N2	OD5	1/21/2019	Exp9	18	25
15	N2	OD5	1/21/2019	Exp9	22	33
15	N2	OD5	1/21/2019	Exp9	23	18
15	N2	OD5	1/21/2019	Exp9	25	49
15	N2	OD5	1/21/2019	Exp9	26	29
15	N2	OD5	1/21/2019	Exp9	27	54
15	N2	OD5	1/21/2019	Exp9	31	53
15	N2	OD5	1/21/2019	Exp9	39	16
15	N2	OD5	1/21/2019	Exp9	41	45
15	N2	OD5	1/21/2019	Exp9	43	39
15	N2	OD5	1/21/2019	Exp9	44	33
15	N2	OD5	1/21/2019	Exp9	50	27
15	N2	OD5	1/21/2019	Exp9	53	42
15	N2	OD5	1/21/2019	Exp9	54	43
15	N2	OD5	1/21/2019	Exp9	55	27
15	N2	OD5	1/21/2019	Exp9	57	27
15	N2	OD5	1/29/2019	Exp13	3	39
15	N2	OD5	1/29/2019	Exp13	4	20
15	N2	OD5	1/29/2019	Exp13	5	27

Table A.1.1 continued

15	N2	OD5	1/29/2019	Exp13	7	47
15	N2	OD5	1/29/2019	Exp13	8	25
15	N2	OD5	1/29/2019	Exp13	12	34
15	N2	OD5	1/29/2019	Exp13	14	29
15	N2	OD5	1/29/2019	Exp13	15	27
15	N2	OD5	1/29/2019	Exp13	16	31
15	N2	OD5	1/29/2019	Exp13	17	41
15	N2	OD5	1/29/2019	Exp13	21	42
15	N2	OD5	1/29/2019	Exp13	22	41
15	N2	OD5	1/29/2019	Exp13	25	48
15	N2	OD5	1/29/2019	Exp13	26	24
15	N2	OD5	1/29/2019	Exp13	28	50
15	N2	OD5	1/29/2019	Exp13	31	31
15	N2	OD5	1/29/2019	Exp13	34	32
15	N2	OD5	1/29/2019	Exp13	35	25
15	N2	OD5	1/29/2019	Exp13	40	22
15	N2	OD5	1/29/2019	Exp13	41	50
15	N2	OD5	1/29/2019	Exp13	42	51
15	N2	OD5	1/29/2019	Exp13	45	57
15	N2	OD5	1/29/2019	Exp13	46	55
15	N2	OD5	1/29/2019	Exp13	47	41
15	N2	OD5	1/29/2019	Exp13	51	36
15	N2	OD5	1/29/2019	Exp13	52	57
15	N2	OD5	1/29/2019	Exp13	56	25
17.5	N2	OD5	1/17/2019	Exp2	8	38
17.5	N2	OD5	1/17/2019	Exp2	9	35
17.5	N2	OD5	1/17/2019	Exp2	10	36
17.5	N2	OD5	1/17/2019	Exp2	11	34
17.5	N2	OD5	1/17/2019	Exp2	13	29
17.5	N2	OD5	1/17/2019	Exp2	24	45
17.5	N2	OD5	1/17/2019	Exp2	25	20
17.5	N2	OD5	1/17/2019	Exp2	27	24
17.5	N2	OD5	1/17/2019	Exp2	28	16
17.5	N2	OD5	1/17/2019	Exp2	29	25
17.5	N2	OD5	1/17/2019	Exp2	32	16
17.5	N2	OD5	1/17/2019	Exp2	33	24
17.5	N2	OD5	1/17/2019	Exp2	35	18
17.5	N2	OD5	1/17/2019	Exp2	37	21
17.5	N2	OD5	1/17/2019	Exp2	41	55
17.5	N2	OD5	1/17/2019	Exp2	43	56
17.5	N2	OD5	1/17/2019	Exp2	44	60
17.5	N2	OD5	1/17/2019	Exp2	45	48
17.5	N2	OD5	1/17/2019	Exp2	46	39
17.5	N2	OD5	1/17/2019	Exp2	47	41
17.5	N2	OD5	1/17/2019	Exp2	48	35

Table A.1.1 continued

17.5	N2	OD5	1/17/2019	Exp2	51	28
17.5	N2	OD5	1/17/2019	Exp2	53	21
17.5	N2	OD5	1/17/2019	Exp2	54	51
17.5	N2	OD5	1/17/2019	Exp2	55	36
17.5	N2	OD5	1/17/2019	Exp2	56	29
17.5	N2	OD5	1/17/2019	Exp2	58	21
17.5	N2	OD5	1/17/2019	Exp2	59	20
17.5	N2	OD5	1/21/2019	Exp10	6	43
17.5	N2	OD5	1/21/2019	Exp10	13	33
17.5	N2	OD5	1/21/2019	Exp10	14	24
17.5	N2	OD5	1/21/2019	Exp10	15	23
17.5	N2	OD5	1/21/2019	Exp10	17	20
17.5	N2	OD5	1/21/2019	Exp10	20	25
17.5	N2	OD5	1/21/2019	Exp10	23	36
17.5	N2	OD5	1/21/2019	Exp10	28	29
17.5	N2	OD5	1/21/2019	Exp10	31	47
17.5	N2	OD5	1/21/2019	Exp10	32	39
17.5	N2	OD5	1/21/2019	Exp10	33	25
17.5	N2	OD5	1/21/2019	Exp10	34	25
17.5	N2	OD5	1/21/2019	Exp10	35	16
17.5	N2	OD5	1/21/2019	Exp10	36	23
17.5	N2	OD5	1/21/2019	Exp10	38	16
17.5	N2	OD5	1/21/2019	Exp10	41	25
17.5	N2	OD5	1/21/2019	Exp10	42	31
17.5	N2	OD5	1/21/2019	Exp10	43	47
17.5	N2	OD5	1/21/2019	Exp10	44	36
17.5	N2	OD5	1/21/2019	Exp10	46	53
17.5	N2	OD5	1/21/2019	Exp10	47	33
17.5	N2	OD5	1/21/2019	Exp10	48	38
17.5	N2	OD5	1/21/2019	Exp10	53	31
17.5	N2	OD5	1/21/2019	Exp10	56	22
17.5	N2	OD5	1/21/2019	Exp10	57	24
17.5	N2	OD5	1/21/2019	Exp10	60	22
17.5	N2	OD5	1/29/2019	Exp14	4	36
17.5	N2	OD5	1/29/2019	Exp14	5	15
17.5	N2	OD5	1/29/2019	Exp14	6	30
17.5	N2	OD5	1/29/2019	Exp14	7	25
17.5	N2	OD5	1/29/2019	Exp14	9	27
17.5	N2	OD5	1/29/2019	Exp14	11	25
17.5	N2	OD5	1/29/2019	Exp14	15	29
17.5	N2	OD5	1/29/2019	Exp14	19	52
17.5	N2	OD5	1/29/2019	Exp14	21	46
17.5	N2	OD5	1/29/2019	Exp14	23	56
17.5	N2	OD5	1/29/2019	Exp14	24	25
17.5	N2	OD5	1/29/2019	Exp14	26	20

Table A.1.1 continued

17.5	N2	OD5	1/29/2019	Exp14	27	26
17.5	N2	OD5	1/29/2019	Exp14	28	30
17.5	N2	OD5	1/29/2019	Exp14	29	28
17.5	N2	OD5	1/29/2019	Exp14	30	32
17.5	N2	OD5	1/29/2019	Exp14	31	25
17.5	N2	OD5	1/29/2019	Exp14	37	20
17.5	N2	OD5	1/29/2019	Exp14	41	62
17.5	N2	OD5	1/29/2019	Exp14	42	20
17.5	N2	OD5	1/29/2019	Exp14	43	26
17.5	N2	OD5	1/29/2019	Exp14	44	45
17.5	N2	OD5	1/29/2019	Exp14	45	28
17.5	N2	OD5	1/29/2019	Exp14	46	51
17.5	N2	OD5	1/29/2019	Exp14	47	43
17.5	N2	OD5	1/29/2019	Exp14	49	26
17.5	N2	OD5	1/29/2019	Exp14	50	49
17.5	N2	OD5	1/29/2019	Exp14	52	40
17.5	N2	OD5	1/29/2019	Exp14	55	42
17.5	N2	OD5	1/29/2019	Exp14	56	29
17.5	N2	OD5	1/29/2019	Exp14	57	25
17.5	N2	OD5	1/29/2019	Exp16	4	22
17.5	N2	OD5	1/29/2019	Exp16	6	32
17.5	N2	OD5	1/29/2019	Exp16	7	23
17.5	N2	OD5	1/29/2019	Exp16	8	14
17.5	N2	OD5	1/29/2019	Exp16	9	26
17.5	N2	OD5	1/29/2019	Exp16	13	24
17.5	N2	OD5	1/29/2019	Exp16	14	17
17.5	N2	OD5	1/29/2019	Exp16	17	33
17.5	N2	OD5	1/29/2019	Exp16	25	37
17.5	N2	OD5	1/29/2019	Exp16	27	21
17.5	N2	OD5	1/29/2019	Exp16	29	27
17.5	N2	OD5	1/29/2019	Exp16	30	42
17.5	N2	OD5	1/29/2019	Exp16	37	16
17.5	N2	OD5	1/29/2019	Exp16	43	40
17.5	N2	OD5	1/29/2019	Exp16	44	22
17.5	N2	OD5	1/29/2019	Exp16	46	57
17.5	N2	OD5	1/29/2019	Exp16	47	41
17.5	N2	OD5	1/29/2019	Exp16	49	23
17.5	N2	OD5	1/29/2019	Exp16	51	27
17.5	N2	OD5	1/29/2019	Exp16	52	20
17.5	N2	OD5	1/29/2019	Exp16	53	38
17.5	N2	OD5	1/29/2019	Exp16	54	25
17.5	N2	OD5	1/29/2019	Exp16	55	12
17.5	N2	OD5	1/29/2019	Exp16	56	15
17.5	N2	OD5	1/29/2019	Exp16	57	23
17.5	N2	OD5	1/29/2019	Exp16	58	25

Table A.1.1 continued

15 ↔ 20	N2	OD5	1/17/2019	Exp3	6	37
15 ↔ 20	N2	OD5	1/17/2019	Exp3	9	29
15 ↔ 20	N2	OD5	1/17/2019	Exp3	11	29
15 ↔ 20	N2	OD5	1/17/2019	Exp3	13	35
15 ↔ 20	N2	OD5	1/17/2019	Exp3	17	24
15 ↔ 20	N2	OD5	1/17/2019	Exp3	19	29
15 ↔ 20	N2	OD5	1/17/2019	Exp3	26	18
15 ↔ 20	N2	OD5	1/17/2019	Exp3	27	28
15 ↔ 20	N2	OD5	1/17/2019	Exp3	29	27
15 ↔ 20	N2	OD5	1/17/2019	Exp3	30	29
15 ↔ 20	N2	OD5	1/17/2019	Exp3	31	25
15 ↔ 20	N2	OD5	1/17/2019	Exp3	34	19
15 ↔ 20	N2	OD5	1/17/2019	Exp3	38	19
15 ↔ 20	N2	OD5	1/17/2019	Exp3	39	25
15 ↔ 20	N2	OD5	1/17/2019	Exp3	40	17
15 ↔ 20	N2	OD5	1/17/2019	Exp3	41	41
15 ↔ 20	N2	OD5	1/17/2019	Exp3	42	21
15 ↔ 20	N2	OD5	1/17/2019	Exp3	43	60
15 ↔ 20	N2	OD5	1/17/2019	Exp3	46	46
15 ↔ 20	N2	OD5	1/17/2019	Exp3	47	48
15 ↔ 20	N2	OD5	1/17/2019	Exp3	48	30
15 ↔ 20	N2	OD5	1/17/2019	Exp3	49	21
15 ↔ 20	N2	OD5	1/17/2019	Exp3	50	48
15 ↔ 20	N2	OD5	1/17/2019	Exp3	52	26
15 ↔ 20	N2	OD5	1/17/2019	Exp3	53	24
15 ↔ 20	N2	OD5	1/17/2019	Exp3	56	25
15 ↔ 20	N2	OD5	1/17/2019	Exp3	57	21
15 ↔ 20	N2	OD5	1/21/2019	Exp11	2	32
15 ↔ 20	N2	OD5	1/21/2019	Exp11	10	32
15 ↔ 20	N2	OD5	1/21/2019	Exp11	11	33
15 ↔ 20	N2	OD5	1/21/2019	Exp11	13	30
15 ↔ 20	N2	OD5	1/21/2019	Exp11	36	16
15 ↔ 20	N2	OD5	1/21/2019	Exp11	37	24
15 ↔ 20	N2	OD5	1/21/2019	Exp11	40	14
15 ↔ 20	N2	OD5	1/21/2019	Exp11	52	57
15 ↔ 20	N2	OD5	1/21/2019	Exp11	53	21
15 ↔ 20	N2	OD5	1/21/2019	Exp11	57	21
15 ↔ 20	N2	OD5	1/21/2019	Exp11	58	25
15 ↔ 20	N2	OD5	1/21/2019	Exp11	59	32
15 ↔ 20	N2	OD5	1/21/2019	Exp11	60	27
15 ↔ 20	N2	OD5	1/29/2019	Exp15	1	28
15 ↔ 20	N2	OD5	1/29/2019	Exp15	2	10
15 ↔ 20	N2	OD5	1/29/2019	Exp15	3	42
15 ↔ 20	N2	OD5	1/29/2019	Exp15	5	30
15 ↔ 20	N2	OD5	1/29/2019	Exp15	6	30

Table A.1.1 continued

15 ↔ 20	N2	OD5	1/29/2019	Exp15	7	32
15 ↔ 20	N2	OD5	1/29/2019	Exp15	9	31
15 ↔ 20	N2	OD5	1/29/2019	Exp15	11	32
15 ↔ 20	N2	OD5	1/29/2019	Exp15	12	26
15 ↔ 20	N2	OD5	1/29/2019	Exp15	13	15
15 ↔ 20	N2	OD5	1/29/2019	Exp15	16	37
15 ↔ 20	N2	OD5	1/29/2019	Exp15	17	15
15 ↔ 20	N2	OD5	1/29/2019	Exp15	18	10
15 ↔ 20	N2	OD5	1/29/2019	Exp15	19	20
15 ↔ 20	N2	OD5	1/29/2019	Exp15	20	11
15 ↔ 20	N2	OD5	1/29/2019	Exp15	22	12
15 ↔ 20	N2	OD5	1/29/2019	Exp15	25	20
15 ↔ 20	N2	OD5	1/29/2019	Exp15	26	35
15 ↔ 20	N2	OD5	1/29/2019	Exp15	27	17
15 ↔ 20	N2	OD5	1/29/2019	Exp15	28	26
15 ↔ 20	N2	OD5	1/29/2019	Exp15	29	37
15 ↔ 20	N2	OD5	1/29/2019	Exp15	30	38
15 ↔ 20	N2	OD5	1/29/2019	Exp15	32	25
15 ↔ 20	N2	OD5	1/29/2019	Exp15	33	14
15 ↔ 20	N2	OD5	1/29/2019	Exp15	35	23
15 ↔ 20	N2	OD5	1/29/2019	Exp15	37	27
15 ↔ 20	N2	OD5	1/29/2019	Exp15	39	38
15 ↔ 20	N2	OD5	1/29/2019	Exp15	40	44
15 ↔ 20	N2	OD5	1/29/2019	Exp15	41	32
15 ↔ 20	N2	OD5	1/29/2019	Exp15	42	30
15 ↔ 20	N2	OD5	1/29/2019	Exp15	44	14
15 ↔ 20	N2	OD5	1/29/2019	Exp15	45	21
15 ↔ 20	N2	OD5	1/29/2019	Exp15	50	38
15 ↔ 20	N2	OD5	1/29/2019	Exp15	51	31
15 ↔ 20	N2	OD5	1/29/2019	Exp15	52	31
15 ↔ 20	N2	OD5	1/29/2019	Exp15	53	29
15 ↔ 20	N2	OD5	1/29/2019	Exp15	55	18
15 ↔ 20	N2	OD5	1/29/2019	Exp15	56	16
15 ↔ 20	N2	OD5	1/29/2019	Exp15	57	28
15 ↔ 20	N2	OD5	1/29/2019	Exp15	58	22
15 ↔ 20	N2	OD5	1/29/2019	Exp15	59	22
15 ↔ 20	N2	OD5	1/29/2019	Exp17	3	29
15 ↔ 20	N2	OD5	1/29/2019	Exp17	4	48
15 ↔ 20	N2	OD5	1/29/2019	Exp17	7	44
15 ↔ 20	N2	OD5	1/29/2019	Exp17	9	17
15 ↔ 20	N2	OD5	1/29/2019	Exp17	10	10
15 ↔ 20	N2	OD5	1/29/2019	Exp17	11	36
15 ↔ 20	N2	OD5	1/29/2019	Exp17	12	45
15 ↔ 20	N2	OD5	1/29/2019	Exp17	13	6
15 ↔ 20	N2	OD5	1/29/2019	Exp17	15	25

Table A.1.1 continued

15 ↔ 20	N2	OD5	1/29/2019	Exp17	24	55
15 ↔ 20	N2	OD5	1/29/2019	Exp17	28	40
15 ↔ 20	N2	OD5	1/29/2019	Exp17	29	23
15 ↔ 20	N2	OD5	1/29/2019	Exp17	30	31
15 ↔ 20	N2	OD5	1/29/2019	Exp17	33	36
15 ↔ 20	N2	OD5	1/29/2019	Exp17	45	41
15 ↔ 20	N2	OD5	1/29/2019	Exp17	47	37
15 ↔ 20	N2	OD5	1/29/2019	Exp17	49	15
15 ↔ 20	N2	OD5	1/29/2019	Exp17	52	30
15 ↔ 20	N2	OD5	1/29/2019	Exp17	53	28
15 ↔ 20	N2	OD5	1/29/2019	Exp17	55	32
15 ↔ 20	N2	OD5	1/29/2019	Exp17	56	14
15 ↔ 20	N2	OD5	1/29/2019	Exp17	59	28
15 ↔ 20	N2	OD5	1/29/2019	Exp17	60	47

Table A.1.2. Lifespan data on plate.

Worms were cultured at 25°C in OD_{600}5 from Day 2 of adulthood to their death.

Strain	Date of L4	Experimenter	Age at Death	Plate	Frequency	Censor
N2	2/19/2018	DP	2	3	1	1
N2	2/19/2018	DP	5	3	1	1
N2	2/19/2018	DP	7	4	1	1
N2	2/19/2018	DP	13	2	1	0
N2	2/19/2018	DP	13	3	1	0
N2	2/19/2018	DP	15	1	3	0
N2	2/19/2018	DP	15	2	1	0
N2	2/19/2018	DP	15	3	2	0
N2	2/19/2018	DP	15	4	3	0
N2	2/19/2018	DP	17	1	3	0
N2	2/19/2018	DP	17	2	4	0
N2	2/19/2018	DP	17	3	3	0
N2	2/19/2018	DP	17	4	2	0
N2	2/19/2018	DP	19	1	3	0
N2	2/19/2018	DP	19	2	3	0
N2	2/19/2018	DP	19	3	5	0
N2	2/19/2018	DP	19	4	7	0
N2	2/19/2018	DP	21	1	6	0
N2	2/19/2018	DP	21	2	6	0
N2	2/19/2018	DP	21	3	4	0
N2	2/19/2018	DP	21	4	5	0
N2	2/19/2018	DP	23	1	5	0
N2	2/19/2018	DP	23	2	3	0
N2	2/19/2018	DP	23	3	3	0
N2	2/19/2018	DP	23	4	2	0
N2	2/19/2018	DP	25	1	1	0
N2	2/19/2018	DP	25	2	1	0
N2	2/19/2018	DP	27	2	2	0
daf-2	2/19/2018	DP	5	4	1	1
daf-2	2/19/2018	DP	7	1	1	1
daf-2	2/19/2018	DP	7	3	1	1
daf-2	2/19/2018	DP	7	4	2	1
daf-2	2/19/2018	DP	9	4	2	1
daf-2	2/19/2018	DP	11	3	1	1
daf-2	2/19/2018	DP	19	1	1	0
daf-2	2/19/2018	DP	19	3	1	0
daf-2	2/19/2018	DP	21	2	1	0
daf-2	2/19/2018	DP	23	2	2	0
daf-2	2/19/2018	DP	25	1	1	0

Table A.1.2 continued

daf-2	2/19/2018	DP	25	2	1	0
daf-2	2/19/2018	DP	27	1	1	0
daf-2	2/19/2018	DP	27	2	2	0
daf-2	2/19/2018	DP	29	1	5	0
daf-2	2/19/2018	DP	29	2	4	0
daf-2	2/19/2018	DP	29	3	4	0
daf-2	2/19/2018	DP	29	4	4	0
daf-2	2/19/2018	DP	31	1	2	0
daf-2	2/19/2018	DP	31	2	3	0
daf-2	2/19/2018	DP	31	3	5	0
daf-2	2/19/2018	DP	31	4	2	0
daf-2	2/19/2018	DP	33	1	3	0
daf-2	2/19/2018	DP	33	2	3	0
daf-2	2/19/2018	DP	33	3	2	0
daf-2	2/19/2018	DP	33	4	3	0
daf-2	2/19/2018	DP	35	1	4	0
daf-2	2/19/2018	DP	35	2	3	0
daf-2	2/19/2018	DP	35	3	4	0
daf-2	2/19/2018	DP	35	4	3	0
daf-2	2/19/2018	DP	37	1	1	0
daf-2	2/19/2018	DP	37	2	1	0
daf-2	2/19/2018	DP	37	3	1	0
daf-2	2/19/2018	DP	37	4	2	0
daf-2	2/19/2018	DP	39	1	1	0
daf-2	2/19/2018	DP	39	3	1	0
daf-2	2/19/2018	DP	39	4	1	0
daf-2	2/19/2018	DP	41	3	1	0
daf-16	2/19/2018	DP	3	1	1	1
daf-16	2/19/2018	DP	3	2	1	1
daf-16	2/19/2018	DP	5	3	1	1
daf-16	2/19/2018	DP	11	1	1	0
daf-16	2/19/2018	DP	11	3	2	0
daf-16	2/19/2018	DP	11	4	2	0
daf-16	2/19/2018	DP	13	1	3	0
daf-16	2/19/2018	DP	13	2	6	0
daf-16	2/19/2018	DP	13	3	2	0
daf-16	2/19/2018	DP	13	4	2	0
daf-16	2/19/2018	DP	15	1	11	0
daf-16	2/19/2018	DP	15	2	10	0
daf-16	2/19/2018	DP	15	3	10	0
daf-16	2/19/2018	DP	15	4	10	0
daf-16	2/19/2018	DP	17	1	3	0
daf-16	2/19/2018	DP	17	2	2	0
daf-16	2/19/2018	DP	17	3	5	0
daf-16	2/19/2018	DP	17	4	5	0

Table A.1.2 continued

daf-16	2/19/2018	DP	19	1	1	0
daf-16	2/19/2018	DP	19	3	1	0
daf-16	2/19/2018	DP	21	1	1	0
daf-16	2/19/2018	DP	21	2	2	0
N2	2/19/2018	JW	2	3	1	1
N2	2/19/2018	JW	3	4	2	1
N2	2/19/2018	JW	5	1	1	1
N2	2/19/2018	JW	5	2	2	1
N2	2/19/2018	JW	7	4	1	1
N2	2/19/2018	JW	9	3	1	1
N2	2/19/2018	JW	9	4	2	1
N2	2/19/2018	JW	11	2	1	0
N2	2/19/2018	JW	15	1	1	0
N2	2/19/2018	JW	15	4	2	0
N2	2/19/2018	JW	17	1	3	0
N2	2/19/2018	JW	17	2	3	0
N2	2/19/2018	JW	17	3	1	0
N2	2/19/2018	JW	19	1	6	0
N2	2/19/2018	JW	19	2	5	0
N2	2/19/2018	JW	19	3	7	0
N2	2/19/2018	JW	19	4	3	0
N2	2/19/2018	JW	21	1	3	0
N2	2/19/2018	JW	21	2	3	0
N2	2/19/2018	JW	21	3	5	0
N2	2/19/2018	JW	21	4	4	0
N2	2/19/2018	JW	23	1	1	0
N2	2/19/2018	JW	23	2	1	0
N2	2/19/2018	JW	23	3	2	0
N2	2/19/2018	JW	23	4	3	0
N2	2/19/2018	JW	25	1	4	0
N2	2/19/2018	JW	25	2	4	0
N2	2/19/2018	JW	25	3	4	0
N2	2/19/2018	JW	25	4	3	0
daf-2	2/19/2018	JW	3	2	2	1
daf-2	2/19/2018	JW	3	3	1	1
daf-2	2/19/2018	JW	5	1	3	1
daf-2	2/19/2018	JW	5	2	2	1
daf-2	2/19/2018	JW	5	4	2	1
daf-2	2/19/2018	JW	7	4	2	1
daf-2	2/19/2018	JW	9	1	2	1
daf-2	2/19/2018	JW	11	1	1	1
daf-2	2/19/2018	JW	11	3	2	1
daf-2	2/19/2018	JW	11	4	1	1
daf-2	2/19/2018	JW	19	4	1	0
daf-2	2/19/2018	JW	23	1	1	0

Table A.1.2 continued

daf-2	2/19/2018	JW	25	3	1	0
daf-2	2/19/2018	JW	25	4	2	0
daf-2	2/19/2018	JW	27	2	3	0
daf-2	2/19/2018	JW	27	3	3	0
daf-2	2/19/2018	JW	29	1	1	0
daf-2	2/19/2018	JW	29	2	2	0
daf-2	2/19/2018	JW	29	3	2	0
daf-2	2/19/2018	JW	29	4	1	0
daf-2	2/19/2018	JW	31	1	7	0
daf-2	2/19/2018	JW	31	2	6	0
daf-2	2/19/2018	JW	31	3	7	0
daf-2	2/19/2018	JW	31	4	6	0
daf-2	2/19/2018	JW	33	1	2	0
daf-2	2/19/2018	JW	33	2	2	0
daf-2	2/19/2018	JW	33	3	1	0
daf-2	2/19/2018	JW	33	4	2	0
daf-2	2/19/2018	JW	35	1	4	0
daf-2	2/19/2018	JW	35	2	2	0
daf-2	2/19/2018	JW	35	3	2	0
daf-2	2/19/2018	JW	35	4	2	0
daf-2	2/19/2018	JW	37	1	2	0
daf-2	2/19/2018	JW	37	2	2	0
daf-2	2/19/2018	JW	37	3	1	0
daf-2	2/19/2018	JW	39	4	1	0
daf-16	2/19/2018	JW	3	2	1	1
daf-16	2/19/2018	JW	3	4	1	1
daf-16	2/19/2018	JW	5	1	2	1
daf-16	2/19/2018	JW	5	2	2	1
daf-16	2/19/2018	JW	5	3	1	1
daf-16	2/19/2018	JW	5	4	3	1
daf-16	2/19/2018	JW	7	1	1	1
daf-16	2/19/2018	JW	7	3	1	1
daf-16	2/19/2018	JW	9	2	1	1
daf-16	2/19/2018	JW	11	1	6	0
daf-16	2/19/2018	JW	11	2	4	0
daf-16	2/19/2018	JW	11	3	5	0
daf-16	2/19/2018	JW	11	4	5	0
daf-16	2/19/2018	JW	13	1	3	0
daf-16	2/19/2018	JW	13	2	5	0
daf-16	2/19/2018	JW	13	3	2	0
daf-16	2/19/2018	JW	13	4	4	0
daf-16	2/19/2018	JW	15	1	3	0
daf-16	2/19/2018	JW	15	2	5	0
daf-16	2/19/2018	JW	15	3	6	0
daf-16	2/19/2018	JW	15	4	5	0

Table A.1.2 continued

daf-16	2/19/2018	JW	17	1	6	0
daf-16	2/19/2018	JW	17	2	1	0
daf-16	2/19/2018	JW	17	3	2	0
daf-16	2/19/2018	JW	17	4	2	0
daf-16	2/19/2018	JW	19	2	2	0
daf-16	2/19/2018	JW	19	3	2	0
daf-16	2/19/2018	JW	19	4	1	0
daf-16	2/19/2018	JW	21	2	1	0
N2	3/27/2018	DP	2	2	1	1
N2	3/27/2018	DP	2	3	1	1
N2	3/27/2018	DP	3	1	2	1
N2	3/27/2018	DP	3	4	1	1
N2	3/27/2018	DP	7	1	1	1
N2	3/27/2018	DP	7	4	1	1
N2	3/27/2018	DP	9	3	1	1
N2	3/27/2018	DP	13	1	2	0
N2	3/27/2018	DP	13	4	2	0
N2	3/27/2018	DP	15	1	4	0
N2	3/27/2018	DP	15	2	5	0
N2	3/27/2018	DP	15	3	3	0
N2	3/27/2018	DP	15	4	4	0
N2	3/27/2018	DP	17	1	4	0
N2	3/27/2018	DP	17	2	8	0
N2	3/27/2018	DP	17	3	7	0
N2	3/27/2018	DP	17	4	6	0
N2	3/27/2018	DP	19	1	5	0
N2	3/27/2018	DP	19	2	4	0
N2	3/27/2018	DP	19	3	4	0
N2	3/27/2018	DP	19	4	4	0
N2	3/27/2018	DP	21	1	2	0
N2	3/27/2018	DP	21	2	2	0
N2	3/27/2018	DP	21	3	4	0
N2	3/27/2018	DP	21	4	2	0
daf-2	3/27/2018	DP	2	4	1	1
daf-2	3/27/2018	DP	7	1	1	1
daf-2	3/27/2018	DP	7	2	3	1
daf-2	3/27/2018	DP	7	3	1	1
daf-2	3/27/2018	DP	11	4	1	1
daf-2	3/27/2018	DP	13	1	1	1
daf-2	3/27/2018	DP	15	2	1	1
daf-2	3/27/2018	DP	17	1	1	1
daf-2	3/27/2018	DP	19	2	2	1
daf-2	3/27/2018	DP	21	4	1	1
daf-2	3/27/2018	DP	23	1	1	0
daf-2	3/27/2018	DP	23	3	2	0

Table A.1.2 continued

daf-2	3/27/2018	DP	23	4	1	0
daf-2	3/27/2018	DP	25	1	1	0
daf-2	3/27/2018	DP	25	3	2	0
daf-2	3/27/2018	DP	25	4	3	0
daf-2	3/27/2018	DP	27	1	1	0
daf-2	3/27/2018	DP	27	2	2	0
daf-2	3/27/2018	DP	27	3	2	0
daf-2	3/27/2018	DP	27	4	2	0
daf-2	3/27/2018	DP	29	1	2	0
daf-2	3/27/2018	DP	29	2	3	0
daf-2	3/27/2018	DP	29	3	3	0
daf-2	3/27/2018	DP	31	1	8	0
daf-2	3/27/2018	DP	31	2	1	0
daf-2	3/27/2018	DP	31	3	1	0
daf-2	3/27/2018	DP	31	4	4	0
daf-2	3/27/2018	DP	34	1	2	0
daf-2	3/27/2018	DP	34	2	7	0
daf-2	3/27/2018	DP	34	3	4	0
daf-2	3/27/2018	DP	34	4	4	0
daf-2	3/27/2018	DP	36	1	1	0
daf-2	3/27/2018	DP	36	2	2	0
daf-2	3/27/2018	DP	36	3	5	0
daf-2	3/27/2018	DP	36	4	2	0
daf-2	3/27/2018	DP	38	1	1	0
daf-16	3/27/2018	DP	2	3	1	1
daf-16	3/27/2018	DP	3	4	1	1
daf-16	3/27/2018	DP	5	4	1	1
daf-16	3/27/2018	DP	7	3	1	0
daf-16	3/27/2018	DP	9	2	2	0
daf-16	3/27/2018	DP	9	3	3	0
daf-16	3/27/2018	DP	9	4	1	1
daf-16	3/27/2018	DP	9	4	1	0
daf-16	3/27/2018	DP	11	1	1	0
daf-16	3/27/2018	DP	11	1	2	1
daf-16	3/27/2018	DP	11	2	4	0
daf-16	3/27/2018	DP	11	3	1	0
daf-16	3/27/2018	DP	11	4	1	0
daf-16	3/27/2018	DP	13	1	9	0
daf-16	3/27/2018	DP	13	2	10	0
daf-16	3/27/2018	DP	13	3	12	0
daf-16	3/27/2018	DP	13	4	12	0
daf-16	3/27/2018	DP	15	1	2	0
daf-16	3/27/2018	DP	15	2	1	0
daf-16	3/27/2018	DP	15	3	1	0
daf-16	3/27/2018	DP	15	4	3	0

Table A.1.2 continued

daf-16	3/27/2018	DP	17	1	3	0
daf-16	3/27/2018	DP	17	2	2	0
daf-16	3/27/2018	DP	19	1	1	0
daf-16	3/27/2018	DP	19	2	1	0
daf-16	3/27/2018	DP	19	3	1	0

A.2 Supplemental Figures

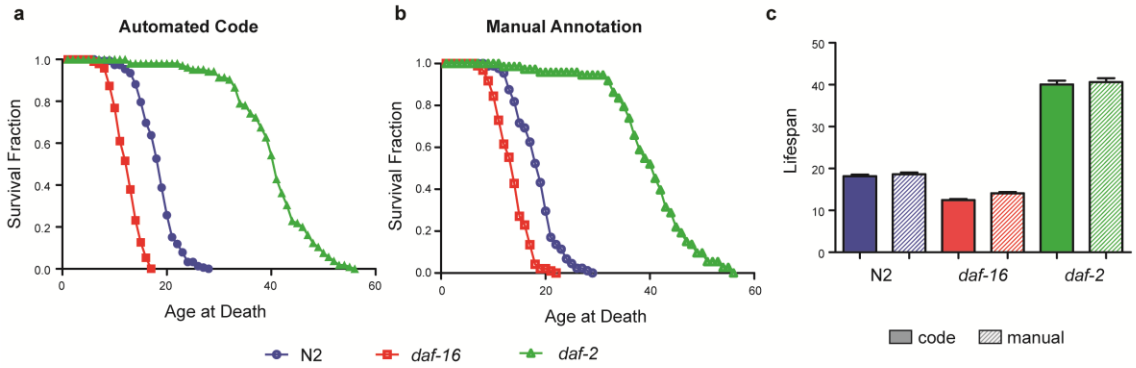

Appendix A.2.1. Validation of automated live/dead code. a) Lifespan curves obtained from the automated analysis code for wild-type (18.20 days ± 0.37, n = 87 individuals), *daf-16* (12.48 days ± 0.26, n = 95 individuals), and *daf-2* (40.08 days ± 0.91, n = 73 individuals) populations. Error is reported as SEM. b) Manual annotation of death for the videos inputted into the automated analysis code for wild-type (18.48 days ± 0.42), *daf-16 (*13.78 days ± 0.32), and *daf-2* (40.29 days ± 0.94) populations. Error is reported as SEM. c) Comparison of average lifespans for wild-type, *daf-16*, and *daf-2* populations as found by the code and manual annotation. Error is reported as SEM. No significant difference was found between code outputted and manually annotated lifespans (log-rank test, *daf-16* p = 0.0162, N2 p = 0.3609, *daf-2* p = 0.6333)

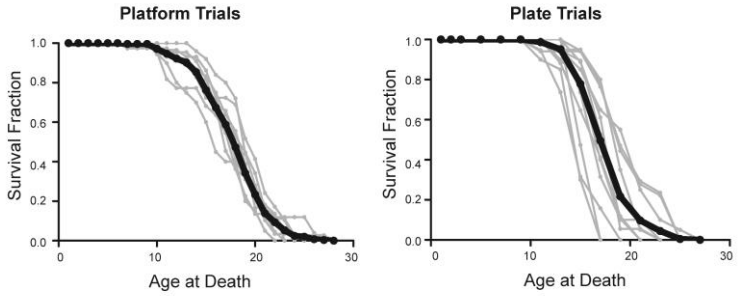

Appendix A.2.2. Characterization of trial-to-trial variability. a) Lifespan curves for each trial for N2, cultured at 25°C with $OD_{600}5$ food concentration on the platform. Gray curves show individual trials while the black curve shows the aggregated lifespan curve. b) Lifespan curves for each trial for N2, cultured at 25°C with $OD_{600}5$ food concentration on plate. Gray curves show individual trials while the black curve shows the aggregated lifespan curve.

Appendix A.2.3. Sources of variability across experimental trials

Variance components and the percent of variance due to difference sources of variability across trials cultured on the platform and on plate. Variance was calculated using a GLM mixed-effect model. Total variation across the two culture methods is comparable. Variance attributed to different trials is lower within the platform. The individual variation is higher; however, this could be due to bacteria. A single trial of the plate assay was seeded with the same batch of bacteria, while multiple batches were grown and used on the platform due to the high consumption rate of bacteria culture. As a result, the high 'individual variation' could be due to variation across bacterial cultures.

	PLATFORM VARIABILITY		**PLATE CONTROL VARIABILITY**	
Source of Variability	Variance	Percent of Variance (%)	Variance	Percent of Variance (%)
Trial	0.8281	6.41	2.2211	27.16
Trial x Plate	0.1568	1.21	0.0237	0.29

Individual Variation	11.9275	92.26	5.9189	72.38
Total	**12.9124**		**8.1773**	

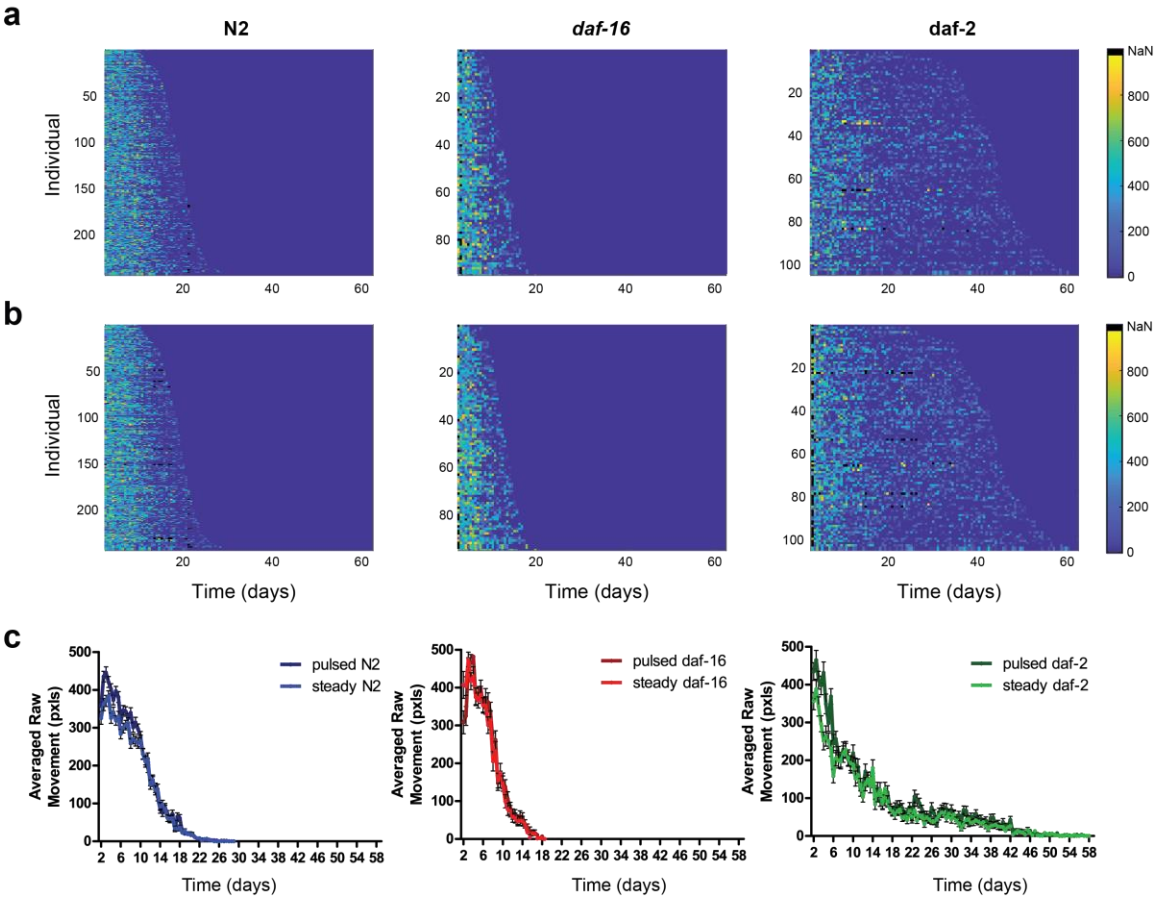

Appendix A.2.4. Worms under constant fluid-flow demonstrated evoked behavior. a) Heatmaps of individual raw movement over time for N2, *daf-16,*and *daf-2* populations under constant flow conditions (~15µL/min). b) Heatmaps of raw movement over time for N2, *daf-16,*and *daf-2* populations after opening the downstream solenoid valve, creating a strong, pulse of fluid flow (~275µL/min) for 5 seconds. c) Population averages of raw movement over time for both the constant flow and 'pulsed' flow conditions across genotypes. No statistical significance was found between the two flow conditions (Kolmogorov-Smirnov test, N2 p = 0.9782, *daf-16* p = 1.000, *daf-2* p = 0.1413), indicating the constant flow conditions create enough of a mechanical stimulus to view stimulated behavior (error bars are SEM).

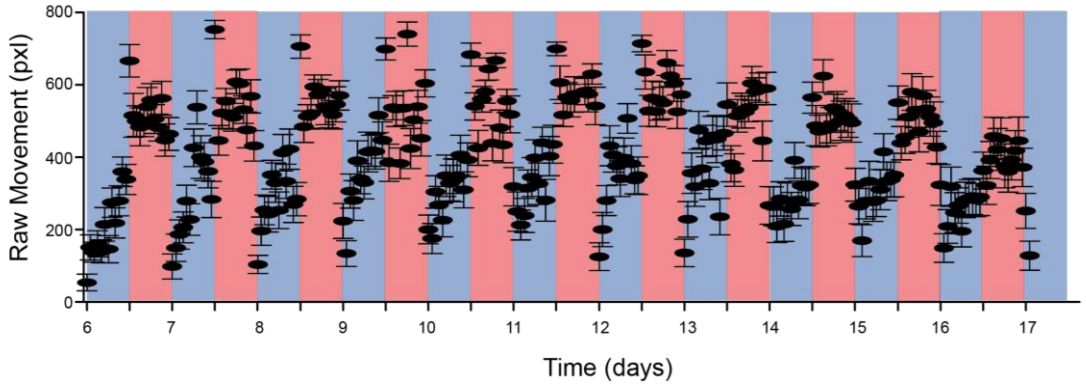

Appendix A.2.5. Average raw movement of a population under oscillatory thermal swings (n = 26 individuals). Error bars are SEM. Blue background indicates a culture temperature of 15°C and a red background indicates a temperature of 20°C.

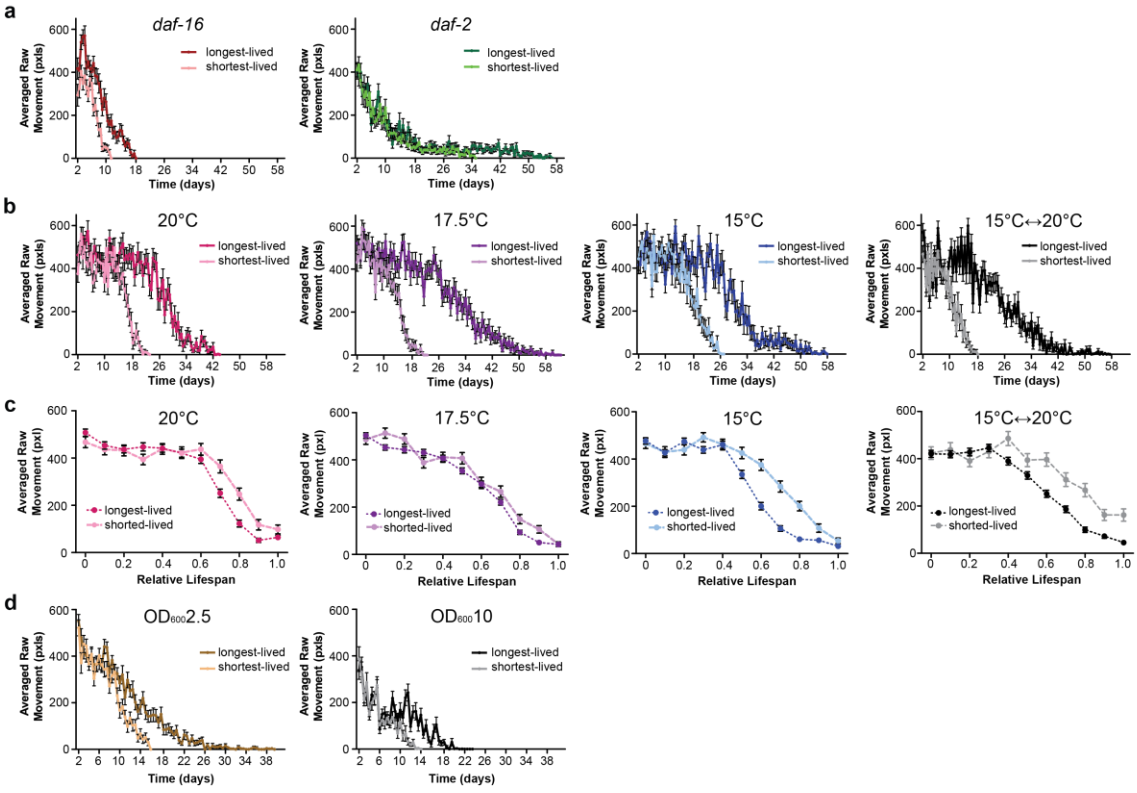

Appendix A.2.6. Intrapopulation behavioral decline across genetic and environmental perturbations. a) Averaged raw movement over time of the short- and long-lived subpopulations at 25°C at OD6005 food level across different genotypes (error bars are SEM). b) (*top)* Averaged raw movement over time of the short- and long-lived wild-type subpopulations at OD6005 food level across different thermal conditions. 20°C short- (n =

16 individuals) and long-lived (n = 16 individuals) subpopulations. 17.5°C short- (n = 24 individuals) and long-lived (n = 22 individuals) subpopulations. 15°C short- (n = 14 individuals) and long-lived (n = 15 individuals) subpopulations. 15°C↔20°C short- (n = 21 individuals) and long-lived (n = 22 individuals) subpopulations (error bars are SEM). *(bottom)* Corresponding average raw movement over normalized, relative lifespan of the short- and long-lived subpopulations across different thermal conditions (error bars are SEM). c) Averaged raw movement over time of the short- and long-lived wild-type subpopulations at 25°C across different food levels (error bars are SEM).

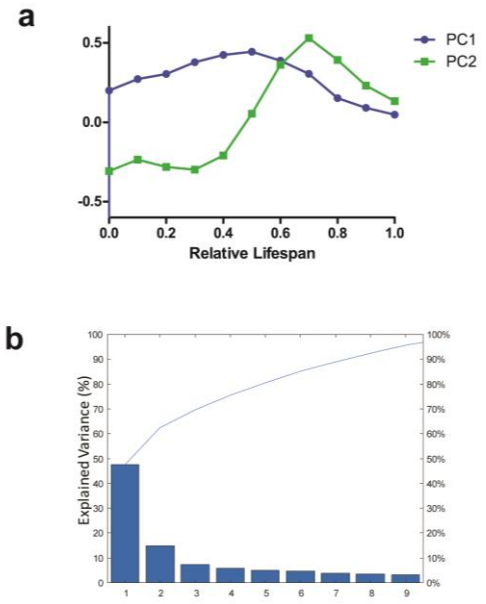

Appendix A.2.7. Characterization of PCA. a) First two principle component curves. b) Scree plot of explained variance with each principle component.

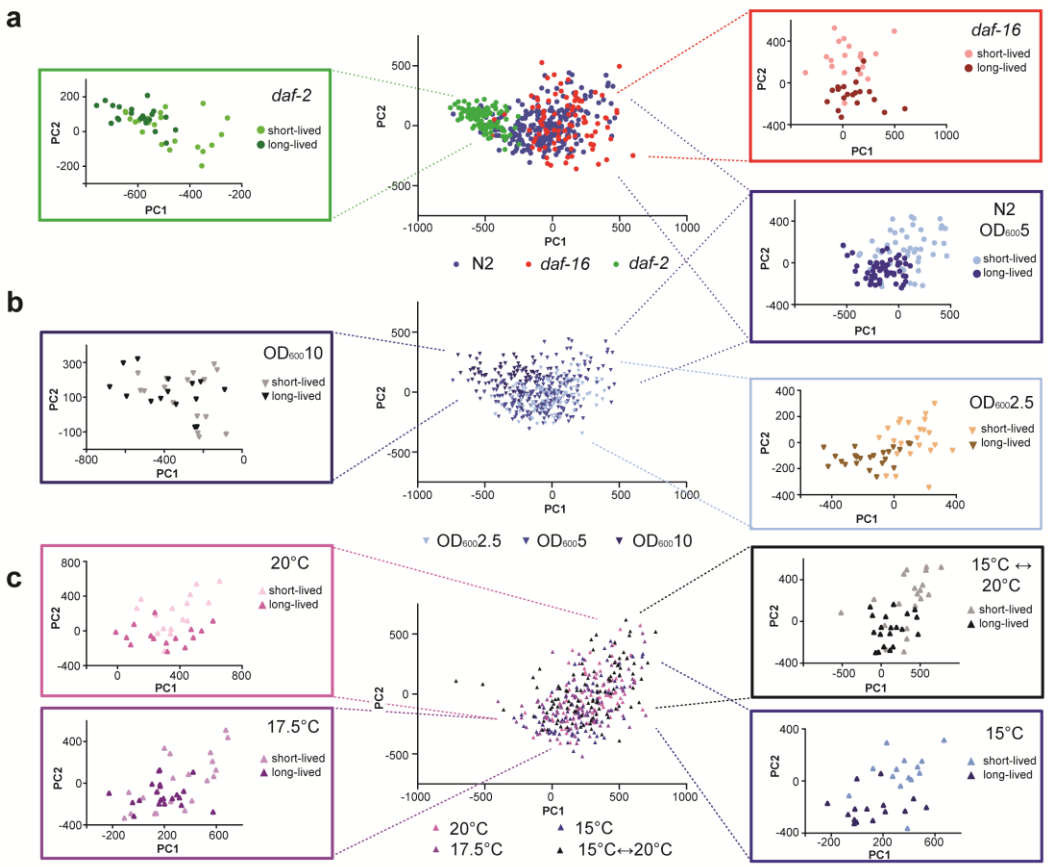

Appendix A.2.8. Intrapopulation variation within the PC space. a) Individuals cultured at 25°C at food level OD6005. Inserts show the spatial location and division of the short-lived and long-lived cohorts across the different genotypes. b) Wild-type individuals cultured at 25°C. Inserts show the spatial location and division of the short-lived and long-lived cohorts across the different food levels. c) Wild-type individuals cultured at food level OD6005. Inserts show the spatial location and division of the short-lived and long-lived cohorts cultured at different thermal conditions.

APPENDIX B. CHAPTER 3 SUPPLEMENTARY MATERIAL

A portion of the figures below are adapted from a research article entitled "Deep learning for robust and flexible tracking in behavioral studies for *C. elegans*", accepted to PLOS Computational Biology (https://doi.org/10.1101/2021.02.08.430359).[105]

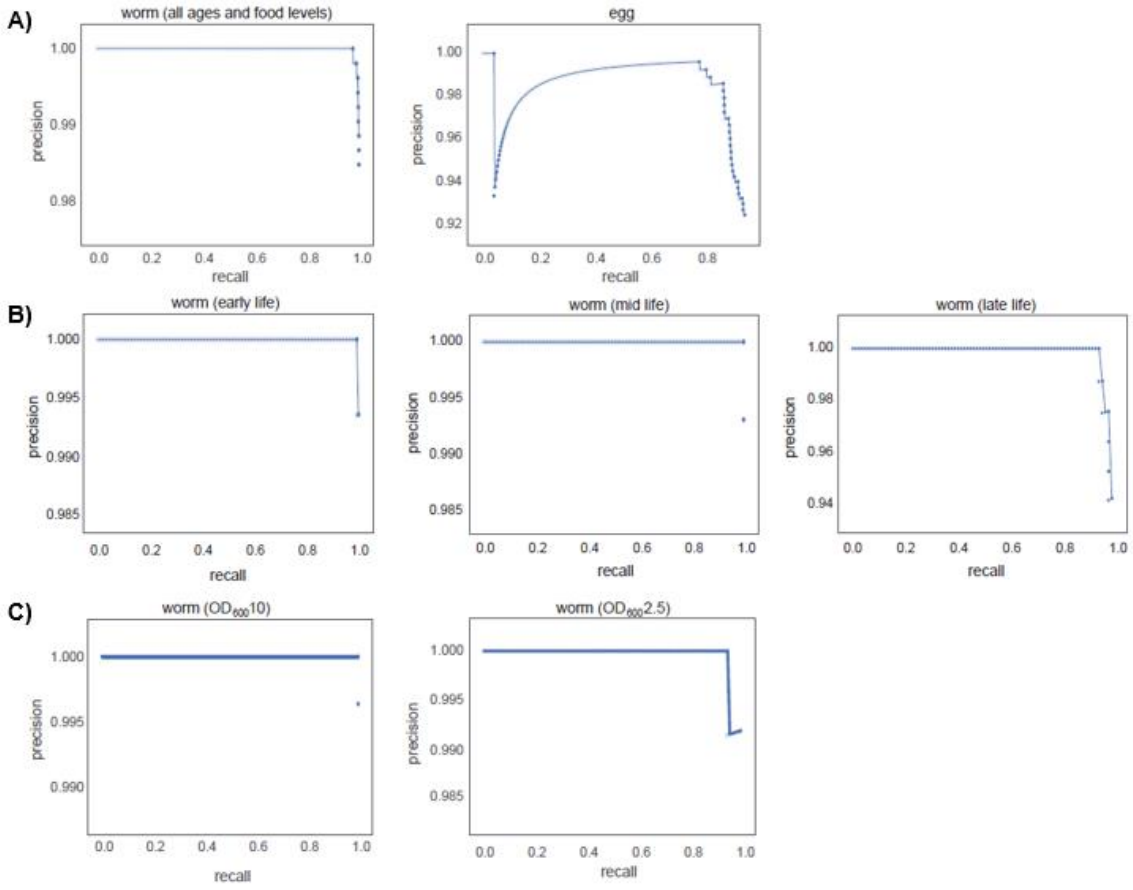

Appendix B.1. Precision-recall curves for the trained Faster R-CNN model. A) Precision-recall curve for the overall worm detection (*left*) and egg detection (*right*) with confidence threshold of 0.5. B) Precision-recall curves for the worm at varying stages in the lifespan with confidence threshold of 0.5. C) Precision-recall curves for the worm at different food levels/contrasts with confidence threshold of 0.5.

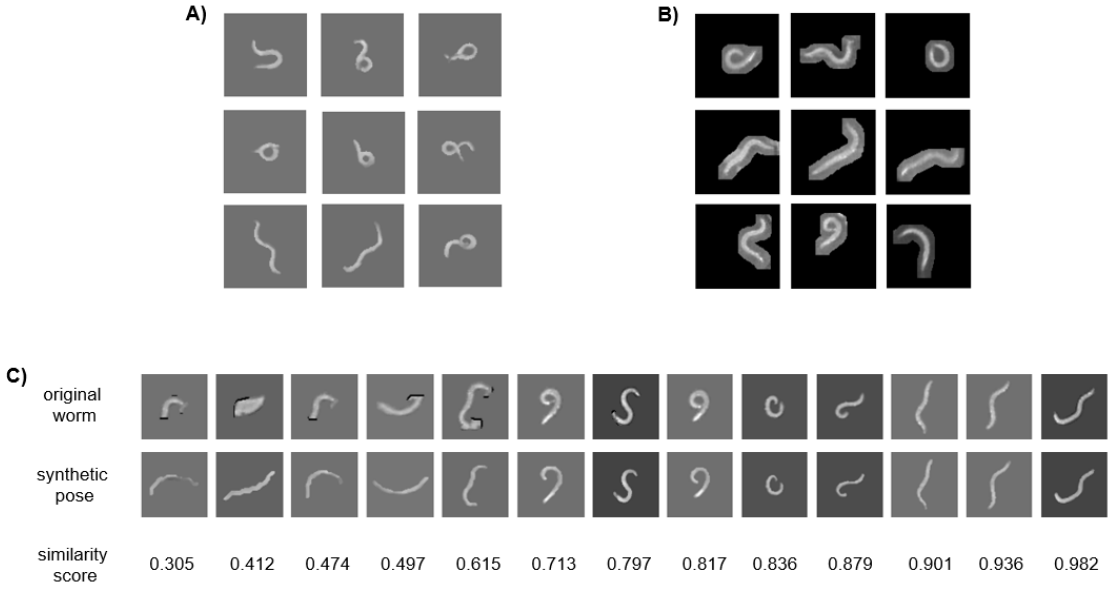

Appendix B.2. Characterizing synthetic poses from WormPose. A) Representative frames of synthetically created postures using WormPose. B) Representative frames of masked experimental data used to train the model. C) Examples of synthetic recreations of inputted frames and their corresponding similarity score for quality control.

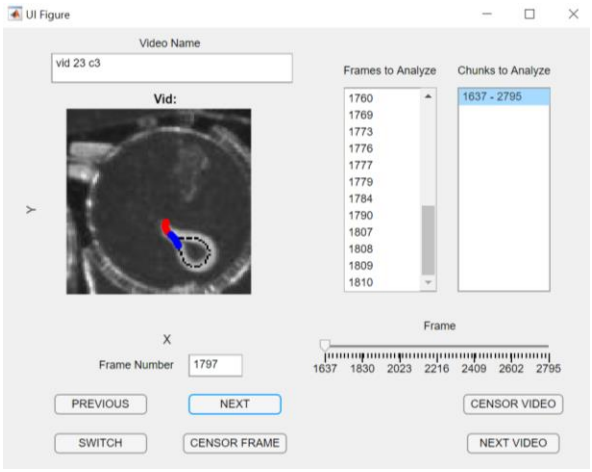

Appendix B.3. A custom GUI for head tracking and post-processing. A screenshot of a MATLAB GUI used to check the location of the head (red) and tail (blue) of the worm during coiled and occluded events.

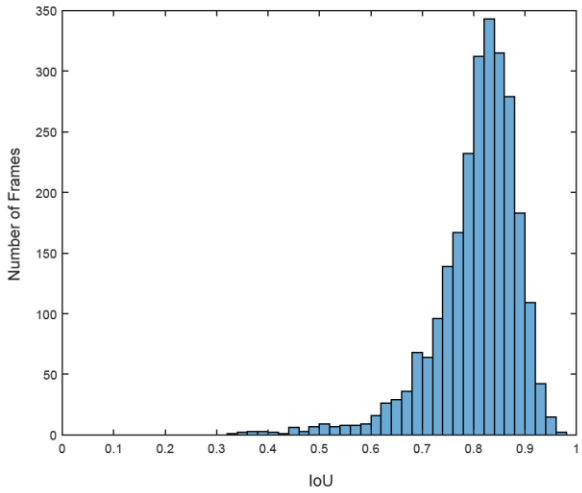

Appendix B.4. Accurate detection of worms using Faster R-CNN. Histogram of IoU values for bounding boxes detected by the Faster R-CNN model compared to bounding boxes of hand annotated, segmented worms of the same frame. (n = 2550 frames).

APPENDIX C. CHAPTER 4 SUPPLEMENTARY MATERIAL

C.1 Raw Data for Survival Analysis

All individuals were WT N2, cultured at 25°C post Day 2 of adulthood. Censored individuals were highlighted in grey.

Food Level	Date of L4	Device		Chamber	Age at Death
OD2.5	1/30/2020	IF_4	Exp3	3	17
OD2.5	1/30/2020	IF_4	Exp3	16	26
OD2.5	1/30/2020	IF_4	Exp3	17	18
OD2.5	1/30/2020	IF_4	Exp3	23	24
OD2.5	1/30/2020	IF_4	Exp3	24	25
OD2.5	1/30/2020	IF_4	Exp3	26	24
OD2.5	1/30/2020	IF_4	Exp3	27	22
OD2.5	1/30/2020	IF_4	Exp3	29	24
OD2.5	1/30/2020	IF_4	Exp3	31	19
OD2.5	1/30/2020	IF_4	Exp3	35	30
OD2.5	1/30/2020	IF_4	Exp3	36	21
OD2.5	1/30/2020	IF_4	Exp3	40	18
OD2.5	1/30/2020	IF_4	Exp3	42	21
OD2.5	1/30/2020	IF_4	Exp3	47	23
OD2.5	1/30/2020	IF_4	Exp3	48	25
OD2.5	1/30/2020	IF_4	Exp3	50	24
OD2.5	1/30/2020	IF_4	Exp3	51	19
OD2.5	1/30/2020	IF_4	Exp3	53	21
OD2.5	1/30/2020	IF_4	Exp3	54	25
OD2.5	1/30/2020	IF_4	Exp3	57	15
OD2.5	1/30/2020	IF_4	Exp3	58	17
OD2.5	1/30/2020	IF_4	Exp3	60	14
OD10	1/30/2020	IF_4	Exp4	2	11
OD10	1/30/2020	IF_4	Exp4	4	18
OD10	1/30/2020	IF_4	Exp4	14	14
OD10	1/30/2020	IF_4	Exp4	15	22
OD10	1/30/2020	IF_4	Exp4	16	20
OD10	1/30/2020	IF_4	Exp4	22	9
OD10	1/30/2020	IF_4	Exp4	25	19
OD10	1/30/2020	IF_4	Exp4	26	18
OD10	1/30/2020	IF_4	Exp4	31	16
OD10	1/30/2020	IF_4	Exp4	33	16

Table C.1 continued

OD10	1/30/2020	IF_4	Exp4	37	19
OD10	1/30/2020	IF_4	Exp4	39	11
OD10	1/30/2020	IF_4	Exp4	41	14
OD10	1/30/2020	IF_4	Exp4	42	15
OD10	1/30/2020	IF_4	Exp4	48	20
OD10	1/30/2020	IF_4	Exp4	53	14
OD10	1/30/2020	IF_4	Exp4	54	18
OD10	1/30/2020	IF_4	Exp4	56	20
OD10	1/30/2020	IF_4	Exp4	58	17
OD2.5	1/30/2020	IF_4	Exp10	3	22
OD2.5	1/30/2020	IF_4	Exp10	6	27
OD2.5	1/30/2020	IF_4	Exp10	16	19
OD2.5	1/30/2020	IF_4	Exp10	18	22
OD2.5	1/30/2020	IF_4	Exp10	19	21
OD2.5	1/30/2020	IF_4	Exp10	20	29
OD2.5	1/30/2020	IF_4	Exp10	21	22
OD2.5	1/30/2020	IF_4	Exp10	23	21
OD2.5	1/30/2020	IF_4	Exp10	24	21
OD2.5	1/30/2020	IF_4	Exp10	29	18
OD2.5	1/30/2020	IF_4	Exp10	30	26
OD2.5	1/30/2020	IF_4	Exp10	42	19
OD2.5	1/30/2020	IF_4	Exp10	43	20
OD2.5	1/30/2020	IF_4	Exp10	44	17
OD2.5	1/30/2020	IF_4	Exp10	45	32
OD2.5	1/30/2020	IF_4	Exp10	46	24
OD2.5	1/30/2020	IF_4	Exp10	51	21
OD2.5	1/30/2020	IF_4	Exp10	56	21
OD2.5	1/30/2020	IF_4	Exp10	57	20
IF (S-Med, OD10)	1/30/2020	IF_4	Exp11	3	36
IF (S-Med, OD10)	1/30/2020	IF_4	Exp11	4	30
IF (S-Med, OD10)	1/30/2020	IF_4	Exp11	7	27
IF (S-Med, OD10)	1/30/2020	IF_4	Exp11	8	29
IF (S-Med, OD10)	1/30/2020	IF_4	Exp11	15	26
IF (S-Med, OD10)	1/30/2020	IF_4	Exp11	17	27
IF (S-Med, OD10)	1/30/2020	IF_4	Exp11	18	27
IF (S-Med, OD10)	1/30/2020	IF_4	Exp11	24	22
IF (S-Med, OD10)	1/30/2020	IF_4	Exp11	25	19
IF (S-Med, OD10)	1/30/2020	IF_4	Exp11	27	19
IF (S-Med, OD10)	1/30/2020	IF_4	Exp11	28	22
IF (S-Med, OD10)	1/30/2020	IF_4	Exp11	29	31
IF (S-Med, OD10)	1/30/2020	IF_4	Exp11	30	19
IF (S-Med, OD10)	1/30/2020	IF_4	Exp11	31	19
IF (S-Med, OD10)	1/30/2020	IF_4	Exp11	33	28
IF (S-Med, OD10)	1/30/2020	IF_4	Exp11	42	25
IF (S-Med, OD10)	1/30/2020	IF_4	Exp11	43	25

Table C.1 continued

IF (S-Med, OD10)	1/30/2020	IF_4	Exp11	44	27
IF (S-Med, OD10)	1/30/2020	IF_4	Exp11	51	33
IF (S-Med, OD10)	1/30/2020	IF_4	Exp11	52	24
IF (S-Med, OD10)	1/30/2020	IF_4	Exp11	53	18
IF (S-Med, OD10)	1/30/2020	IF_4	Exp11	55	26
IF (S-Med, OD10)	1/30/2020	IF_4	Exp11	56	22
IF (S-Med, OD10)	1/30/2020	IF_4	Exp11	57	21
IF (S-Med, OD10)	1/30/2020	IF_4	Exp11	58	22
IF (S-Med, OD10)	1/30/2020	IF_4	Exp11	59	28
OD10	2/7/2020	IF_5	Exp20	1	20
OD10	2/7/2020	IF_5	Exp20	2	16
OD10	2/7/2020	IF_5	Exp20	3	10
OD10	2/7/2020	IF_5	Exp20	5	10
OD10	2/7/2020	IF_5	Exp20	7	23
OD10	2/7/2020	IF_5	Exp20	8	22
OD10	2/7/2020	IF_5	Exp20	10	15
OD10	2/7/2020	IF_5	Exp20	15	13
OD10	2/7/2020	IF_5	Exp20	17	22
OD10	2/7/2020	IF_5	Exp20	18	7
OD10	2/7/2020	IF_5	Exp20	19	18
OD10	2/7/2020	IF_5	Exp20	22	19
OD10	2/7/2020	IF_5	Exp20	23	20
OD10	2/7/2020	IF_5	Exp20	24	11
OD10	2/7/2020	IF_5	Exp20	25	21
OD10	2/7/2020	IF_5	Exp20	26	13
OD10	2/7/2020	IF_5	Exp20	27	20
OD10	2/7/2020	IF_5	Exp20	28	21
OD10	2/7/2020	IF_5	Exp20	30	18
OD10	2/7/2020	IF_5	Exp20	32	13
OD10	2/7/2020	IF_5	Exp20	33	14
OD10	2/7/2020	IF_5	Exp20	35	7
OD10	2/7/2020	IF_5	Exp20	37	17
OD10	2/7/2020	IF_5	Exp20	38	22
OD10	2/7/2020	IF_5	Exp20	39	21
OD10	2/7/2020	IF_5	Exp20	42	23
OD10	2/7/2020	IF_5	Exp20	43	16
OD10	2/7/2020	IF_5	Exp20	48	19
OD10	2/7/2020	IF_5	Exp20	50	21
OD10	2/7/2020	IF_5	Exp20	51	19
OD10	2/7/2020	IF_5	Exp20	52	18
OD10	2/7/2020	IF_5	Exp20	54	18
OD10	2/7/2020	IF_5	Exp20	55	22
OD10	2/7/2020	IF_5	Exp20	56	20
OD10	2/7/2020	IF_5	Exp20	57	18
OD10	2/7/2020	IF_5	Exp20	59	10

Table C.1 continued

IF (S-Med, OD10)	2/7/2020	IF_5	Exp21	1	24
IF (S-Med, OD10)	2/7/2020	IF_5	Exp21	5	25
IF (S-Med, OD10)	2/7/2020	IF_5	Exp21	6	34
IF (S-Med, OD10)	2/7/2020	IF_5	Exp21	8	21
IF (S-Med, OD10)	2/7/2020	IF_5	Exp21	9	26
IF (S-Med, OD10)	2/7/2020	IF_5	Exp21	12	22
IF (S-Med, OD10)	2/7/2020	IF_5	Exp21	18	30
IF (S-Med, OD10)	2/7/2020	IF_5	Exp21	19	27
IF (S-Med, OD10)	2/7/2020	IF_5	Exp21	21	33
IF (S-Med, OD10)	2/7/2020	IF_5	Exp21	22	35
IF (S-Med, OD10)	2/7/2020	IF_5	Exp21	26	23
IF (S-Med, OD10)	2/7/2020	IF_5	Exp21	27	33
IF (S-Med, OD10)	2/7/2020	IF_5	Exp21	28	24
IF (S-Med, OD10)	2/7/2020	IF_5	Exp21	29	29
IF (S-Med, OD10)	2/7/2020	IF_5	Exp21	30	28
IF (S-Med, OD10)	2/7/2020	IF_5	Exp21	31	37
IF (S-Med, OD10)	2/7/2020	IF_5	Exp21	32	28
IF (S-Med, OD10)	2/7/2020	IF_5	Exp21	33	27
IF (S-Med, OD10)	2/7/2020	IF_5	Exp21	34	35
IF (S-Med, OD10)	2/7/2020	IF_5	Exp21	39	24
IF (S-Med, OD10)	2/7/2020	IF_5	Exp21	40	17
IF (S-Med, OD10)	2/7/2020	IF_5	Exp21	41	22
IF (S-Med, OD10)	2/7/2020	IF_5	Exp21	42	37
IF (S-Med, OD10)	2/7/2020	IF_5	Exp21	43	32
IF (S-Med, OD10)	2/7/2020	IF_5	Exp21	44	24
IF (S-Med, OD10)	2/7/2020	IF_5	Exp21	45	22
IF (S-Med, OD10)	2/7/2020	IF_5	Exp21	47	31
IF (S-Med, OD10)	2/7/2020	IF_5	Exp21	48	24
IF (S-Med, OD10)	2/7/2020	IF_5	Exp21	50	31
IF (S-Med, OD10)	2/7/2020	IF_5	Exp21	51	28
IF (S-Med, OD10)	2/7/2020	IF_5	Exp21	53	18
IF (S-Med, OD10)	2/7/2020	IF_5	Exp21	54	18
IF (S-Med, OD10)	2/7/2020	IF_5	Exp21	56	33
IF (S-Med, OD10)	2/7/2020	IF_5	Exp21	58	33
IF (S-Med, OD10)	2/7/2020	IF_5	Exp21	59	25
IF (S-Med, OD10)	2/7/2020	IF_5	Exp21	60	23
IF (S-Med, OD10)	2/7/2020	IF_6	Exp25	3	28
IF (S-Med, OD10)	2/7/2020	IF_6	Exp25	4	24
IF (S-Med, OD10)	2/7/2020	IF_6	Exp25	5	28
IF (S-Med, OD10)	2/7/2020	IF_6	Exp25	7	24
IF (S-Med, OD10)	2/7/2020	IF_6	Exp25	8	27
IF (S-Med, OD10)	2/7/2020	IF_6	Exp25	9	27
IF (S-Med, OD10)	2/7/2020	IF_6	Exp25	13	28
IF (S-Med, OD10)	2/7/2020	IF_6	Exp25	17	30
IF (S-Med, OD10)	2/7/2020	IF_6	Exp25	22	14

Table C.1 continued

IF (S-Med, OD10)	2/7/2020	IF_6	Exp25	23	33
IF (S-Med, OD10)	2/7/2020	IF_6	Exp25	24	23
IF (S-Med, OD10)	2/7/2020	IF_6	Exp25	25	35
IF (S-Med, OD10)	2/7/2020	IF_6	Exp25	26	39
IF (S-Med, OD10)	2/7/2020	IF_6	Exp25	29	21
IF (S-Med, OD10)	2/7/2020	IF_6	Exp25	30	26
IF (S-Med, OD10)	2/7/2020	IF_6	Exp25	31	23
IF (S-Med, OD10)	2/7/2020	IF_6	Exp25	32	22
IF (S-Med, OD10)	2/7/2020	IF_6	Exp25	39	30
IF (S-Med, OD10)	2/7/2020	IF_6	Exp25	41	34
IF (S-Med, OD10)	2/7/2020	IF_6	Exp25	41	26
IF (S-Med, OD10)	2/7/2020	IF_6	Exp25	44	26
IF (S-Med, OD10)	2/7/2020	IF_6	Exp25	45	31
IF (S-Med, OD10)	2/7/2020	IF_6	Exp25	47	23
IF (S-Med, OD10)	2/7/2020	IF_6	Exp25	48	19
IF (S-Med, OD10)	2/7/2020	IF_6	Exp25	49	26
IF (S-Med, OD10)	2/7/2020	IF_6	Exp25	51	16
IF (S-Med, OD10)	2/7/2020	IF_6	Exp25	52	25
IF (S-Med, OD10)	2/7/2020	IF_6	Exp25	53	25
IF (S-Med, OD10)	2/7/2020	IF_6	Exp25	54	28
IF (S-Med, OD10)	2/7/2020	IF_6	Exp25	55	20
IF (S-Med, OD10)	2/7/2020	IF_6	Exp25	56	29
IF (S-Med, OD10)	2/7/2020	IF_6	Exp25	57	15
IF (S-Med, OD10)	2/7/2020	IF_6	Exp25	59	19
IF (S-Med, OD10)	2/7/2020	IF_6	Exp28	4	30
IF (S-Med, OD10)	2/7/2020	IF_6	Exp28	6	24
IF (S-Med, OD10)	2/7/2020	IF_6	Exp28	10	29
IF (S-Med, OD10)	2/7/2020	IF_6	Exp28	26	35
IF (S-Med, OD10)	2/7/2020	IF_6	Exp28	27	4
IF (S-Med, OD10)	2/7/2020	IF_6	Exp28	31	26
IF (S-Med, OD10)	2/7/2020	IF_6	Exp28	40	24
IF (S-Med, OD10)	2/7/2020	IF_6	Exp28	43	27
IF (S-Med, OD10)	2/7/2020	IF_6	Exp28	46	20
IF (S-Med, OD10)	2/7/2020	IF_6	Exp28	47	26
IF (S-Med, OD10)	2/7/2020	IF_6	Exp28	50	30
IF (S-Med, OD10)	2/7/2020	IF_6	Exp28	51	20
IF (S-Med, OD10)	2/7/2020	IF_6	Exp28	54	38
IF (S-Med, OD10)	2/7/2020	IF_6	Exp28	55	38
IF (S-Med, OD10)	2/7/2020	IF_6	Exp28	56	23
IF (S-Med, OD10)	2/7/2020	IF_6	Exp28	58	39
OD10	2/7/2020	IF_6	Exp32	1	17
OD10	2/7/2020	IF_6	Exp32	4	21
OD10	2/7/2020	IF_6	Exp32	5	21
OD10	2/7/2020	IF_6	Exp32	8	16
OD10	2/7/2020	IF_6	Exp32	9	16

Table C.1 continued

OD10	2/7/2020	IF_6	Exp32	14	16
OD10	2/7/2020	IF_6	Exp32	15	17
OD10	2/7/2020	IF_6	Exp32	16	19
OD10	2/7/2020	IF_6	Exp32	19	22
OD10	2/7/2020	IF_6	Exp32	20	19
OD10	2/7/2020	IF_6	Exp32	21	19
OD10	2/7/2020	IF_6	Exp32	22	21
OD10	2/7/2020	IF_6	Exp32	23	17
OD10	2/7/2020	IF_6	Exp32	25	19
OD10	2/7/2020	IF_6	Exp32	28	11
OD10	2/7/2020	IF_6	Exp32	30	14
OD10	2/7/2020	IF_6	Exp32	31	12
OD10	2/7/2020	IF_6	Exp32	33	21
OD10	2/7/2020	IF_6	Exp32	38	19
OD10	2/7/2020	IF_6	Exp32	41	17
OD10	2/7/2020	IF_6	Exp32	42	10
OD10	2/7/2020	IF_6	Exp32	44	21
OD10	2/7/2020	IF_6	Exp32	47	17
OD10	2/7/2020	IF_6	Exp32	49	20
OD10	2/7/2020	IF_6	Exp32	50	14
OD10	2/7/2020	IF_6	Exp32	51	22
OD10	2/7/2020	IF_6	Exp32	52	21
OD10	2/7/2020	IF_6	Exp32	54	20
OD10	2/7/2020	IF_6	Exp32	55	17
OD10	2/7/2020	IF_6	Exp32	57	12
OD2.5	9/27/2019	IF_2	Exp8	1	24
OD2.5	9/27/2019	IF_2	Exp8	5	28
OD2.5	9/27/2019	IF_2	Exp8	8	21
OD2.5	9/27/2019	IF_2	Exp8	9	22
OD2.5	9/27/2019	IF_2	Exp8	10	23
OD2.5	9/27/2019	IF_2	Exp8	15	21
OD2.5	9/27/2019	IF_2	Exp8	16	23
OD2.5	9/27/2019	IF_2	Exp8	17	22
OD2.5	9/27/2019	IF_2	Exp8	21	21
OD2.5	9/27/2019	IF_2	Exp8	25	22
OD2.5	9/27/2019	IF_2	Exp8	26	23
OD2.5	9/27/2019	IF_2	Exp8	27	26
OD2.5	9/27/2019	IF_2	Exp8	28	24
OD2.5	9/27/2019	IF_2	Exp8	32	34
OD2.5	9/27/2019	IF_2	Exp8	33	24
OD2.5	9/27/2019	IF_2	Exp8	35	23
OD2.5	9/27/2019	IF_2	Exp8	40	28
OD2.5	9/27/2019	IF_2	Exp8	41	31
OD2.5	9/27/2019	IF_2	Exp8	42	30
OD2.5	9/27/2019	IF_2	Exp8	46	23

Table C.1 continued

OD2.5	9/27/2019	IF_2	Exp8	47	22
OD2.5	9/27/2019	IF_2	Exp8	48	26
OD2.5	9/27/2019	IF_2	Exp8	49	22
OD2.5	9/27/2019	IF_2	Exp8	50	26
OD2.5	9/27/2019	IF_2	Exp8	51	27
OD2.5	9/27/2019	IF_2	Exp8	53	27
OD2.5	9/27/2019	IF_2	Exp8	54	27
OD2.5	9/27/2019	IF_2	Exp8	55	24
OD2.5	9/27/2019	IF_2	Exp8	56	28
OD2.5	9/27/2019	IF_2	Exp8	57	17
OD2.5	9/27/2019	IF_2	Exp8	58	12
OD2.5	9/27/2019	IF_3	Exp15	1	0
OD2.5	9/27/2019	IF_3	Exp15	4	18
OD2.5	9/27/2019	IF_3	Exp15	5	33
OD2.5	9/27/2019	IF_3	Exp15	7	16
OD2.5	9/27/2019	IF_3	Exp15	9	21
OD2.5	9/27/2019	IF_3	Exp15	10	21
OD2.5	9/27/2019	IF_3	Exp15	13	19
OD2.5	9/27/2019	IF_3	Exp15	15	25
OD2.5	9/27/2019	IF_3	Exp15	19	25
OD2.5	9/27/2019	IF_3	Exp15	21	25
OD2.5	9/27/2019	IF_3	Exp15	22	24
OD2.5	9/27/2019	IF_3	Exp15	23	30
OD2.5	9/27/2019	IF_3	Exp15	25	25
OD2.5	9/27/2019	IF_3	Exp15	28	20
OD2.5	9/27/2019	IF_3	Exp15	32	27
OD2.5	9/27/2019	IF_3	Exp15	34	22
OD2.5	9/27/2019	IF_3	Exp15	35	14
OD2.5	9/27/2019	IF_3	Exp15	36	23
OD2.5	9/27/2019	IF_3	Exp15	37	25
OD2.5	9/27/2019	IF_3	Exp15	38	22
OD2.5	9/27/2019	IF_3	Exp15	41	29
OD2.5	9/27/2019	IF_3	Exp15	42	18
OD2.5	9/27/2019	IF_3	Exp15	45	27
OD2.5	9/27/2019	IF_3	Exp15	47	31
OD2.5	9/27/2019	IF_3	Exp15	48	26
OD2.5	9/27/2019	IF_3	Exp15	49	0
OD2.5	9/27/2019	IF_3	Exp15	50	25
OD2.5	9/27/2019	IF_3	Exp15	52	25
OD2.5	9/27/2019	IF_3	Exp15	53	25
OD2.5	9/27/2019	IF_3	Exp15	55	23
OD2.5	9/27/2019	IF_3	Exp15	56	25
OD2.5	9/27/2019	IF_3	Exp15	58	22
OD2.5	9/27/2019	IF_3	Exp15	59	24
OD10	9/27/2019	IF_2	Exp6	1	13

Table C.1 continued

OD10	9/27/2019	IF_2	Exp6	4	14
OD10	9/27/2019	IF_2	Exp6	5	15
OD10	9/27/2019	IF_2	Exp6	6	14
OD10	9/27/2019	IF_2	Exp6	9	14
OD10	9/27/2019	IF_2	Exp6	14	19
OD10	9/27/2019	IF_2	Exp6	15	10
OD10	9/27/2019	IF_2	Exp6	16	15
OD10	9/27/2019	IF_2	Exp6	32	22
OD10	9/27/2019	IF_2	Exp6	33	17
OD10	9/27/2019	IF_2	Exp6	35	13
OD10	9/27/2019	IF_2	Exp6	39	20
OD10	9/27/2019	IF_2	Exp6	42	16
OD10	9/27/2019	IF_2	Exp6	45	25
OD10	9/27/2019	IF_2	Exp6	50	15
OD10	9/27/2019	IF_2	Exp6	53	13
OD10	9/27/2019	IF_2	Exp6	55	13
OD10	9/27/2019	IF_2	Exp6	56	14
OD10	9/27/2019	IF_2	Exp6	59	15
OD10	9/27/2019	IF_2	Exp6	60	17
OD10	9/27/2019	IF_2	Exp7	2	14
OD10	9/27/2019	IF_2	Exp7	4	19
OD10	9/27/2019	IF_2	Exp7	6	11
OD10	9/27/2019	IF_2	Exp7	7	22
OD10	9/27/2019	IF_2	Exp7	10	8
OD10	9/27/2019	IF_2	Exp7	14	22
OD10	9/27/2019	IF_2	Exp7	17	24
OD10	9/27/2019	IF_2	Exp7	20	19
OD10	9/27/2019	IF_2	Exp7	21	23
OD10	9/27/2019	IF_2	Exp7	23	17
OD10	9/27/2019	IF_2	Exp7	26	24
OD10	9/27/2019	IF_2	Exp7	27	19
OD10	9/27/2019	IF_2	Exp7	28	13
OD10	9/27/2019	IF_2	Exp7	32	11
OD10	9/27/2019	IF_2	Exp7	40	18
OD10	9/27/2019	IF_2	Exp7	44	11
OD10	9/27/2019	IF_2	Exp7	45	18
OD10	9/27/2019	IF_2	Exp7	52	14
OD10	9/27/2019	IF_2	Exp7	55	11
OD10	9/27/2019	IF_2	Exp7	57	12
OD10	9/27/2019	IF_3	Exp14	1	19
OD10	9/27/2019	IF_3	Exp14	7	19
OD10	9/27/2019	IF_3	Exp14	12	13
OD10	9/27/2019	IF_3	Exp14	13	15
OD10	9/27/2019	IF_3	Exp14	14	9
OD10	9/27/2019	IF_3	Exp14	27	19

Table C.1 continued

OD10	9/27/2019	IF_3	Exp14	28	26
OD10	9/27/2019	IF_3	Exp14	30	13
OD10	9/27/2019	IF_3	Exp14	33	18
OD10	9/27/2019	IF_3	Exp14	36	16
OD10	9/27/2019	IF_3	Exp14	38	18
OD10	9/27/2019	IF_3	Exp14	39	19
OD10	9/27/2019	IF_3	Exp14	40	15
OD10	9/27/2019	IF_3	Exp14	46	15
OD10	9/27/2019	IF_3	Exp14	49	0
OD10	9/27/2019	IF_3	Exp14	54	13
OD10	9/27/2019	IF_3	Exp14	56	17
OD10	9/27/2019	IF_3	Exp14	59	11
OD10	9/27/2019	IF_3	Exp14	60	23

C.2 Supplemental Figures

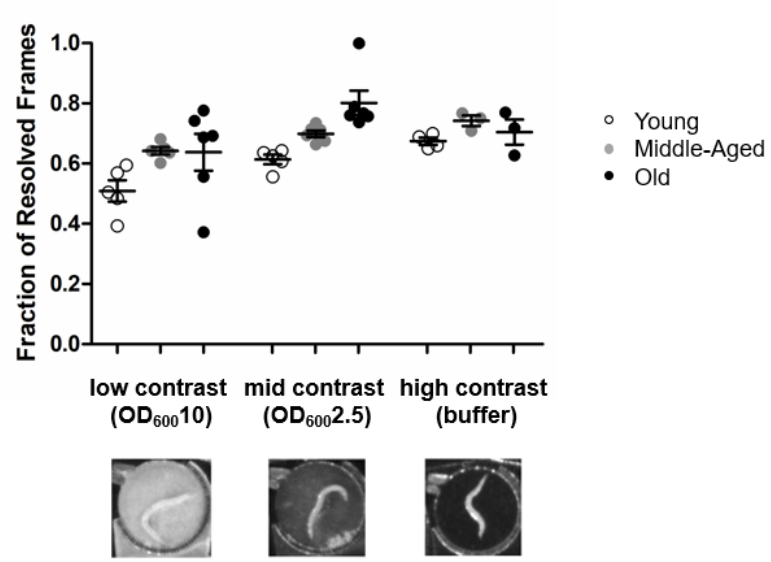

Appendix C.2.1. Characterizing the performance of the deep learning pipeline on the IF dataset. *(top)* Fraction of resolved frames for worms cultured under different food conditions with age. Each point is the fraction of resolved frames across an entire day of recordings. *(bottom)* Representative images of worms under the different food and contrast conditions.

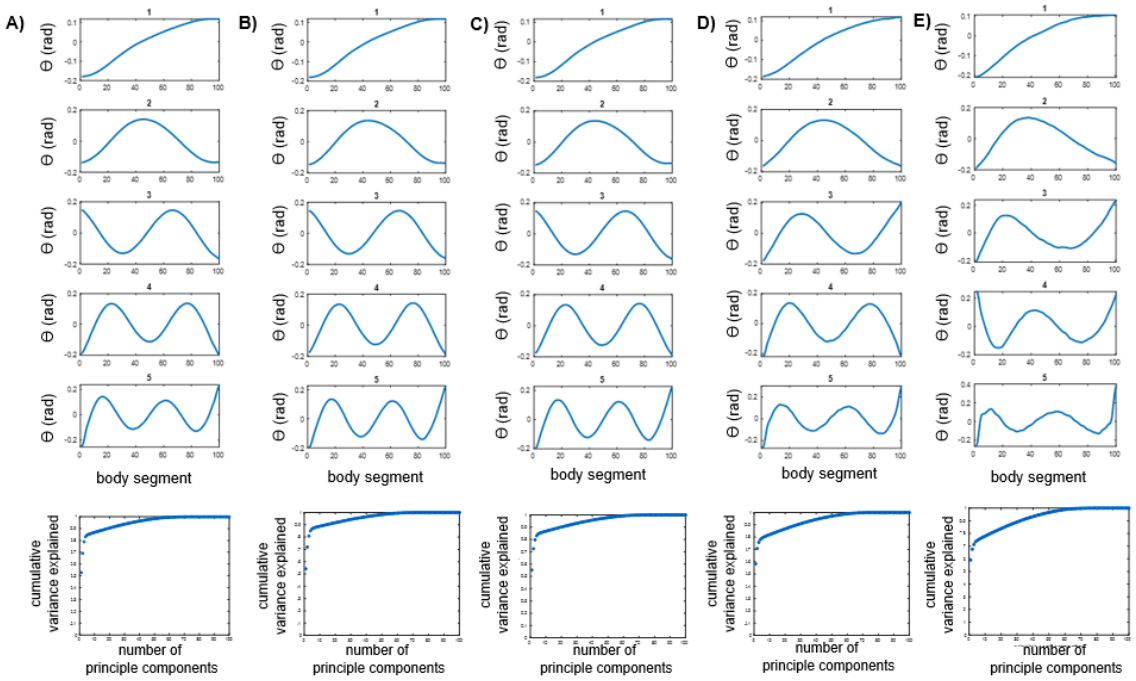

Appendix C.2.2. Eigenworms for *C. elegans* cultured on-chip across different age ranges. A) *(top)* The first five eigenworms for worms cultured on-chip for the 0-20% of the relative lifespan. *(bottom)* The first five modes capture 84.63% of postural variance. B) *(top)* The first five eigenworms for worms cultured on-chip for the 20-40% of the relative lifespan. *(bottom)* The first five modes capture 86.66% of postural variance. C) *(top)* The first five eigenworms for worms cultured on-chip for the 40-60% of the relative lifespan. *(bottom)* The first five modes capture 84.45% of postural variance. D) *(top)* The first five eigenworms for worms cultured on-chip for the 60-80% of the relative lifespan. *(bottom)* The first five modes capture 79.15% of postural variance. E) *(top)* The first five eigenworms for worms cultured on-chip for the 80-100% of the relative lifespan. *(bottom)* The first five modes capture 74.39% of postural variance.

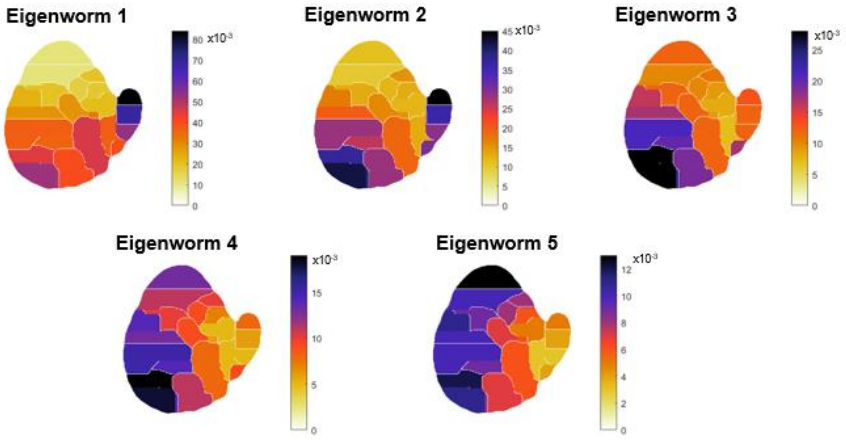

Appendix C.2.3. Wavelet amplitudes across eigenworms for the discretized behavioral regions.

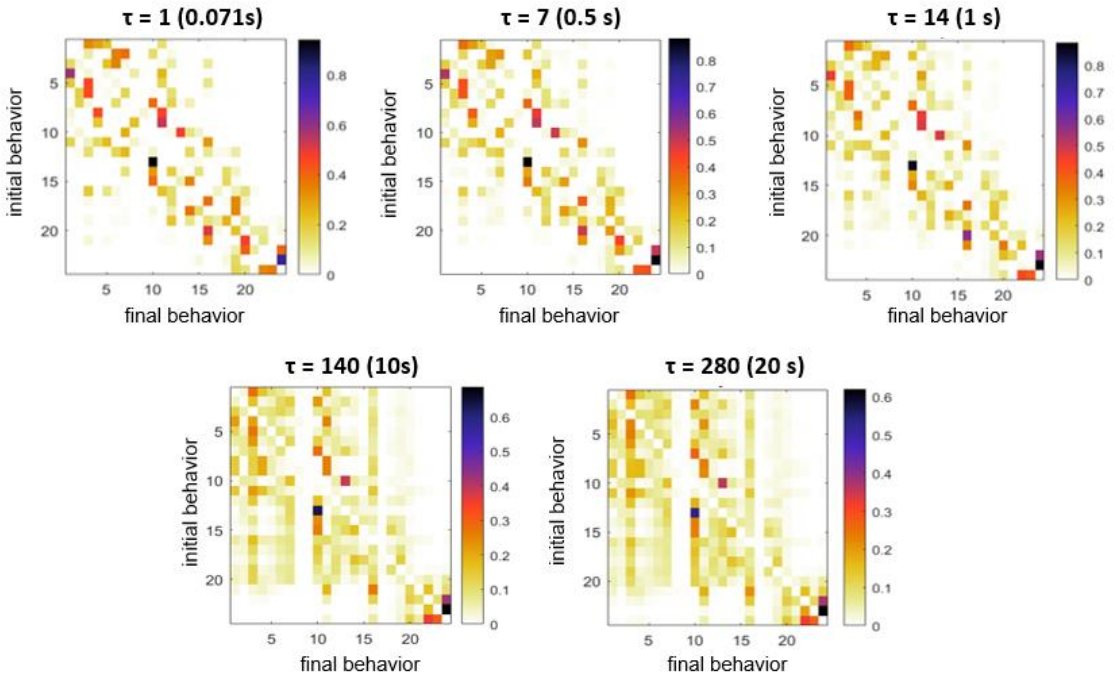

Appendix C.2.4. Behavioral transition probabilities are non-Markovian in *C. elegans*. Behavioral transition matrices retain a structure past τ = 7 frames, the expected decay in a Markovian system. Past τ = 140 frames the transition matrix begins to lose its structure.

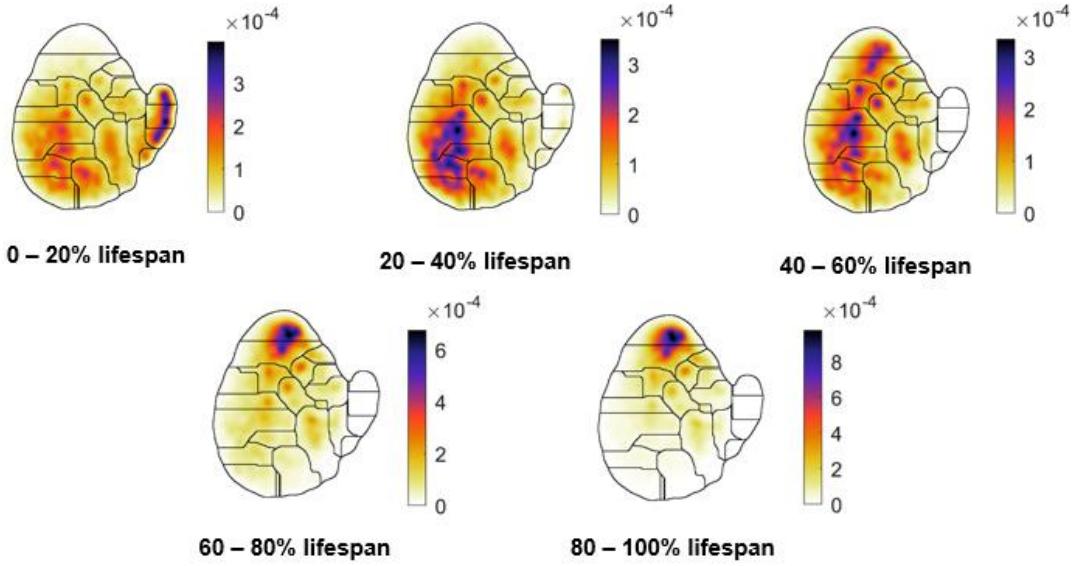

Appendix C.2.5. Differences in behavior across relative age. Behavioral PDF maps of individuals cultured with no DR across their lifespan.

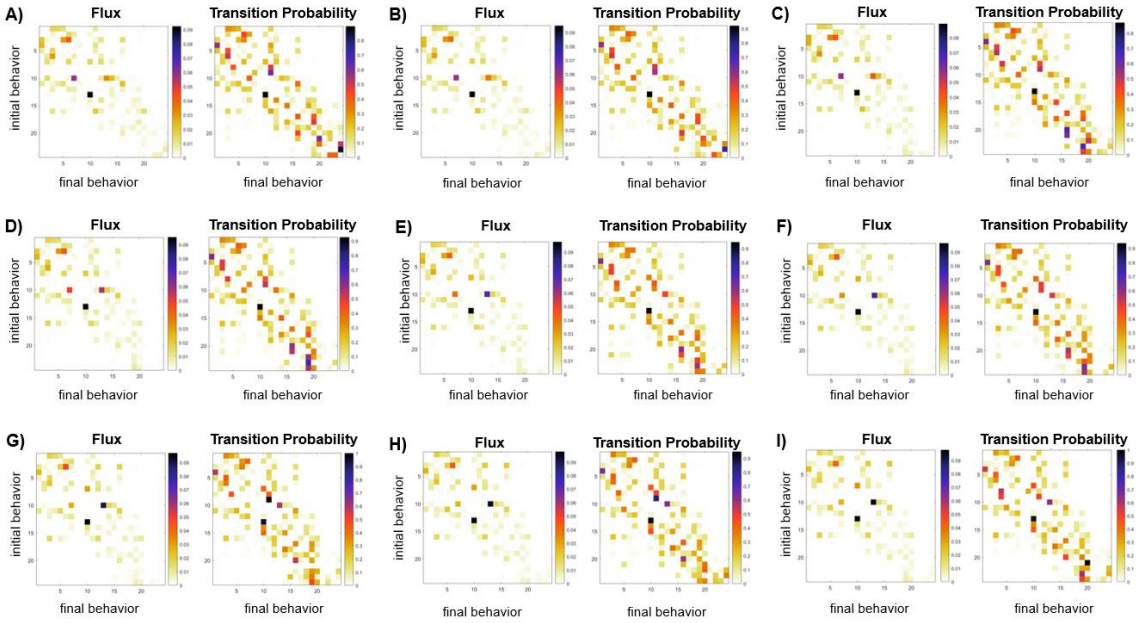

Appendix C.2.6. Worms transition to similar behaviors throughout the behavioral map across their lifespan. Flux matrix and transition probability matrix (τ = 1 frame) across the 24 regions for individuals under no DR across 2-day aged cohorts. A) Day 2-4 aged worms. B) Day 4-6 aged worms. C) Day 6-8 aged worms. D) Day 8-10 aged worms. E) Day 10-12

aged worms. F) Day 12-14 aged worms. G) Day 14-16 aged worms. H) Day 16-18 aged worms. I) Day 18-20 aged worms.

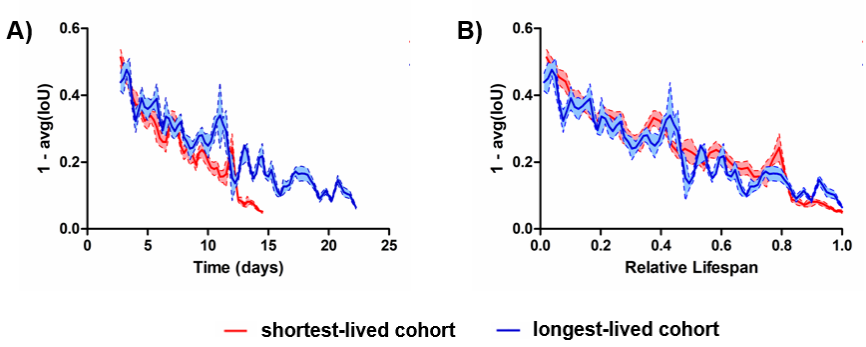

Appendix C.2.7. Differences in movement decline across short- and long-lived individuals within an isogenic population. A) Average movement decline over time (error bars are SEM). B) Average movement decline across the normalized lifespan (error bars are SEM).

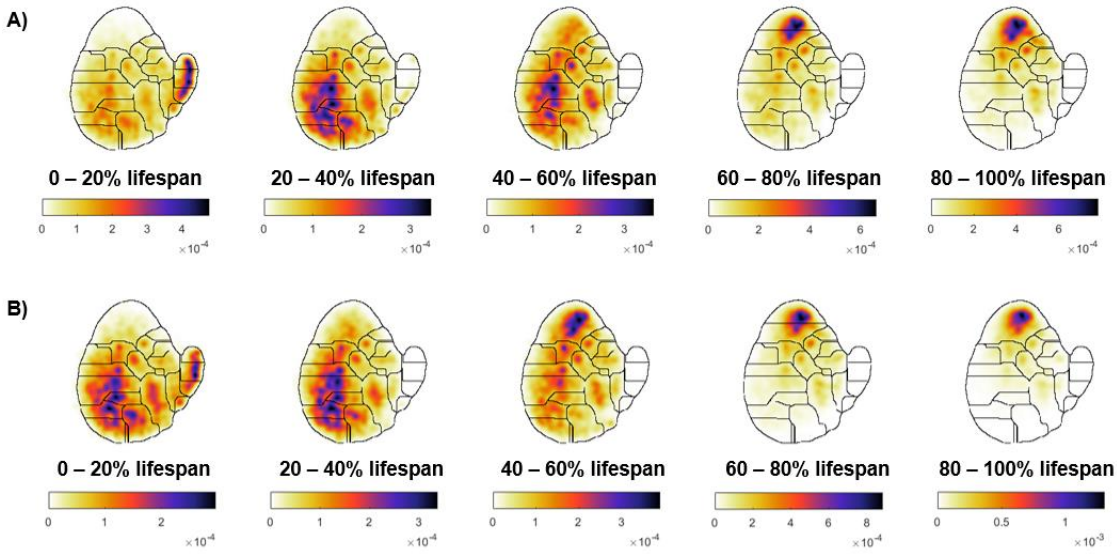

Appendix C.2.8. Differences in behavior across short- and long-lived individuals within an isogenic population across age. A) Behavioral PDF maps of short-lived individuals cultured with no DR across their relative lifespan. B) Behavioral PDF maps of long-lived individuals cultured with no DR across their relative lifespan.

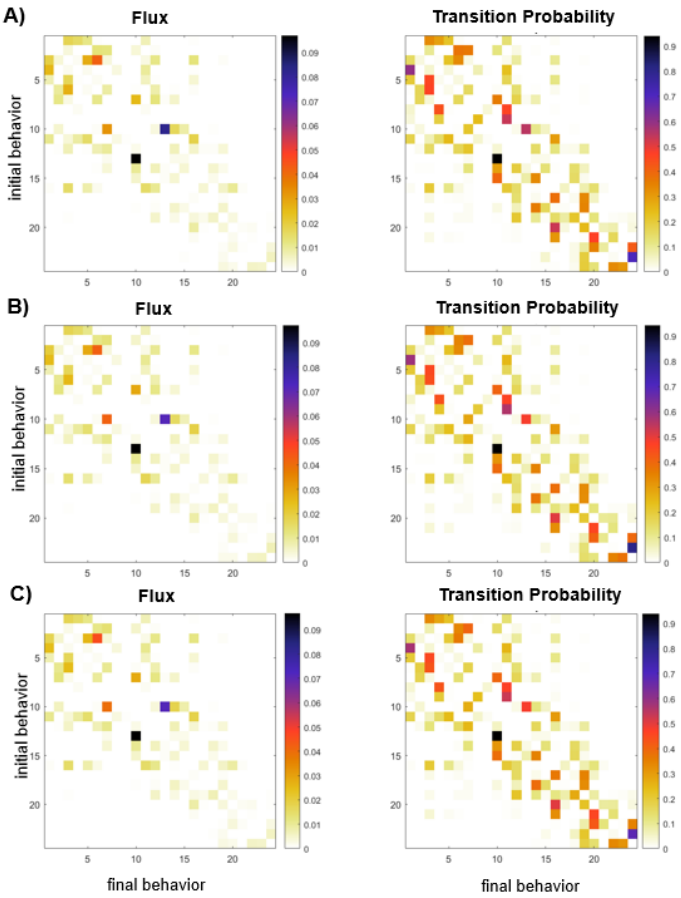

Appendix C.2.9. Worms transition to similar behaviors throughout the behavioral map across different food conditions. *(left)* Flux matrix and *(right)* transition probability matrix (τ = 1 frame) across the 24 regions across recordings for individuals across all time points. A) Worms cultured under no DR. B) Worms cultured under CR. C) Worms cultured under IF.

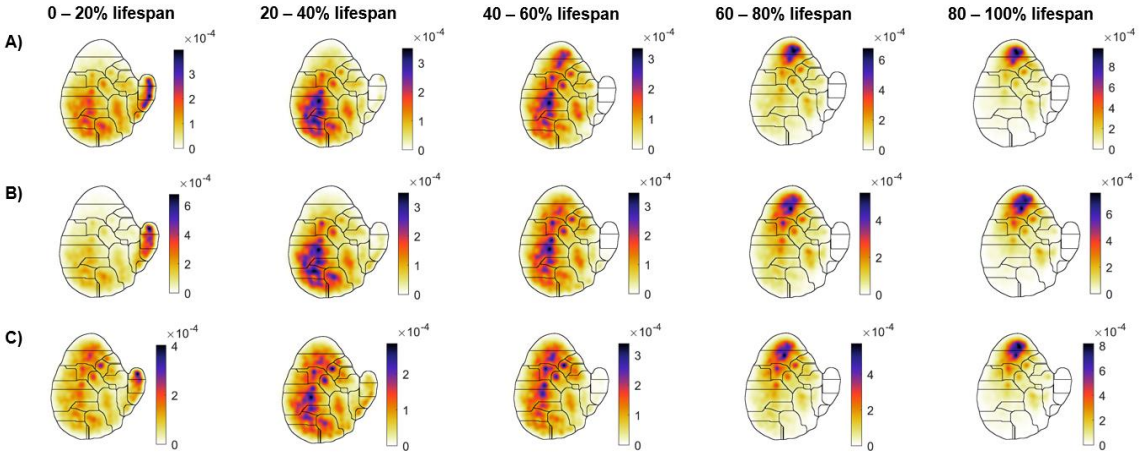

Appendix C.2.10. Differences in behavior across food conditions across age. A) Behavioral PDF maps of individuals cultured with no DR across their relative lifespan. B) Behavioral PDF maps of individuals cultured with CR across their relative lifespan. C) Behavioral PDF maps of individuals cultured with IF across their relative lifespan.

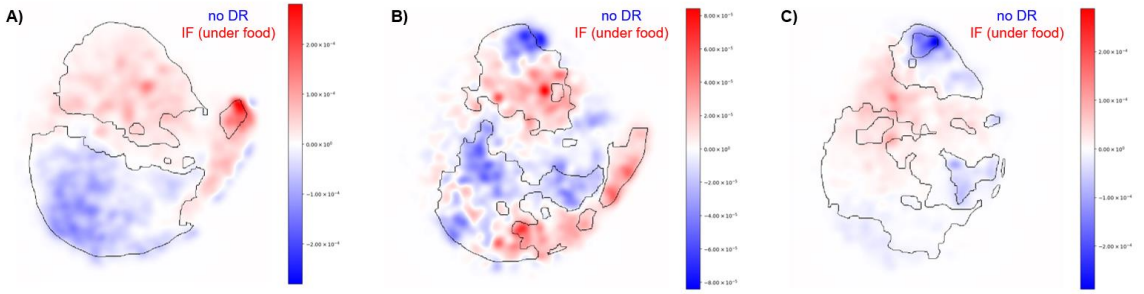

Appendix C.2.11. Significant differences in behaviors from individuals across no DR and IF conditions with age. A) Difference between the PDFs of individuals under no DR (Day 4-8) and IF with food present (Day 8-10). Outlined areas are statistically significantly different regions across the two maps. B) Difference between the PDFs of individuals under no DR (Day 8-12) and IF with food present (Day 12-14). Outlined areas are statistically significantly different regions across the two maps. C) Difference between the PDFs of individuals under no DR (Day 12-16) and IF with food present (Day 20-22).

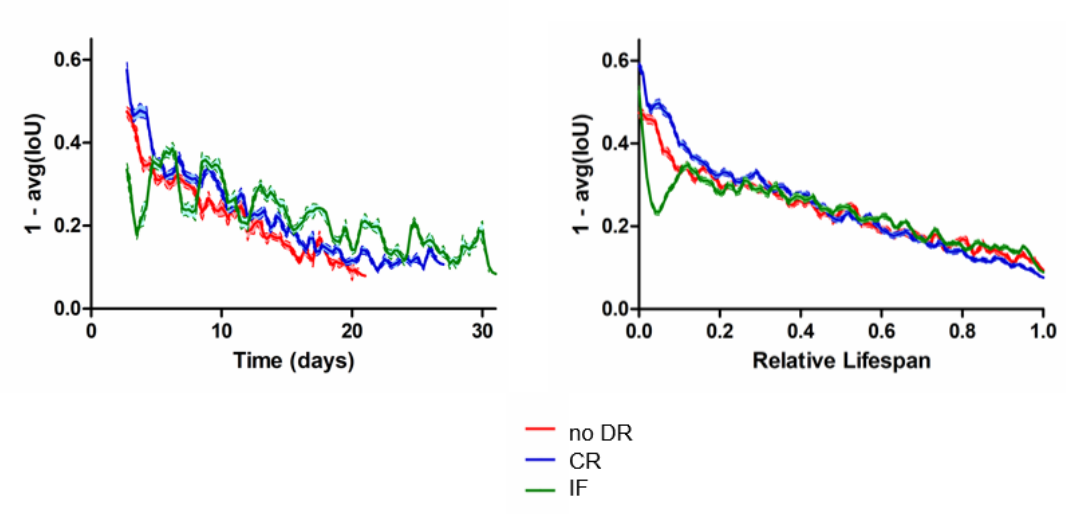

Appendix C.2.12. Differences in movement decline across food conditions. *(left)* Average movement decline over time (error bars are SEM). *(right)* Average movement decline across the normalized lifespan (error bars are SEM).

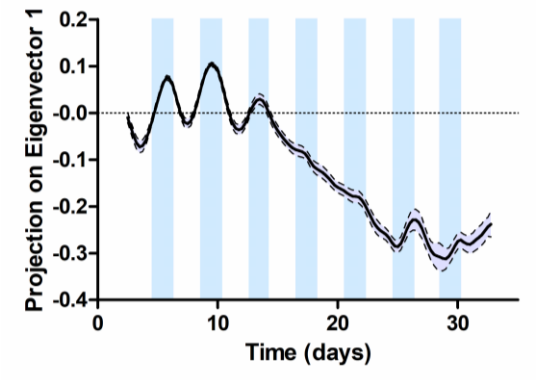

Appendix C.2.13. Behavior under IF is dependent on the presented food condition. Projection onto the first eigenvector from the behavioral covariance matrix across time (error bars are the standard deviation from bootstrapped samples). Areas shaded in blue are times where worms were exposed to food. Areas in white indicate periods where no food was present.

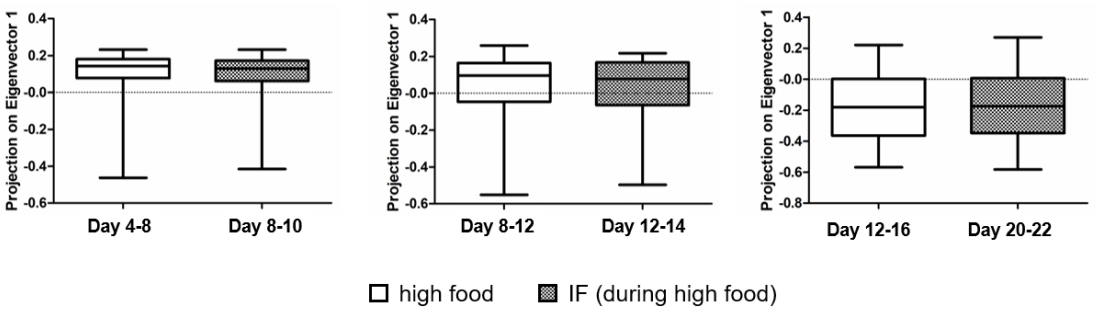

Appendix C.2.14. Individuals in no DR and IF have similar behaviors across the shifted age ranges. Projection values for all recordings under the designated time and food conditions indicate similar behaviors for individuals under no DR and older IF individuals exposed to food. There was no significant difference between any of the aged comparisons (t-test, $p > 0.001$).

REFERENCES

1. Roth, G. A. *et al.* Global Burden of Cardiovascular Diseases and Risk Factors, 1990–2019: Update From the GBD 2019 Study. *J. Am. Coll. Cardiol.* **76**, 2982–3021 (2020).

2. Virani, S. S. *et al.* Heart Disease and Stroke Statistics—2021 Update. *Circulation* E254–E743 (2021). doi:10.1161/CIR.0000000000000950

3. Sung, H. *et al.* Global Cancer Statistics 2020: GLOBOCAN Estimates of Incidence and Mortality Worldwide for 36 Cancers in 185 Countries. *CA. Cancer J. Clin.* **71**, 209–249 (2021).

4. Matthews, K. *et al.* Racial and ethnic estimates of Alzheimer's disease and related dementias in the United States (2015-2060) in adults aged ≥65 years. *Alzheimers. Dement.* **15**, 17–24 (2019).

5. López-Otín, C., Blasco, M. A., Partridge, L., Serrano, M. & Kroemer, G. The Hallmarks of Aging. *Cell* **153**, 1194–1217 (2013).

6. DiLoreto, R. & Murphy, C. T. The cell biology of aging. *Mol. Biol. Cell* **26**, 4524–4531 (2015).

7. Kennedy, B. K. *et al.* Geroscience: Linking aging to chronic disease. *Cell* **159**, 709–713 (2014).

8. Shaye, D. D. & Greenwald, I. OrthoList: A Compendium of C. elegans Genes with Human Orthologs. *PLoS One* **6**, e20085 (2011).

9. Kenyon, C., Chang, J., Gensch, E., Rudner, A. & Tabtlang, R. A C. elegans mutant that lives twice as long as wild type. *Nature* **366**, (1993).

10. Kimura, K. D., Tissenbaum, H. A., Liu, Y. & Ruvkun, G. daf-2, an insulin receptor-like gene that regulates longevity and diapause in Caenorhabditis elegans. *Science* **277**, 942–946 (1997).

11. Kenyon, C. The plasticity of aging: Insights from long-lived mutants. *Cell* **120**, 449–460 (2005).

12. Ogg, S. *et al.* The Fork head transcription factor DAF-16 transduces insulin-like metabolic and longevity signals in C. elegans. *Nature* **389**, 994–999 (1997).

13. Lin, K., Dorman, J. B., Rodan, A. & Kenyon, C. daf-16: An HNF-3/forkhead family member that can function to double the life-span of Caenorhabditis elegans. *Science* **278**, 1319–1322 (1997).

14. Hsu, A.-L., Murphy, C. T. & Kenyon, C. Regulation of Aging and Age-Related Disease by DAF-16 and Heat-Shock Factor. *Science (80-.).* **300**, 1142–1145 (2003).

15. Morley, J. F. & Morimoto, R. I. Regulation of longevity in Caenorhabditis elegans by heat shock factor and molecular chaperones. *Mol. Biol. Cell* **15**, 657–664 (2004).

16. Bishop, N. A. & Guarente, L. Two neurons mediate diet-restriction-induced longevity in C. elegans. *Nature* **447**, 545–549 (2007).

17. Tullet, J. M. A. *et al.* Direct inhibition of the longevity-promoting factor SKN-1 by insulin-like signaling in C. elegans. *Cell* **132**, 1025–1038 (2008).

18. Tatar, M., Bartke, A. & Antebi, A. The Endocrine Regulation of Aging by Insulin-like Signals. *Science (80-.).* **299**, 1346–1351 (2003).

19. Holzenberger, M. *et al.* IGF-1 receptor regulates lifespan and resistance to oxidative stress in mice. *Nature* **421**, 182–187 (2003).

20. Suh, Y. *et al.* Functionally significant insulin-like growth factor I receptor mutations in centenarians. *Proc. Natl. Acad. Sci. U. S. A.* **105**, 3438–3442 (2008).

21. Willcox, B. J. *et al.* FOXO3A genotype is strongly associated with human longevity. *Proc. Natl. Acad. Sci.* **105**, 13987 LP – 13992 (2008).

22. Vellai, T. *et al.* Influence of TOR kinase on lifespan in C. elegans. *Nature* **426**, 620 (2003).

23. Kaeberlein, M. *et al.* Regulation of yeast replicative life span by TOR and Sch9 in response to nutrients. *Science* **310**, 1193–1196 (2005).

24. Greer, E. L. *et al.* An AMPK-FOXO pathway mediates longevity induced by a novel method of dietary restriction in C. elegans. *Curr. Biol.* **17**, 1646–1656 (2007).

25. Rogina, B. & Helfand, S. L. Sir2 mediates longevity in the fly through a pathway related to calorie restriction. *Proc. Natl. Acad. Sci. U. S. A.* **101**, 15998–16003 (2004).

26. Bitterman, K. J., Anderson, R. M., Cohen, H. Y., Latorre-Esteves, M. & Sinclair, D. A. Inhibition of silencing and accelerated aging by nicotinamide, a putative negative regulator of yeast sir2 and human SIRT1. *J. Biol. Chem.* **277**, 45099–45107 (2002).

27. Fontana, L., Partridge, L. & Longo, V. D. Extending healthy life span-from yeast to humans. *Science* **328**, 321–326 (2010).

28. Masoro, E. J. Overview of caloric restriction and ageing. *Mech. Ageing Dev.* **126**, 913–922 (2005).

29. Mair, W., Goymer, P., Pletcher, S. D. & Partridge, L. Demography of dietary

restriction and death in Drosophila. *Science (80-.).* **301**, 1731–1733 (2003).

30. Colman, R. J. *et al.* Caloric restriction delays disease onset and mortality in rhesus monkeys. *Science (80-.).* **325**, 201–204 (2009).

31. Partridge, L., Piper, M. D. W. & Mair, W. Dietary restriction in Drosophila. *Mech. Ageing Dev.* **126**, 938–950 (2005).

32. Wang, X. L., Liu, S. X. & Wilcken, D. E. Circulating transforming growth factor beta 1 and coronary artery disease. *Cardiovasc Res* **34**, 404–410 (1997).

33. Stekovic, S. *et al.* Alternate Day Fasting Improves Physiological and Molecular Markers of Aging in Healthy, Non-obese Humans. *Cell Metab.* **30**, 462-476.e6 (2019).

34. Greer, E. L. & Brunet, A. Different dietary restriction regimens extend lifespan by both independent and overlapping genetic pathways in C. elegans. *Aging Cell* **8**, 113–127 (2009).

35. Kenyon, C. J. The genetics of ageing. *Nature* **464**, 504–512 (2010).

36. Alcedo, J. & Kenyon, C. Regulation of C. elegans Longevity by Specific Gustatory and Olfactory Neurons. *Neuron* **41**, 45–55 (2004).

37. Apfeld, J. & Kenyon, C. Regulation of lifespan by sensory perception in Caenorhabditis elegans. *Nature* **402**, 804–809 (1999).

38. Libert, S. *et al.* Regulation of Drosophila life span by olfaction and food-derived odors. *Science (80-.).* **315**, 1133–1137 (2007).

39. Libert, S. & Pletcher, S. D. Modulation of Longevity by Environmental Sensing. *Cell* **131**, 1231–1234 (2007).

40. Lithgow, G. J., White, T. M., Melov, S. & Johnson, T. E. Thermotolerance and extended life-span conferred by single-gene mutations and induced by thermal stress. *Proc. Natl. Acad. Sci. U. S. A.* **92**, 7540–7544 (1995).

41. Xiao, R. *et al.* A Genetic Program Promotes C. elegans Longevity at Cold Temperatures via a Thermosensitive TRP Channel. *Cell* **152**, 806–817 (2013).

42. Zhang, B. *et al.* Environmental Temperature Differentially Modulates C. elegans Longevity through a Thermosensitive TRP Channel. *Cell Rep.* **11**, 1414–1424 (2015).

43. Lee, S. J. & Kenyon, C. Regulation of the Longevity Response to Temperature by Thermosensory Neurons in Caenorhabditis elegans. *Curr. Biol.* **19**, 715–722 (2009).

44. Partridge, L., Deelen, J. & Slagboom, P. E. Facing up to the global challenges of

ageing. *Nature* **561**, 45–56 (2018).

45. Ross, R. *et al.* Importance of Assessing Cardiorespiratory Fitness in Clinical Practice: A Case for Fitness as a Clinical Vital Sign: A Scientific Statement From the American Heart Association. *Circulation* **134**, e653–e699 (2016).

46. Boustani, M., Peterson, B., Hanson, L., Harris, R. & Lohr, K. N. Screening for Dementia in Primary Care: A Summary of the Evidence for the U.S. Preventive Services Task Force. *Ann. Intern. Med.* **138**, (2003).

47. Guralnik, J. *et al.* A short physical performance battery assessing lower extremity function: association with self-reported disability and prediction of mortality and nursing home admission. *J. Gerontol.* **49**, (1994).

48. Herndon, L. A. *et al.* Stochastic and genetic factors influence tissue-specific decline in ageing C. elegans. *Nature* **419**, 808–814 (2002).

49. Gerstbrein, B., Stamatas, G., Kollias, N. & Driscoll, M. In vivo spectrofluorimetry reveals endogenous biomarkers that report healthspan and dietary restriction in Caenorhabditis elegans. *Aging Cell* **4**, 127–137 (2005).

50. Bansal, A., Zhu, L. J., Yen, K. & Tissenbaum, H. A. Uncoupling lifespan and healthspan in Caenorhabditis elegans longevity mutants. *Proc. Natl. Acad. Sci.* **112**, E277–E286 (2015).

51. Hahm, J. *et al.* C. elegans maximum velocity correlates with healthspan and is maintained in worms with an insulin receptor mutation. *Nat. Commun.* **6**, 1–7 (2015).

52. Pincus, Z. & Slack, F. J. Developmental biomarkers of aging in Caenorhabditis elegans. *Dev. Dyn.* **239**, 1306–1314 (2010).

53. Huang, C., Xiong, C. & Kornfeld, K. Measurements of age-related changes of physiological processes that predict lifespan of Caenorhabditis elegans. *Proc. Natl. Acad. Sci.* **101**, 8084–8089 (2004).

54. Newell Stamper, B. L. *et al.* Movement decline across lifespan of *Caenorhabditis elegans* mutants in the insulin/insulin-like signaling pathway. *Aging Cell* e12704 (2017). doi:10.1111/acel.12704

55. Partridge, L. & Gems, D. Benchmarks for ageing studies. *Nature* **450**, 165–167 (2007).

56. Park, H. *et al.* A PTEN variant uncouples longevity from impaired fitness in Caenorhabditis elegans with reduced insulin/IGF-1 signaling. *Nat. Commun.* **12**, (2021).

57. Stroustrup, N. *et al.* The Caenorhabditis elegans Lifespan Machine. *Nat. Methods*

10, 665–70 (2013).

58. Stroustrup, N. *et al.* The temporal scaling of Caenorhabditis elegans ageing. *Nature* (2016). doi:10.1038/nature16550

59. Zhang, W. B. *et al.* Extended Twilight among Isogenic C. elegans Causes a Disproportionate Scaling between Lifespan and Health. *Cell Syst.* **3**, 333–345 (2016).

60. Churgin, M. A. *et al.* Longitudinal imaging of *Caenorhabditis elegans* in a microfabricated device reveals variation in behavioral decline during aging. *Elife* **6**, e26652 (2017).

61. Stern, S., Kirst, C. & Bargmann, C. I. Neuromodulatory Control of Long-Term Behavioral Patterns and Individuality across Development. *Cell* **171**, 1649-1662.e10 (2017).

62. Pitt, J. N. *et al.* WormBot, an open-source robotics platform for survival and behavior analysis in C. elegans. *GeroScience 2019 416* **41**, 961–973 (2019).

63. Honjoh, S., Yamamoto, T., Uno, M. & Nishida, E. Signalling through RHEB-1 mediates intermittent fasting-induced longevity in C. elegans. *Nature* **457**, 726–730 (2009).

64. Wu, D., Rea, S. L., Cypser, J. R. & Johnson, T. E. Mortality shifts in *Caenorhabditis elegans* : remembrance of conditions past. *Aging Cell* **8**, 666–675 (2009).

65. Chung, K., Crane, M. M. & Lu, H. Automated on-chip rapid microscopy, phenotyping and sorting of C. elegans. *Nat. Methods 2008 57* **5**, 637–643 (2008).

66. Gray, J. M. *et al.* Oxygen sensation and social feeding mediated by a C. elegans guanylate cyclase homologue. *Nat. 2004 4306997* **430**, 317–322 (2004).

67. Chronis, N., Zimmer, M. & Bargmann, C. I. Microfluidics for in vivo imaging of neuronal and behavioral activity in Caenorhabditis elegans. *Nat. Methods 2007 49* **4**, 727–731 (2007).

68. Chalasani, S. H. *et al.* Dissecting a circuit for olfactory behaviour in Caenorhabditis elegans. *Nat. 2007 4507166* **450**, 63–70 (2007).

69. Crane, M. M., Chung, K., Stirman, J. & Lu, H. Microfluidics-enabled phenotyping, imaging, and screening of multicellular organisms. *Lab Chip* **10**, 1509–1517 (2010).

70. McCormick, K. E., Gaertner, B. E., Sottile, M., Phillips, P. C. & Lockery, S. R. Microfluidic Devices for Analysis of Spatial Orientation Behaviors in Semi-Restrained Caenorhabditis elegans. *PLoS One* **6**, e25710 (2011).

71. McDonald, J. C. *et al.* Fabrication of microfluidic systems in

poly(dimethylsiloxane). *Electrophoresis* **21**, 27–40 (2000).

72. David C. Duffy, J. Cooper McDonald, Olivier J. A. Schueller, and & Whitesides*, G. M. Rapid Prototyping of Microfluidic Systems in Poly(dimethylsiloxane). *Anal. Chem.* **70**, 4974–4984 (1998).

73. McDonald, J. C. & Whitesides, G. M. Poly(dimethylsiloxane) as a material for fabricating microfluidic devices. *Acc. Chem. Res.* **35**, 491–499 (2002).

74. Hulme, S. E., Shevkoplyas, S. S., Apfeld, J., Fontana, W. & Whitesides, G. M. A microfabricated array of clamps for immobilizing and imaging C. elegans. *Lab Chip* **7**, 1515–1523 (2007).

75. Lee, H. *et al.* A multi-channel device for high-density target-selective stimulation and long-term monitoring of cells and subcellular features in C. elegans. *Lab Chip* **14**, 4513–4522 (2014).

76. Keil, W., Kutscher, L. M., Shaham, S. & Siggia, E. D. Long-Term High-Resolution Imaging of Developing C. elegans Larvae with Microfluidics. *Dev. Cell* **40**, 202–214 (2017).

77. Li, S., Stone, H. a & Murphy, C. T. A microfluidic device and automatic counting system for the study of C. elegans reproductive aging. *Lab Chip* **15**, 524–31 (2015).

78. Kopito, R. B. & Levine, E. Durable spatiotemporal surveillance of Caenorhabditis elegans response to environmental cues. *Lab Chip* **14**, 764–770 (2014).

79. Hulme, S. E. *et al.* Lifespan-on-a-chip: microfluidic chambers for performing lifelong observation of C. elegans. *Lab Chip* **10**, 589–597 (2010).

80. Rahman, M. *et al.* NemaLife chip: a micropillar-based microfluidic culture device optimized for aging studies in crawling C. elegans. *Sci. Rep.* **10**, 16190 (2020).

81. Xian, B. *et al.* WormFarm: A quantitative control and measurement device toward automated Caenorhabditis elegans aging analysis. *Aging Cell* **12**, 398–409 (2013).

82. Ge, A. *et al.* Logarithmic bacterial gradient chip for analyzing the effects of dietary restriction on C. elegans growth. *Sensors Actuators B Chem.* **255**, 735–744 (2018).

83. Javer, A. *et al.* An open-source platform for analyzing and sharing worm-behavior data. *Nature Methods* **15**, 645–646 (2018).

84. Swierczek, N. A., Giles, A. C., Rankin, C. H. & Kerr, R. A. High-throughput behavioral analysis in C. elegans. *Nat. Methods* **8**, 592–602 (2011).

85. Ramot, D., Johnson, B. E., Jr, T. L. B., Carnell, L. & Goodman, M. B. The Parallel Worm Tracker: A Platform for Measuring Average Speed and Drug-Induced Paralysis in Nematodes. *PLoS One* **3**, e2208 (2008).

86. Buckingham, S. D. & Sattelle, D. B. Fast, automated measurement of nematode swimming (thrashing) without morphometry. *BMC Neurosci. 2009 101* **10**, 1–6 (2009).

87. Restif, C. *et al.* CeleST: Computer Vision Software for Quantitative Analysis of C. elegans Swim Behavior Reveals Novel Features of Locomotion. *PLOS Comput. Biol.* **10**, e1003702 (2014).

88. Le, K. N. *et al.* An automated platform to monitor long-term behavior and healthspan in Caenorhabditis elegans under precise environmental control. *Commun. Biol.* **3**, 1–13 (2020).

89. Sutphin, G. L. & Kaeberlein, M. Measuring Caenorhabditis elegans life span on solid media. *J. Vis. Exp.* (2009). doi:10.3791/1152

90. Zhan, M. New Toolsets to Understand Environmental Sensation and Variability in the Aging Process. (Georgia Institute of Technology, 2014).

91. Chung, K. *et al.* Microfluidic chamber arrays for whole-organism behavior-based chemical screening. *Lab Chip* **11**, 3689–3697 (2011).

92. Entchev, E. V *et al.* A gene-expression-based neural code for food abundance that modulates lifespan. *Elife* **4**, 1–22 (2015).

93. Lucanic, M. *et al.* Impact of genetic background and experimental reproducibility on identifying chemical compounds with robust longevity effects. *Nat. Commun.* **8**, 14256 (2017).

94. Ward, A., Liu, J., Feng, Z. & Xu, X. Z. S. Light-sensitive neurons and channels mediate phototaxis in C. elegans. *Nat. Neurosci.* **11**, 916–22 (2008).

95. De Magalhaes Filho, C. D. *et al.* Visible light reduces C. elegans longevity. *Nat. Commun.* **9**, (2018).

96. Sutphin, G. L. & Kaeberlein, M. Measuring Caenorhabditis elegans life span on solid media. *J. Vis. Exp.* (2009). doi:10.3791/1152

97. Mitchell, D. H., Stiles, J. W., Santelli, J. & Sanadi, D. R. Synchronous growth and aging of Caenorhabditis elegans in the presence of fluorodeoxyuridine. *J. Gerontol.* **34**, 28–36 (1979).

98. Aitlhadj, L. & Stürzenbaum, S. R. The use of FUdR can cause prolonged longevity in mutant nematodes. *Mech. Ageing Dev.* **131**, 364–365 (2010).

99. Anderson, E. N. *et al.* C. elegans lifespan extension by osmotic stress requires FUdR, base excision repair, FOXO, and sirtuins. *Mech. Ageing Dev.* **154**, 30–42 (2016).

100. Weicksel, S. E. *et al.* A novel small molecule that disrupts a key event during the oocyte- to-embryo transition in C. elegans. doi:10.1242/dev.140046

101. Hibshman, J. D., Webster, A. K. & Baugh, L. R. Liquid-culture protocols for synchronous starvation, growth, dauer formation, and dietary restriction of Caenorhabditis elegans. *STAR Protoc.* **2**, 100276 (2021).

102. Martineau, C. N., Brown, A. E. X. & Laurent, P. Multidimensional phenotyping predicts lifespan and quantifies health in Caenorhabditis elegans. *PLOS Comput. Biol.* **16**, e1008002 (2020).

103. Rollins, J. A., Howard, A. C., Dobbins, S. K., Washburn, E. H. & Rogers, A. N. Assessing Health Span in Caenorhabditis elegans: Lessons From Short-Lived Mutants. *Journals Gerontol. Ser. A* **72**, 473–480 (2017).

104. Gong, J. *et al.* A Cold-Sensing Receptor Encoded by a Glutamate Receptor Gene. *Cell* (2019). doi:10.1016/j.cell.2019.07.034

105. Bates, K., Le, K. & Lu, H. Deep learning for robust and flexible tracking in behavioral studies for C. elegans *bioRxiv* 2021.02.08.430359 (2021). doi:10.1101/2021.02.08.430359

106. Brown, A. E. X. & De Bivort, B. Ethology as a physical science. *Nat. Phys.* **14**, 653–657 (2018).

107. Niepoth, N. & Bendesky, A. How Natural Genetic Variation Shapes Behavior. *Annu. Rev. Genomics Hum. Genet.* **21**, 437–463 (2020).

108. Krakauer, J. W., Ghazanfar, A. A., Gomez-Marin, A., MacIver, M. A. & Poeppel, D. Neuroscience Needs Behavior: Correcting a Reductionist Bias. *Neuron* **93**, 480–490 (2017).

109. Anderson, D. J. & Perona, P. Toward a science of computational ethology. *Neuron* **84**, 18–31 (2014).

110. Stephens, G. J. *et al.* Dimensionality and Dynamics in the Behavior of C. elegans. *PLoS Comput. Biol.* **4**, e1000028 (2008).

111. Brown, A. E. X., Yemini, E. I., Grundy, L. J., Jucikas, T. & Schafer, W. R. A dictionary of behavioral motifs reveals clusters of genes affecting Caenorhabditis elegans locomotion. *Proc. Natl. Acad. Sci. U. S. A.* **110**, 791–6 (2013).

112. Brown, A. E. X., Gomez-Marin, A. & Stephens, G. J. Hierarchical compression of Caenorhabditis elegans locomotion reveals phenotypic differences in the organization of behaviour. *J. R. Soc. Interface* **04**, (2016).

113. Chalfie, M. *et al. The Neural Circuit for Touch Sensitivity in Caenorhabditis elegans'*. *The Journal of Neuroscience* **5**, (1985).

114. Gray, J. M., Hill, J. J. & Bargmann, C. I. A circuit for navigation in Caenorhabditis elegans. *Proc. Natl. Acad. Sci. U. S. A.* **102**, 3184–3191 (2005).

115. Hedgecock, E. M. & Russell, R. L. Normal and mutant thermotaxis in the nematode Caenorhabditis elegans. *Proc. Natl. Acad. Sci. U. S. A.* **72**, 4061–4065 (1975).

116. Schindelin, J. *et al.* Fiji: an open-source platform for biological-image analysis. *Nat. Methods 2012 97* **9**, 676–682 (2012).

117. Berg, S. *et al.* ilastik: interactive machine learning for (bio)image analysis. *Nat. Methods* **16**, 1226–1232 (2019).

118. Geng, W. *et al.* Automatic Tracking, Feature Extraction and Classification of C. elegans Phenotypes. *IEEE Trans. Biomed. Eng.* **10**, (2004).

119. von Ziegler, L., Sturman, O. & Bohacek, J. Big behavior: challenges and opportunities in a new era of deep behavior profiling. *Neuropsychopharmacol. 2020 461* **46**, 33–44 (2020).

120. Lin, T. Y. *et al.* Microsoft COCO: Common objects in context. in *Lecture Notes in Computer Science (including subseries Lecture Notes in Artificial Intelligence and Lecture Notes in Bioinformatics)* **8693 LNCS**, 740–755 (Springer Verlag, 2014).

121. LeCun, Y., Bengio, Y. & Hinton, G. Deep learning. *Nat. 2015 5217553* **521**, 436–444 (2015).

122. Moen, E. *et al.* Deep learning for cellular image analysis. *Nat. Methods 2019 1612* **16**, 1233–1246 (2019).

123. He, K., Gkioxari, G., Dollár, P. & Girshick, R. Mask R-CNN.

124. Ren, S., He, K., Girshick, R. & Sun, J. *Faster R-CNN: Towards Real-Time Object Detection with Region Proposal Networks*.

125. Huang, J. *et al.* Speed/accuracy trade-offs for modern convolutional object detectors. in *Proceedings - 30th IEEE Conference on Computer Vision and Pattern Recognition, CVPR 2017* **2017-Janua**, 3296–3305 (Institute of Electrical and Electronics Engineers Inc., 2017).

126. Hung, J. *et al.* Applying Faster R-CNN for Object Detection on Malaria Images. (2018).

127. Chew, Y. L. *et al.* Recordings of Caenorhabditis elegans locomotor behaviour following targeted ablation of single motorneurons. *Sci. Data 2017 41* **4**, 1–7 (2017).

128. Salvador, L. C. M., Bartumeus, F., Levin, S. A. & Ryu, W. S. Mechanistic analysis of the search behaviour of Caenorhabditis elegans. *J. R. Soc. Interface* **11**, (2014).

129. Pierce-Shimomura, J. T., Morse, T. M. & Lockery, S. R. The Fundamental Role of Pirouettes in Caenorhabditis elegans Chemotaxis. *J. Neurosci.* **19**, 9557–9569 (1999).

130. Bates, K. *et al.* Fast, versatile and quantitative annotation of complex images. *https://doi.org/10.2144/btn-2019-0010* **66**, 269–275 (2019).

131. Nagy, S., Goessling, M., Amit, Y. & Biron, D. A Generative Statistical Algorithm for Automatic Detection of Complex Postures. *PLOS Comput. Biol.* **11**, e1004517 (2015).

132. Huang, K. M., Cosman, P. & Schafer, W. R. Machine vision based detection of omega bends and reversals in C. elegans. *J. Neurosci. Methods* **158**, 323–336 (2006).

133. Roussel, N., Sprenger, J., Tappan, S. J. & Glaser, J. R. Robust tracking and quantification of C. elegans body shape and locomotion through coiling, entanglement, and omega bends. *Worm* **3**, e982437 (2014).

134. Broekmans, O. D., Rodgers, J. B., Ryu, W. S. & Stephens, G. J. Resolving coiled shapes reveals new reorientation behaviors in C. elegans. *Elife* **5**, (2016).

135. Hebert, L., Ahamed, T., Costa, A. C., O'Shaughnessy, L. & Stephens, G. J. WormPose: Image synthesis and convolutional networks for pose estimation in C. elegans. *PLOS Comput. Biol.* **17**, e1008914 (2021).

136. Kokel, D. *et al.* Rapid behavior-based identification of neuroactive small molecules in the zebrafish. *Nat. Chem. Biol. 2010 63* **6**, 231–237 (2010).

137. de Chaumont, F. *et al.* Computerized video analysis of social interactions in mice. *Nat. Methods 2012 94* **9**, 410–417 (2012).

138. Jhuang, H. *et al.* Automated home-cage behavioural phenotyping of mice. *Nat. Commun. 2010 11* **1**, 1–10 (2010).

139. Schwarz, R. F. *et al.* Changes in Postural Syntax Characterize Sensory Modulation and Natural Variation of C. elegans Locomotion. *PLOS Comput. Biol.* **11**, e1004322 (2015).

140. Berman, G. J., Choi, D. M., Bialek, W. & Shaevitz, J. W. Mapping the stereotyped behaviour of freely moving fruit flies. *J. R. Soc. Interface* **11**, 1–22 (2014).

141. Berman, G. J., Bialek, W., Shaevitz, J. W. & Goldenfeld, N. Predictability and hierarchy in Drosophila behavior. *Proc. Natl. Acad. Sci. U. S. A.* **113**, 11943–11948 (2016).

142. Overman, K. E., Choi, D. M., Leung, K., Shaevitz, J. W. & Berman, G. J. *Measuring the repertoire of age-related behavioral changes in Drosophila melanogaster*.

143. Liu, M., Sharma, A. K., Shaevitz, J. W. & Leifer, A. M. Temporal processing and context dependency in caenorhabditis elegans response to mechanosensation. *Elife* **7**, (2018).

144. Saravanan, V., Berman, G. J. & Sober, S. J. Application of the Hierarchical Bootstrap to Multi-Level Data in Neuroscience. (2020). doi:10.1101/819334

145. Kirkwood, T. B. L. *et al.* What accounts for the wide variation in life span of genetically identical organisms reared in a constant environment? in *Mechanisms of Ageing and Development* **126**, 439–443 (2005).

146. Ghosh, R. & Emmons, S. W. Episodic swimming behavior in the nematode C. elegans. *J. Exp. Biol.* **211**, 3703–3711 (2008).

147. Ghosh, R. & Emmons, S. W. Calcineurin and Protein kinase G regulate C. elegans behavioral quiescence during locomotion in liquid. (2010).

148. Hughes, S. E., Evason, K., Xiong, C. & Kornfeld, K. Genetic and Pharmacological Factors That Influence Reproductive Aging in Nematodes. *PLOS Genet.* **3**, e25 (2007).

149. Berg, B. N. & Simms, H. S. Nutrition and longevity in the rat. II. Longevity and onset of disease with different levels of food intake. *J. Nutr.* **71**, 255–263 (1960).

150. Austad, S. N. & Fischer, K. E. Sex Differences in Lifespan. *Cell Metab.* **23**, 1022–1033 (2016).

151. Sampathkumar, N. K. *et al.* Widespread sex dimorphism in aging and age-related diseases. *Hum. Genet.* **139**, 333–356 (2020).

152. Honjoh, S. *et al.* The Sexual Dimorphism of Dietary Restriction Responsiveness in Caenorhabditis elegans. *Cell Rep.* **21**, 3646–3652 (2017).

153. Gems, D. & Riddle, D. L. Genetic, Behavioral and Environmental Determinants of Male Longevity in Caenorhabditis elegans. *Genetics* **154**, 1597–1610 (2000).

154. Shi, C., Runnels, A. M. & Murphy, C. T. Mating and male pheromone kill Caenorhabditis males through distinct mechanisms. *Elife* **6**, (2017).

155. Templeman, N. M. & Murphy, C. T. Regulation of reproduction and longevity by nutrient-sensing pathways. *J. Cell Biol.* **217**, 93 (2018).